

University of Alberta

**Experimental Study of Submerged Hydraulic Jumps with
Baffle Blocks**

by

Alireza Habibzadeh Gharehbaba

A thesis submitted to the Faculty of Graduate Studies and Research
in partial fulfillment of the requirements for the degree of

Doctor of Philosophy

in

Water Resources Engineering

Department of Civil & Environmental Engineering

© Alireza Habibzadeh Gharehbaba

Fall 2013

Edmonton, Alberta

Permission is hereby granted to the University of Alberta Libraries to reproduce single copies of this thesis and to lend or sell such copies for private, scholarly or scientific research purposes only. Where the thesis is converted to, or otherwise made available in digital form, the University of Alberta will advise potential users of the thesis of these terms.

The author reserves all other publication and other rights in association with the copyright in the thesis and, except as herein before provided, neither the thesis nor any substantial portion thereof may be printed or otherwise reproduced in any material form whatsoever without the author's prior written permission.

*Dedicated to the love of my life,
Sahar*

Abstract

The current work presents the results of an experimental study on the effects of submergence on the performance of a submerged hydraulic jump with baffle blocks downstream of a sluice gate. A wide range of Froude numbers, submergence factors, and block sizes, locations and arrangements were covered in the experiments. It was observed that, depending on the submergence factor, two different flow regimes could be established; i.e. the deflected surface jet (DSJ) and the reattaching wall jet (RWJ). Empirical equations were presented for the transitional submergence factor between the two regimes. Also, a theoretical equation was derived for the drag force acting on the blocks. To study the flow field, an acoustic Doppler velocimeter was used to measure the three-dimensional instantaneous velocities. The effect of the block size, location and arrangement on bulk energy dissipation was found to be insignificant. However, the block characteristics played an important role in determining the flow regime. As the size of the blocks increases, or they were moved further downstream, or a second row of blocks was added, the establishment of the DSJ flow regime was enhanced. It was observed that the DSJ flow regime is more efficient in dissipating the kinetic energy of the incoming flow. Also, the rate of reduction of the longitudinal velocity was faster in this flow regime. It was found that a larger portion of the flow depth is influenced by the blocks in the DSJ flow regime compared to the RWJ regime and significant mixing was observed between the centerplane and off-centerplane of the former. The turbulence flow field showed that the turbulence characteristics including turbulence intensities, Reynolds

stress, turbulence kinetic energy and energy dissipation are influenced by the blocks in both planes of the two flow regimes, but the magnitudes were significantly larger in the off-centerplane of the DSJ regime. The considerable difference between the two planes of the DSJ flow regime creates a significant shear mixing interface, which is, in turn, responsible for enhancing the dissipation of energy and decaying of the velocity.

Acknowledgments

I feel deeply honored and privileged to have the experience of working under the supervision of Dr. Mark R. Loewen and Dr. Nallamuthu Rajaratnam. I gratefully acknowledge their guidance and encouragement throughout the entire course of my studies. Appreciation is also expressed to the committee members for their valuable comments and suggestions.

I am thankful to Perry Fedun and Chris Kraft for helping me with the experimental arrangements during this research.

I wish to give special thanks to my parents for their major influence on my life. Words cannot express how appreciative I am of the love and support I've received from them.

During this journey, I met the most cherished one, the love of my life, Sahar. I feel fortunate to have her unwavering support, and deeply thank her for her love, support and sacrifices and for giving me the strength and courage to sail through challenges. Thank you for keeping life joyful for me with your love, liveliness and beauty.

Table of Contents

Topic	Page
List of Tables	i
List of Figures	ii
List of Symbols	v
List of Abbreviations	viii
Chapter 1 : Introduction	1
Motivation and Objectives.....	1
Thesis Content	2
Chapter 2 : An Exploratory Study of Submerged Hydraulic Jumps with Blocks ..	4
Introduction	4
Theory of Submerged Jumps with Baffle Blocks.....	6
Experimental Setup and Procedures	7
Results and Analysis.....	9
Conclusions	13
References	14
Chapter 3 : Performance of Baffle Blocks in Submerged Hydraulic Jumps	17
Introduction	17
Experimental Setup	19
Results and Discussion	21
Flow Observations	21
Drag Coefficient.....	26
Energy Dissipation	29
Practical Considerations	32
Conclusions	34
References	35
Chapter 4 : Mean Flow in a Submerged Hydraulic Jump with Baffle Blocks.....	38
Introduction	38
Experimental Setup and Procedures	42
Results and Discussion	48
Summary and Conclusion.....	68
References	69
Chapter 5 : Turbulence Characteristics of Submerged Hydraulic Jumps with Baffle Blocks	75
Introduction	75
Experimental Setup and Procedures	78
Results and Discussion	85
Conclusions	106
References	109
Chapter 6 : Conclusions and Recommendations for Future Research.....	115
Conclusions	115
Recommendations for Future Research.....	119

Appendix 1 : Some Observations on Submerged Hydraulic Jumps with Blocks	120
Introduction	120
Experimental Setup	121
Results and Analysis.....	123
Summary and Conclusion.....	131
References	131
Appendix 2 : Data Quality and Analysis	133
Error Analysis.....	133
ADV Measurements	133
Data Quality	133
Sampling Duration	137
Accuracy Compared to LDA.....	139
Uncertainty.....	140
References	144

List of Tables

Table	Page
Table 2-1 A summary of the experimental conditions ($y_I=2.4$ cm for all tests)	8
Table 3-1 The ranges of the experimental parameters.....	21
Table 4-1 The range of the experimental parameters ($y_I=19.1$ mm for all runs).....	44
Table 5-1 Range of the experimental parameters ($y_I=19.1$ mm for all runs).....	80
Table A2.1. The range of parameters in the replicate experiments.	139
Table A2.2. The range of the ADV measurement errors compared to LDA.....	140

List of Figures

Figure	Page
Figure 2.1 Definition sketch of a submerged jump with blocks	6
Figure 2.2 Comparison between measured and calculated drag coefficients for the baffle wall series.....	9
Figure 2.3 Dimensionless backup depth against dimensionless tailwater depth for the baffle-block series.....	10
Figure 2.4 Energy dissipation efficiency of the submerged jumps with blocks versus the submergence factor (S).....	11
Figure 2.5 Maximum energy dissipation efficiencies as a function of Froude number.....	12
Figure 2.6 Energy dissipation efficiency ratio as a function of tailwater depth	13
Figure 3.1 Schematic view of a submerged hydraulic jump with blocks; a) side view, b) top view.	20
Figure 3.2 Sketch of the centerplane flow pattern for a) Deflected Surface Jet (DSJ) and b) Reattaching Wall Jet (RWJ).	22
Figure 3.3 Dimensionless drag force (F_D/P_I) versus the submergence factor (S) with $w_b/y_I=2.36$ (the three numbers in the legend refer to h_b/y_I , x_b/y_I , and F_I , respectively).	27
Figure 3.4 The drag coefficient (C_D) versus dimensionless distance (x_b/y_I) for $h_b/y_I=2.0$ and $w_b/y_I=2.36$	29
Figure 3.5 The energy dissipation efficiency ratio (η) versus the submergence factor (S) (the three numbers in the legend refer to h_b/y_I , x_b/y_I , and F_I , respectively).....	30
Figure 4.1 Schematic view of the experimental arrangement; a) side view, b) top view.	43
Figure 4.2 Normalized velocity vector plot for the DSJ regime (Run #4); a) centerplane, and b) off-centerplane (blocks are located at $x=19.1$ cm or $x/y_I=10$).	48
Figure 4.3 Normalized longitudinal velocity profiles for the DSJ regime (Run #4).	50
Figure 4.4 Normalized vertical velocity profiles for the DSJ regime (Run #4); a) centerplane, and b) off-centerplane.	52
Figure 4.5 Normalized velocity vector plot for the RWJ regime (Run #6); a) centerplane, and b) off-centerplane (blocks are located at $x=19.1$ cm or $x/y_I=10$).	53
Figure 4.6 Normalized longitudinal velocity profiles for the RWJ regime (Run #6).	54
Figure 4.7 Normalized vertical velocity profiles for the RWJ regime (Run #6); a) centerplane, and b) off-centerplane.	56
Figure 4.8 Normalized velocity vector plot for the two-row block arrangement (Run #14); a) centerplane, and b) off-centerplane (first row of blocks is located at $x=19.1$ cm or $x/y_I=10$ and the second row at $x=28.6$ cm or $x/y_I=15$).	57

Figure 4.9 Normalized longitudinal velocity profiles for the two-row block arrangement (Run #14).	58
Figure 4.10 Normalized longitudinal velocity profiles upstream of the blocks ($x/y_1 < 10$) for the DSJ (a and b) and RWJ (c and d) regimes in the centerplane (a and c) and off-centerplane (b and d). .	60
Figure 4.11 The maximum normalized longitudinal velocity versus the normalized longitudinal distance for the DSJ regime; a) centerplane, and b) off-centerplane (wall jet curve from Rajaratnam 1976 and free jump curve from Rajaratnam 1965a).....	62
Figure 4.12 The maximum normalized longitudinal velocity versus the normalized longitudinal distance for the RWJ regime; a) centerplane, and b) off-centerplane (wall jet curve from Rajaratnam 1976 and free jump curve from Rajaratnam 1965a).....	63
Figure 4.13 Average curves of the maximum normalized longitudinal velocity versus the normalized longitudinal distance for runs with $x_b/y_1 = 10$ (wall jet curve from Rajaratnam 1976; free and submerged jump curves from Wu and Rajaratnam 1995).	65
Figure 4.14 Average curves showing the variation of the a) normalized jet half-width and b) normalized location of u_m versus the normalized longitudinal distance for runs with $x_b/y_1 = 10$	67
Figure 5.1 Schematic view of the experimental arrangement; a) side view, b) top view.	79
Figure 5.2 Vector plots of the mean flow field in (a) the centerplane and (b) off-centerplane of the DSJ flow regime (run BB3, $F_J = 5.32$ and $S = 0.54$) and (c) the submerged jump without blocks (run NB3, $F_J = 5.33$ and $S = 0.49$).	86
Figure 5.3 Vector plots of the mean flow field in the centerplane (a) and off-centerplane (b) of the RWJ flow regime (run BB4, $F_J = 5.25$ and $S = 1.55$) and the submerged jump without blocks (run NB4, $F_J = 5.28$ and $S = 1.53$).	87
Figure 5.4 Typical streamwise variation of the longitudinal turbulence intensity (I_x) for a) the DSJ regime (run BB3, $F_J = 5.32$, $S = 0.54$) and b) the RWJ regime (run BB4, $F_J = 5.25$, $S = 1.55$) and the corresponding submerged jump without blocks.	89
Figure 5.5 Typical streamwise variation of the vertical turbulence intensity (I_y) for a) the DSJ regime (run BB3, $F_J = 5.32$, $S = 0.54$) and b) the RWJ regime (run BB4, $F_J = 5.25$, $S = 1.55$) and the corresponding submerged jump without blocks.	92
Figure 5.6 Typical streamwise variation of the normalized Reynolds stress for a) the DSJ regime (run BB3, $F_J = 5.32$, $S = 0.54$) and b) the RWJ regime (run BB4, $F_J = 5.25$, $S = 1.55$) and the corresponding submerged jump without blocks.	94
Figure 5.7 Typical streamwise variation of the normalized turbulence kinetic energy for a) the DSJ regime (run BB3, $F_J = 5.32$, $S = 0.54$) and b) the RWJ regime (run BB4, $F_J = 5.25$, $S = 1.55$) and the corresponding submerged jump without blocks.	96
Figure 5.8 Typical streamwise variation of the dimensionless energy dissipation rate for a) the DSJ regime (run BB3, $F_J = 5.32$, $S = 0.54$) and b) the RWJ regime (run BB4, $F_J = 5.25$, $S = 1.55$) and the corresponding submerged jump without blocks.	98
Figure 5.9 Average curves for the streamwise variation of a) the maximum longitudinal turbulence intensity $(I_x)_{max}$ and b) maximum Reynolds stress. (Error bars represent the range of the computed 95% confidence limits of the runs used in the averaging.)	100

Figure 5.10 Average curves for the streamwise variation of the vertically-averaged turbulence kinetic energy. (Error bars represent the range of the computed 95% confidence limits of the runs used in the averaging.).....	102
Figure 5.11 Average curves for the streamwise variation of the vertically-averaged turbulence dissipation rate. (Error bars represent the range of the computed 95% confidence limits of the runs used in the averaging.).....	104
Figure A1.1 Schematic view of the experimental set-up.....	122
Figure A1.2 Shape and parameters of the blocks.	122
Figure A1.3 Flow visualization for DSJ (a, b, and c) and RWJ regimes (d, e, and f) (dye injected in the $z=0$ plane (a and d), $z=4.5$ cm plane (b and e), and behind the block (c and f)).	124
Figure A1.4 u -velocity profiles of the DSJ regime for $F_I=4.59$ and $S=0.52$ at $z=0$ and $z=4.5$ cm	125
Figure A1.5 Sketch of the streamlines of the DSJ regime at (a) $z=0$ and (b) $z=4.5$ cm.....	126
Figure A1.6 u -velocity profiles of the RWJ regime ($F_I=4.63$, $S=1.73$) for $z=0$ and $z=4.5$ cm.....	127
Figure A1.7 Sketch of the streamlines of the RWJ regime for (a) $z=0$ and (b) $z=4.5$ cm.....	128
Figure A1.8 Nondimensional velocity profiles along the $z=4.5$ cm plane.....	129
Figure A2.1 Distribution pattern for the spikes (a), correlation coefficients (b), and signal-to-noise ratios (c) of the u -velocity in the centerplane of the DSJ flow regime (run BB3).	134
Figure A2.2 Distribution pattern for the spikes (a), correlation coefficients (b), and signal-to-noise ratios (c) of the u -velocity in the off-centerplane of the DSJ flow regime (run BB3).	135
Figure A2.3 Distribution pattern for the spikes (a), correlation coefficients (b), and signal-to-noise ratios (c) of the u -velocity in the centerplane of the RWJ flow regime (run BB4).	136
Figure A2.4 Distribution pattern for the spikes (a), correlation coefficients (b), and signal-to-noise ratios (c) of the u -velocity in the off-centerplane of the RWJ flow regime (run BB4).	137
Figure A2.5 Sensitivity of the measured u (a) and I_x (b) to sampling duration (colors represent different measurement points).	138
Figure A2.6 Distribution pattern of the coefficient of variation (a) and relative error (b) of I_x in the centerplane of the DSJ flow regime (run BB3).	142
Figure A2.7 Distribution pattern of the coefficient of variation (a) and relative error (b) of I_x in the off-centerplane of the DSJ flow regime (run BB3).	143
Figure A2.8 Distribution pattern of the coefficient of variation (a) and relative error (b) of I_x in the centerplane of the RWJ flow regime (run BB4).	143
Figure A2.9 Distribution pattern of the coefficient of variation (a) and relative error (b) of I_x in the off-centerplane of the RWJ flow regime (run BB4).	144

List of Symbols

A	=	cross sectional area of baffles subjected to the flow;
B	=	width of the channel;
C_D	=	drag coefficient;
E_1	=	specific energy of the supercritical flow at the gate;
E_L	=	energy dissipation in the jump;
E_t	=	specific energy at the tailwater section downstream of the jump;
F	=	Froude number;
F_1	=	Froude number of the supercritical stream at the gate;
F_D	=	drag force;
I_x	=	normalized longitudinal turbulence intensities;
$(I_x)_{max}$	=	maximum normalized longitudinal turbulence intensities;
I_y	=	normalized vertical turbulence intensities;
L_e	=	length of the standing eddy behind each baffle block;
L_j	=	length of a free hydraulic jump;
L_r	=	length of the surface roller;
L_t	=	characteristic turbulence length scale;
L_x	=	turbulence integral length scale in the longitudinal (x) direction;
L_y	=	turbulence integral length scale in the vertical (y) direction;
L_z	=	turbulence integral length scale in the transverse (z) direction;
M	=	momentum flux;
P_f	=	pressure force;
P_t	=	pressure force at the subcritical section (tailwater) downstream of the jump;
Q	=	volumetric flow rate;
R_1	=	Reynolds number at the gate section;
S	=	submergence factor;
S_1	=	maximum submergence factor for the flow to be in the DSJ regime;
S_2	=	minimum submergence factor for the flow to be in the RWJ regime;
U	=	mean longitudinal velocity;
U_1	=	uniform longitudinal velocity at the gate opening;
V_t	=	characteristic turbulence velocity;
b	=	jet half-width; vertical distance y at which $u=1/2 u_m$ and $\partial u/\partial y < 0$;

g	=	acceleration due to gravity;
h_b	=	height of blocks;
k	=	turbulent kinetic energy;
\hat{k}	=	normalized turbulent kinetic energy;
\hat{k}_0	=	vertically-averaged normalized turbulent kinetic energy;
l_b	=	thickness of baffles (walls and blocks) in streamwise direction;
u	=	longitudinal (streamwise) velocity component;
u_m	=	maximum longitudinal velocity;
u'	=	longitudinal (streamwise) fluctuating velocity component;
v	=	vertical (normal to the bed) velocity component;
v'	=	vertical (normal to bed) fluctuating velocity component;
w	=	lateral (cross-stream) velocity component;
w'	=	transverse (cross-stream) fluctuating velocity component;
w_b	=	width of the blocks in transverse direction;
w_s	=	width of space between blocks;
x	=	longitudinal distance measured from the gate (in the direction of flow);
x_b	=	distance between the front face of blocks and the gate;
y	=	vertical distance measured from the flume bed;
y_0	=	height of the highest point at which velocity measurements were conducted;
y_1	=	vertical gate opening, depth of the supercritical flow;
y_2	=	subcritical sequent depth of the jump;
y_3	=	depth of flow just downstream of the gate, the back-up depth;
y_t	=	tailwater depth;
z	=	transverse distance measured from the flume centerline;
Δh	=	head loss in a free hydraulic jump;
δ	=	y at which $u = u_m$ at each station;
ε	=	energy dissipation rate per unit mass;
$\hat{\varepsilon}_0$	=	normalized vertically-averaged energy dissipation rate per unit mass;
ε_{ave}	=	average energy dissipation rate per unit mass of the corresponding free jump;
η	=	energy dissipation efficiency ratio;
λ	=	spacing parameter equal to the ratio of blocked width to the total flow width;
ν	=	kinematic viscosity of water;
ρ	=	mass density of water;
$\hat{\tau}_R$	=	normalized Reynolds stress;

$(\hat{\tau}_R)_{max}$ = maximum (at a given x/y_I) normalized Reynolds stress.

List of Abbreviations

ADV	=	acoustic Doppler velocimeter
BB	=	submerged jump experiments with baffle blocks
CFD	=	computational fluid dynamics
COR	=	correlation coefficient of ADV measurements
CV	=	coefficient of variation
DSJ	=	deflected surface jet (flow regime)
LDA	=	laser Doppler anemometer
NB	=	submerged jump experiments without baffle blocks
PIV	=	particle image velocimetry
RE	=	relative error in percent
RMS	=	root mean square
RS	=	Reynolds stress
RWJ	=	reattaching wall jet (flow regime)
SAD	=	sum of absolute deviations
SJ	=	submerged jump (flow regime)
SNR	=	signal-to-noise ratio of ADV measurements
SSD	=	sum of squared deviations
MKE	=	mean kinetic energy
TKE	=	turbulent kinetic energy
USBR	=	United States Bureau of Reclamation

Chapter 1: Introduction

Motivation and Objectives

Downstream of dams and outlet structures, the water flow has a high velocity; namely a supercritical flow, which has the potential to scour the downstream river channel. To avoid this undesirable issue, stilling basins are built at those locations. Stilling basins force a hydraulic phenomenon to occur which is named a '*hydraulic jump*'. In a hydraulic jump, the high-velocity (supercritical) flow is converted into a low-velocity (subcritical) one and will no longer have the mentioned unfavorable result. Depending on the depth of flow at the downstream channel, the toe (entrance to the jump) of the hydraulic jump can either have a free surface exposed to the atmospheric pressure, which is called a '*free jump*', or the toe occurs inside the ambient water with no contact to the free atmosphere, which is called a '*submerged jump*'. The free jump can change to the submerged one whenever the tailwater (downstream depth) increases. The tailwater increase can be, for example, a result of the backwater due to the construction of a structure located further downstream. Stilling basins are designed for the free jump conditions and the effect of submergence on their performance is not considered. However, the submergence of the jump can dramatically influence the functioning of the jump. The main role of a jump is to dissipate the excess energy of the incoming flow and decay its high velocity to release it safely into the downstream channel.

At the present time, the design of traditional stilling basins is based on free jump conditions and there are no design guidelines for submerged jumps with baffles. One major advantage of submerged jumps is that they are more stable than free jumps when downstream water levels vary. Also, the risk of downstream scouring can be eliminated by considering submergence in the design. In order to

Chapter 1: Introduction

do this a standard stilling basin design for submerged jumps must be made available to engineers so that they can design more cost-effective, safer and environmentally friendly hydraulic structures.

The objective of the present research was to investigate the performance of a submerged hydraulic jump with baffle blocks downstream of a sluice gate. The study consisted of an experimental study which covered a wide range of parameters observed in practice. The goal was to find out what modifications are required to be made to the structure to maintain its effectiveness so that the safety of the structure is ensured.

Thesis Content

The study is initiated with an exploratory investigation of the integral flow features in Chapter 2. A theoretical equation is derived for the drag force acting on the blocks as well as an empirical equation for the back-up depth; i.e. the depth just downstream of the gate. Also, some preliminary results are presented for the bulk energy dissipation within the submerged jump with blocks and a comparison was made with free hydraulic jumps.

The effects of the blocks size (height and width), location and arrangement (one-row and two-row) are studied in Chapter 3. Based on the experimental observations, two flow regimes were distinguished; i.e. the deflected surface jet (DSJ) and the reattaching wall jet (RWJ). Using dimensional analysis and nonlinear multiple regression analysis, empirical equations are also presented for the transitional submergence factor for the two flow regimes as a function the Froude number and blocks characteristics. It is demonstrated how the empirical equation can be used to modify design to consider the effect of submergence.

In Chapter 4, the time-averaged (mean) flow field is studied in detail. Three-dimensional velocities were measured with an acoustic Doppler velocimeter (ADV) for different flow conditions and block characteristics. The magnitude and location of the maximum longitudinal (streamwise) velocity

Chapter 1: Introduction

component is also studied in the streamwise direction. And, the results of the two flow regimes are compared with each other.

The turbulence properties of the flow field are studied in Chapter 5. The distribution patterns of turbulence intensities, Reynolds stress, turbulent kinetic energy, and energy dissipation are compared in the two flow regimes with the case of a submerged jump without blocks. Also, the longitudinal distributions of these parameters are investigated.

In Chapter 6, a summary of the results is presented and recommendations are provided for future study.

Chapter 2: An Exploratory Study of Submerged Hydraulic Jumps with Blocks¹

Introduction

Supercritical flow, in which the Froude number ($F = U/\sqrt{gy}$, where U is velocity, g acceleration due to gravity, and y is depth of water) is greater than unity, can be transformed into a subcritical flow ($F < 1$) through a hydraulic jump. This rapid transformation occurs when the tailwater depth is equal to the subcritical sequent depth of the incoming supercritical flow. The sequent depths are related by the Belanger equation,

$$\frac{y_2}{y_1} = \frac{1}{2} \left[\sqrt{1 + 8F_1^2} - 1 \right] \quad 2-1$$

where y_1 and y_2 are, respectively, the supercritical and subcritical sequent depths of the jump and F_1 is the Froude number at the supercritical section of the jump. The hydraulic jump under these circumstances is called a free hydraulic jump and this flow has been studied extensively (Mignot and Cienfuegos 2010, Castro-Orgaz and Hager 2009, Liu et al. 2004, Long et al. 1991, McCorquodale and Khalifa 1983, Rouse et al. 1958, Bakhmeteff and Matzke 1936). The transition from a high-velocity flow to a slow one is associated with high turbulence generated at the shear interface between the forward flow and the backward surface roller which helps in dissipating the excess energy of the supercritical flow. As a result, the hydraulic jump is a beneficial phenomenon and an efficient energy dissipator (Chow 1959). Baffle walls (sills) or blocks are sometimes introduced into the jump to increase the energy dissipation efficiency, as well as to stabilize it (Hager 1992).

¹A version of this chapter has been published (reused with permission from ASCE). Habibzadeh, A., Wu, S., Ade, F., Rajaratnam, N., and Loewen, M. R., *ASCE Journal of Hydraulic Engineering*, 137(6), 706-710, June 2011. DOI: [http://dx.doi.org/10.1061/\(ASCE\)HY.1943-7900.0000347](http://dx.doi.org/10.1061/(ASCE)HY.1943-7900.0000347)

If the tailwater depth is less than the subcritical sequent depth, the jump will be swept out of the basin, resulting in scour of the downstream channel. However, when the tailwater depth is greater than the subcritical sequent depth, the jump will become submerged. It has been observed that when the submergence of the jump increases, jet mixing decreases. This results in less dissipation of energy compared to free jumps, and the decay of the high velocity jet is retarded (Rajaratnam 1967, Rajaratnam 1965, Govinda Rao and Rajaratnam 1963). This may be considered an unfavorable characteristic of a submerged jump because it lowers the energy dissipation efficiency, and as a result, a longer stilling basin is needed if a submerged jump is to be used as an energy dissipator. However, submerged jumps are less sensitive to tailwater variations, which is an advantage over free jumps. Stilling basins below low-head structures are often required to operate under submerged conditions, and as a result, submerged jumps often occur in basins designed for free jumps.

Submerged jumps have been studied by many researchers (Dey and Sarkar 2008, Leutheusser and Fan 2001, Long et al. 1990, Narasimhan and Bhargava 1976, Rajaratnam 1965, Govinda Rao and Rajaratnam 1963) and the performance of baffles in free jumps has also attracted numerous investigations (Ohtsu et al. 1991, Tyagi et al. 1978, Basco and Adams 1971, Rajaratnam 1964, Shukry 1957, Harleman 1955) but the presence of baffle walls or blocks in a submerged jump has received less attention. Wu and Rajaratnam (1995) only studied the flow in a submerged jump with a baffle wall. The flow was classified into two regimes, namely deflected surface jet and reattaching wall jet, depending on the baffle wall height and tailwater depth. A detailed study of the flow properties in the two regimes was carried out, and the deflected surface jet regime was suggested as a safe method of dissipating energy using a submerged jump.

The effects of baffle blocks in submerged jumps have not been studied in detail. This paper is a preliminary attempt to investigate the behavior of a submerged jump with baffle blocks.

Theory of Submerged Jumps with Baffle Blocks

A definition sketch of a submerged jump with baffle blocks below a sluice gate is shown in Figure 2.1. In this figure, y_1 is the depth of the supercritical incoming flow, y_3 is the depth at the gate section (backup depth), y_t is the tailwater depth, h_b is the height of wall or block, and F_D is the drag force on the baffle. Assuming the pressure distribution to be hydrostatic and the velocity profile to be uniform at the two end sections of the jump, the momentum equation for a submerged jump with blocks (neglecting bottom shear stress) can be written as,

$$F_D = (P_1 + M_1) - (P_t + M_t) \tag{2-2}$$

where the drag force (F_D) is equal to the difference between the sum of the pressure force (P_f) and momentum flux ($M = \rho QU$, where ρ is the mass density of water and Q is the volumetric flow rate) at the two ends of the jump. Here, indices 1 and t refer to the supercritical (gate) and tailwater sections, respectively.

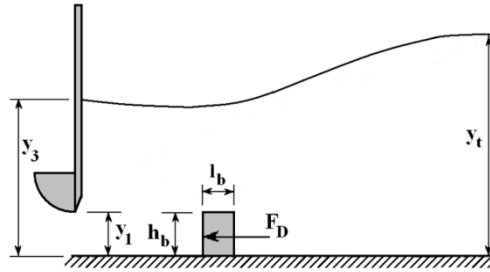


Figure 2.1 Definition sketch of a submerged jump with blocks

Using the customary definition of the drag force; i.e. $F_D = 1/2 C_D \rho A U^2$ (where C_D is the drag coefficient, A is the area projected to the flow, and U is velocity), and assuming the momentum flux correction coefficient to be unity, the solution of Eq. 2-2) leads to the following relation for the drag coefficient C_D ,

$$C_D = \frac{F_D}{1/2 \lambda \rho h_b U_1^2} = \frac{(y_3/y_1)^2 - (1+S)^2 (y_2/y_1)^2 - 2F_1^2 \{ [(1+S)(y_2/y_1)]^{-1} - 1 \}}{\lambda h_b / y_1 F_1^2} \tag{2-3}$$

where U_1 is velocity at the efflux section, F_1 is the Froude number at the efflux section, λ is the spacing parameter equal to the ratio of blocked width to the total basin width, and S is the submergence factor, defined as,

$$S = \frac{y_1 - y_2}{y_2} \quad 2-4$$

Note that for baffle walls $\lambda=1$, and for three-dimensional baffle blocks λ is a function of the block width (w_b) and the space between them (w_s) as follows: $\lambda=w_b/(w_b + w_s)$.

In a submerged jump without blocks, the depth of flow just downstream of the gate, y_3 , is used as a measure of the level of submergence of the gate. The ratio y_3/y_1 , the inlet depth factor, can be calculated in a submerged jump without blocks by applying the momentum equation to the two ends of the jump (Govinda Rao and Rajaratnam 1963),

$$\frac{y_3}{y_1} = \sqrt{(1+S)^2 (y_2/y_1)^2 - 2F_1^2 + \frac{2F_1^2}{(1+S)(y_2/y_1)}} \quad 2-5$$

In the case of a submerged jump with blocks, no such theoretical solution exists since the drag force enters the relation as a third parameter. The solution of Eq. 2-3) is possible if a relation between the inlet depth factor and submergence can be established.

Experimental Setup and Procedures

The experiments were conducted in a horizontal flume 46.4 cm wide, 62 cm high, and 9.2 m long. The side walls of the flume were made of glass with an aluminum bed. A false wooden bottom was installed over the entire flume bed to facilitate mounting of the baffles. The discharge was controlled by a valve, and a magnetic flowmeter in the supply pipe was used to measure the flow rate. The flow entered an upstream head tank and flowed beneath a sluice gate with a streamlined lip. The gate opening was set at 2.4 cm, creating a supercritical

stream with a depth of $y_1=2.4$ cm. A Prandtl type Pitot-static tube with an outer diameter of 3 mm was used to measure velocity profiles as well as pressures.

Two series of experiments were completed. The experimental conditions of the two series are listed in Table 2-1. The first series consisted of three runs with baffle walls of varying heights $h_b=2.54$ cm ($h_b/y_1=1.06$ for runs 1 and 3) and $h_b=3.8$ cm ($h_b/y_1=1.58$ for run 2). The baffle walls were installed at distances equal to $x_b=23.5$ cm ($x_b/y_1=9.79$ for run 1) and $x_b=33.3$ cm ($x_b/y_1=13.88$ for runs 2 and 3) from the gate. Froude numbers corresponding to these experiments were 2.44, 2.60 and 4.66, with submergences equal to 0.646, 0.683, and -0.073, respectively.

Table 2-1 A summary of the experimental conditions ($y_1=2.4$ cm for all tests)

Parameter	Symbol	Baffle Wall			Baffle Block
		Run 1	Run 2	Run 3	
height	h_b/y_1	1.06	1.58	1.06	1.58
wall thickness	l_b/y_1	0.79	0.79	0.79	0.79
distance from the gate	x_b/y_1	9.79	13.88	13.88	13.88
Froude number	F_1	2.60	4.66	2.44	3.92 ~ 7.37
submergence	S	0.683	-0.073	0.646	-0.14 ~ 0.89

For the second series, five baffle blocks were mounted across the flume covering half of the width. The blocks were at a distance of $x_b=33.3$ cm ($x_b/y_1=13.88$) from the gate. The width of the blocks, w_b , and their spacing, w_s , were both equal to 4.5 cm ($w_b/y_1=w_s/y_1=1.88$), which corresponds to a spacing parameter of $\lambda=1/2$. The blocks had a height of $h_b=3.8$ cm ($h_b/y_1=1.58$). The baffle walls and blocks were made of wood with a rectangular cross section and a streamwise thickness of $l_b=1.9$ cm ($l_b/y_1=0.79$). Five Froude numbers ranging from 3.92 to 7.37 and various submergences from -0.14 to 0.89 were included in this series of experiments.

In the baffle-wall experiments, the drag force acting on the baffle wall was calculated using measurements of the pressure distribution on both sides of the baffle. Pressures were measured using the static pressure holes of the Pitot tube kept near and parallel to the baffle wall. This method is based on the assumption

that the very small velocities near the baffle do not contribute to the pressure. The pressure on the front face was found to first decrease from the value on the bed and then rises to a maximum value followed by a fall to the minimum at the top edge of the baffle. The general trend of the pressure distribution is similar to the earlier measurements of Rajaratnam and Murahari (1971) and Ohtsu et al. (1991).

The measured drag coefficients of the baffle-wall experiments were first used to validate Eq. (2-3), then this equation was used to predict the drag coefficient in the block series. Submergence factors were calculated using the tailwater depth in the submerged jump with baffles and the subcritical sequent depth of a corresponding free jump without baffles (Eq. 2-1).

Results and Analysis

A comparison between the measured values of the drag coefficient and those calculated using Eq. (2-3) for the baffle-wall series is shown in Figure 2.2. It can be observed that the measured drag coefficients are in close agreement with the calculated values with a maximum deviation of -3.3%.

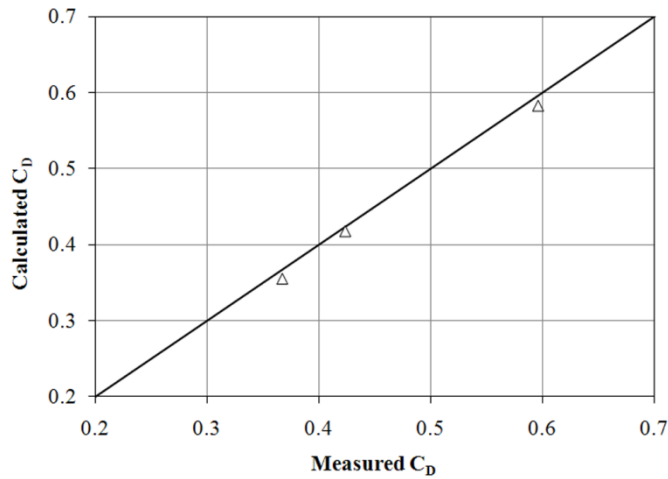


Figure 2.2 Comparison between measured and calculated drag coefficients for the baffle wall series

The measured inlet depth factors for the submerged jump with blocks were compared with those calculated for a submerged jump without blocks using Eq.

(2-5). It was found that the inlet depth factor was 9% to 189% larger in the presence of baffle blocks. The difference tended to increase for larger Froude numbers. Submerged jumps with and without blocks having the same values of F_1 , y_1 , and y_t were compared and it can be concluded that a direct consequence of the blocks on the jump is to increase the inlet depth factor. It is interesting to note that when blocks were present in the jump, it could become submerged at tailwater depths less than the corresponding subcritical sequent depth. In such cases, the corresponding submerged jump without blocks could not be established because the submergence factor was negative.

As shown in Figure 2.3, the dimensionless backup depths (y_3/y_2) collapsed to a single curve for $y_t/y_2 > 1$ (or $S > 0$). A linear regression of this data provides the following equation,

$$\frac{y_3}{y_2} = 1.384 \left(\frac{y_t}{y_2} \right) - 0.8 \quad 2-6$$

which has an $R^2=0.98$. Recalling Eq. (2-1), it is seen that y_2 includes the effects of both y_1 and F_1 .

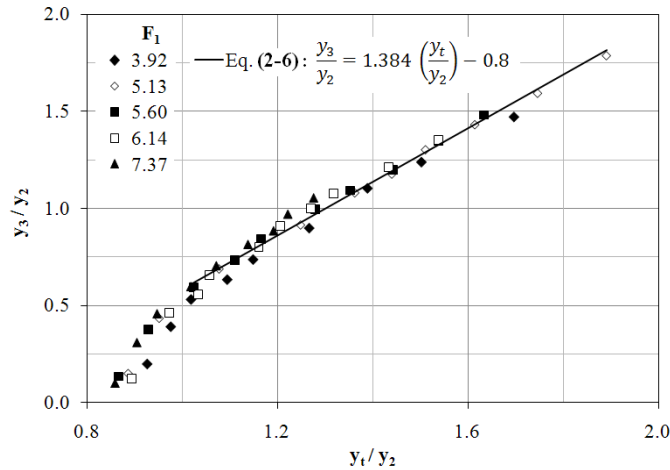


Figure 2.3 Dimensionless backup depth against dimensionless tailwater depth for the baffle-block series

The energy dissipation in a jump (E_L) can be defined as the difference between the specific energies before and after the jump (E_1 and E_2 , respectively). The energy dissipation efficiency can be defined as the ratio of the energy dissipation to the specific energy upstream of the jump; i.e. E_L/E_1 . The energy dissipation efficiencies for the submerged jumps with blocks are plotted in Figure 2.4 as a function of the submergence factor (S). As expected, the energy loss is larger for larger F_1 while a similar trend can be observed for all of the Froude numbers. For a given F_1 , the energy loss first increases with S , reaches its maximum value then gradually decreases in a linear manner. However, the difference between the maximum and minimum efficiencies was not greater than 10% for a given F_1 . The peak of the energy loss curve was found to be located at the same value of S where a linear relation could be established between the inlet and tailwater depths, i.e. the optimum point at $S \approx 0$. The peak shifted to slightly larger S values as F_1 decreased (see Figure 2.4).

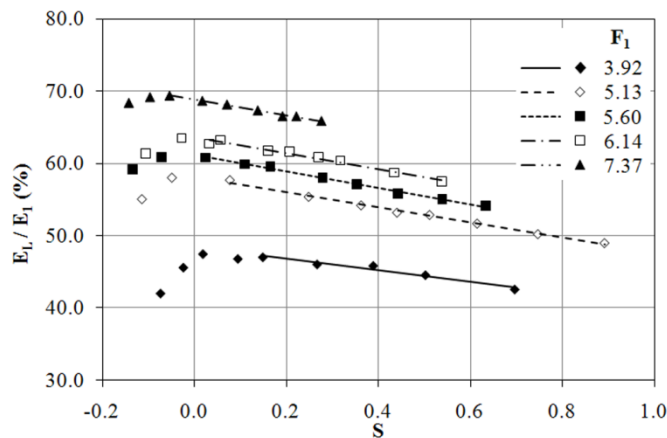


Figure 2.4 Energy dissipation efficiency of the submerged jumps with blocks versus the submergence factor (S)

The maximum energy dissipation efficiencies are compared to the values for free jumps and free jumps with blocks in Figure 2.5 as a function of F_1 . Energy losses at all five Froude numbers are in excess of the corresponding free jump having the same supercritical depth and Froude number; i.e. y_1 and F_1 . Without the blocks, the energy loss would be less than that of a free jump for

large submergences (Govinda Rao and Rajaratnam 1963). However, blocks increase the energy loss by increasing the mixing in the jump. The maximum energy loss is largest for the submerged jump with blocks and smallest for the free jump at all values of F_1 . The difference between submerged jumps with blocks and free jumps with blocks is insignificant, but the former is more efficient than a free jump; the difference being 9.2% for $F_1=3.92$ and 5.6% for $F_1=7.37$.

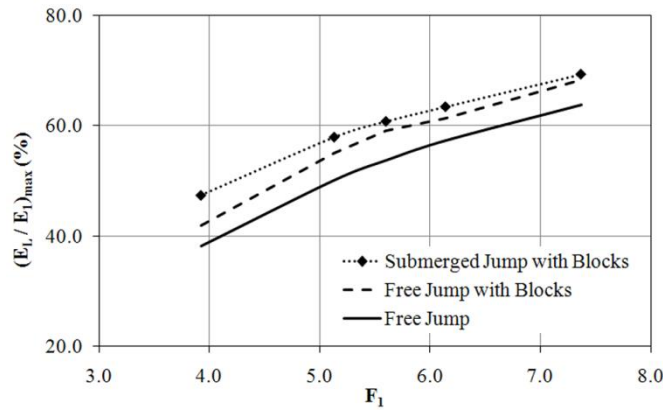


Figure 2.5 Maximum energy dissipation efficiencies as a function of Froude number

To compare the energy dissipation efficiencies, a dimensionless parameter η was defined as,

$$\eta = \frac{(E_L/E_1)_{SB}}{(E_L/E_1)_{FJ}} \quad 2-7$$

where, η is the ratio of the energy dissipation efficiency in the submerged jump with blocks (index SB) to that in the corresponding free jump (index FJ). The energy dissipation in a free jump can be calculated by simply applying the energy and momentum equations, and therefore this parameter can be used to compare the energy dissipation occurring in the two types of jumps and to determine the effectiveness of the blocks in a submerged jump.

The variation of η with dimensionless tailwater depth y_2/y_1 is shown in Figure 2.6. The values of this parameter for the three baffle-wall runs were 1.66, 1.23, and 1.78. For each value of F_1 , η increases from ~ 1.1 , reaches a maximum,

then gradually decreases to ~ 1.0 as y_t/y_1 increases. Again, the peak was located at the same optimal tailwater depth. Considering Figure 2.6, η is smaller for larger Froude numbers while this trend is reversed for $y_t/y_1 > 9$. Beyond this point, η is larger for larger Froude numbers and its variation is more gradual. This means that the energy dissipation efficiency of the submerged jump with blocks is more than that of a free jump without blocks when $y_t/y_1 < 9.0$. But with the increasing tailwater depth or submergence, the difference becomes insignificant. At large values of the tailwater depth ($y_t/y_1 \approx 12 \sim 14$), the efficiency becomes even less than that of the corresponding free jump; i.e. $\eta < 1$. This point ($\eta \leq 1$) occurs at a larger tailwater depth ratio (submergence) for larger Froude numbers. The magnitude of the peak is also seen to be higher for smaller F_1 , so the effect of the blocks is most beneficial at small Froude numbers.

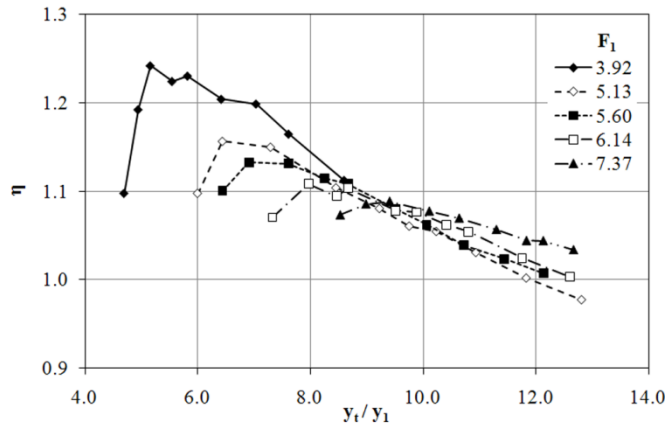


Figure 2.6 Energy dissipation efficiency ratio as a function of tailwater depth

Conclusions

It was shown that the theoretical equation for the drag coefficient derived using the momentum equation can be applied to submerged jumps with baffle walls. A new form of this equation (Eq. 2-3) was introduced for baffle blocks. A linear relation between the dimensionless backup and tailwater depths (using the sequent depth as the length scale) was derived using regression analysis. This equation along with Eq. (2-3) can be used to estimate the drag force on baffle

blocks. The energy dissipation efficiency of submerged jumps with blocks was found to be a function of F_1 and S . The efficiency first increases with submergence, reaching its maximum, then slightly decreasing. The maximum energy dissipation efficiency of submerged jumps with blocks was shown to be more than the efficiency of the free jump, and a free jump with the same blocks at the same F_1 . However, the difference decreases with increasing Froude number. The energy dissipation efficiency of submerged jumps with blocks is larger than that of free jumps at first but the efficiency decreases as tailwater depth increases. More detailed studies covering a wider range of the parameters pertinent to blocks are required to fully understand and make use of submerged jumps with baffle blocks as energy dissipators.

References

- Bakhmeteff, B. A., and Matzke, A. E. (1936). "The hydraulic jump in terms of dynamic similarity." *Trans. Am. Soc. Civ. Eng.*, 101 630-647. Discussion : Vol. 101, pp. 648-680.
- Basco, D. R., and Adams, J. R. (1971). "Drag forces on baffle blocks in hydraulic jumps." *J. Hyd. Div.*, 97(HY12), 2023-2035.
- Castro-Orgaz, O., and Hager, W. H. (2009). "Classical hydraulic jump: basic flow features." *J. Hydraul. Res.*, 47(6), 744-754.
- Chow, V. (1959). *Open-channel hydraulics*. McGraw-Hill, New York.
- Dey, S., and Sarkar, A. (2008). "Characteristics of Turbulent Flow in Submerged Jumps on Rough Beds." *J. Engrg. Mech.*, 134(1), 49-59.
- Govinda Rao, N. S., and Rajaratnam, N. (1963). "The submerged hydraulic jump." *J. Hyd. Div.*, 89(HY1), 139-162.
- Hager, W. H. (1992). *Energy dissipators and hydraulic jump*. Kluwer, London.
- Harleman, D. R. F. (1955). "Effect of baffle piers on stilling basin performance." *J. Boston Soc. of Civil Engrs*, 42(2), 84-99.

- Leutheusser, H. J., and Fan, J. J. (2001). "Backward Flow Velocities of Submerged Hydraulic Jumps." *J.Hydr.Engng.*, 127(6), 514-517.
- Liu, M., Rajaratnam, N., and Zhu, D. Z. (2004). "Turbulence Structure of Hydraulic Jumps of Low Froude Numbers." *J.Hydr.Engng.*, 130(6), 511-520.
- Long, D., Rajaratnam, N., Steffler, P. M., and Smy, P. R. (1991). "Structure of flow in hydraulic jumps." *J. Hydraul. Res.*, 29(2), 207-218.
- Long, D., Steffler, P. M., and Rajaratnam, N. (1990). "LDA study of flow structure in submerged hydraulic jump." *J. Hydraul. Res.*, 28(4), 437-460.
- McCorquodale, J. A., and Khalifa, A. (1983). "Internal Flow in hydraulic jumps." *J. Hydr. Engng.*, 109(5), 684-701.
- Mignot, E., and Cienfuegos, R. (2010). "Energy Dissipation and Turbulent Production in Weak Hydraulic Jumps." *J.Hydr.Engng.*, 136(2), 116-121.
- Narasimhan, S., and Bhargava, V. P. (1976). "Pressure fluctuations in submerged jump." *J. Hyd. Div.*, 102(3), 339-350.
- Ohtsu, I., Yasuda, Y., and Yamanaka, Y. (1991). "Drag on vertical sill of forced jump." *J. Hydraul. Res.*, 29(1), 29-47.
- Rajaratnam, N. (1967). "Hydraulic Jumps." *Advances in Hydrosience Vol. 4*, Academic Press Inc., 197-280.
- Rajaratnam, N. (1965). "Submerged hydraulic jump." *J. Hyd. Div.*, 91(HY4), 71-96.
- Rajaratnam, N. (1964). "The forced hydraulic jump." *Water Power*, Part I - January and Part II - February.
- Rajaratnam, N., and Murahari, V. (1971). "A contribution to forced hydraulic jumps." *J. Hydraul. Res.*, 9(2), 217-240.
- Rouse, H., Siao, T. T., and Nagaratnam, S. (1958). "Turbulence characteristics of the hydraulic jump." *J. Hyd. Div.*, 84(HY1), Proc. Paper 1528.
- Shukry, A. (1957). "The efficiency of floor sills under drowned hydraulic jumps." *J. Hyd. Div.*, 83(Hy3), Proc. Paper 1260.

Chapter 2: An Exploratory Study of Submerged Hydraulic Jumps with Blocks

Tyagi, D. M., Pande, P. K., and Mittal, M. K. (1978). "Drag on baffle walls in hydraulic jump." J. Hyd. Div., 104(HY4), 515-525.

Wu, S., and Rajaratnam, N. (1995). "Effect of Baffles on Submerged Flows." J.Hydr.Engrg., 121(9), 644-652.

Chapter 3: Performance of Baffle Blocks in Submerged Hydraulic Jumps¹

Introduction

Hydraulic jumps occur in natural systems; e.g. rivers and streams, as well as man-made systems. Examples of the latter occurrence are jumps in water distribution and irrigation networks formed downstream of hydraulic structures such as spillways, sluice gates, and drops. These structures are usually designed for a specific tailwater depth (along with other parameters; e.g. discharge and Froude number) corresponding to the design discharge, so that the jump is restricted to a length not more than the length of the stilling basin. However, the flow rate and hence the tailwater depth may vary and as a result, the location of the jump can vary. Usually a tailwater depth in excess of the one required for the free jump is maintained to ensure that the jump will not be swept downstream (Peterka 1984). If the flow rate is larger than the design discharge, the tailwater depth will be greater than the one required for a free jump. These situations are common in low head hydraulic structures including downstream of low diversion dam spillways and sluice gates. Under such conditions the hydraulic jump will be submerged. The purpose of stilling basins downstream of these types of hydraulic structures is to dissipate the excess kinetic energy of the supercritical flow in a hydraulic jump. When the jump is submerged, the energy dissipation rate, being a function of submergence, could be less than that of the free jump depending on the submergence (Rajaratnam 1967). In submerged jumps the flow behavior, including jet expansion and streamwise velocity decay, differ significantly from a free jump (Rajaratnam 1967).

Baffle walls and blocks are often used to stabilize the jump, decrease its length and increase the energy dissipation. Performance of baffle walls and blocks

¹ A version of this chapter has been published (reused with permission from ASCE). Habibzadeh, A., Loewen, M.R., and Rajaratnam, N., *ASCE Journal of Hydraulic Engineering*, 138(10), 902-908, October 2012. DOI: [http://dx.doi.org/10.1061/\(ASCE\)HY.1943-7900.0000587](http://dx.doi.org/10.1061/(ASCE)HY.1943-7900.0000587)

in free hydraulic jumps has been studied by numerous researchers (e.g. Rajaratnam 1964a and 1964b, Basco and Adams 1971, Rajaratnam and Murahari 1971, Ohtsu et al. 1991, Hager 1992, and Thompson and Kilgore 2006). Submerged hydraulic jumps have also been the subject of many papers (e.g. Long et al. 1990 and Dey and Sarkar 2008), but submerged jumps with baffles (walls or blocks) have received much less attention. Wu and Rajaratnam (1995) studied submerged flows with baffle walls and observed that the flow could be classified into two regimes. For low submergences the incoming stream, after impacting the baffle wall, was deflected towards the water surface and a region of circulating flow was established. This type of flow was called the “Deflected Surface Jet” (DSJ) regime. When the tailwater depth was larger than a certain threshold, the incoming jet was first deflected away from the bed and then impinged on the bed further downstream. This flow regime was called the “Reattaching Wall Jet” (RWJ).

Onyshko et al. (2002) employed the particle image velocimetry (PIV) method to study the flow field in a deflected wall jet. The formation of two eddies was observed on the upstream and downstream sides of the jet trajectory. Variation of the vorticity field as well as the mean and turbulent kinetic energy was studied. Habibzadeh et al. (2011) conducted a preliminary study of the flow properties of submerged jumps with baffle blocks. A general theoretical equation for the drag force on the blocks was derived. The energy dissipation in submerged jumps with blocks was also compared with free jumps. The energy dissipation efficiency, defined as the ratio of the dissipated energy to the initial energy of the supercritical flow in the submerged jump to that in the free jump, was found to be a function of submergence factor with the maximum efficiency being slightly larger than in the corresponding free jump. An empirical equation was derived for the back-up depth; i.e. the ratio of the depth just downstream of the gate to the gate opening. The energy dissipation was found to be a function of submergence

factor as well as the Froude number. However, their experiments included only one block shape and location.

The current study was designed to investigate the global features and hydraulic behavior of this flow over a wide range of Froude numbers, submergence factors, and block shapes and locations. This range of the experimental parameters was selected based on the practical ranges which are common in low head structures where hydraulic jump stilling basins are widely used. The main objective of this study was to determine the conditions under which submerged hydraulic jumps with blocks can be used as energy dissipators and to derive practical measures to do so.

Experimental Setup

The experiments were conducted in the Hydraulics Laboratory in the Department of Civil and Environmental Engineering at the University of Alberta. Measurements were conducted in a horizontal flume with a width of 0.467 m, height of 0.60 m, and length of 7.5 m and an aluminum bed and glass walls. Water was pumped from an underground sump into a head tank and the discharge was measured with a magnetic flowmeter. At the downstream end of the head tank there was a sluice gate with an opening of $y_1=1.9$ cm into the flume. The edge of the sluice gate has a streamlined lip in the shape of a quarter-cylinder of diameter 20 cm to minimize flow contraction and provide a uniform supercritical flow. A PVC sheet 19.1 mm thick was mounted on the original bed of the flume to facilitate baffle block installation. This false bed extended 1.2 m upstream and 3.5 m downstream of the gate. A tailgate located at the downstream end of the flume was used to control the tailwater depth. A point gauge with an accuracy of 0.1 mm was used to measure water depths. In order to visualize the flow field, the dye-injection method and a high speed camera were employed.

A sketch of the side view of a submerged hydraulic jump with blocks is shown in Figure 3.1a. In this figure, y_t is the tailwater depth, y_3 is the back-up

depth downstream of the gate, and y_1 is the depth of the supercritical jet equal to the gate opening. The plan view of the block arrangement is also shown in Figure 3.2b.

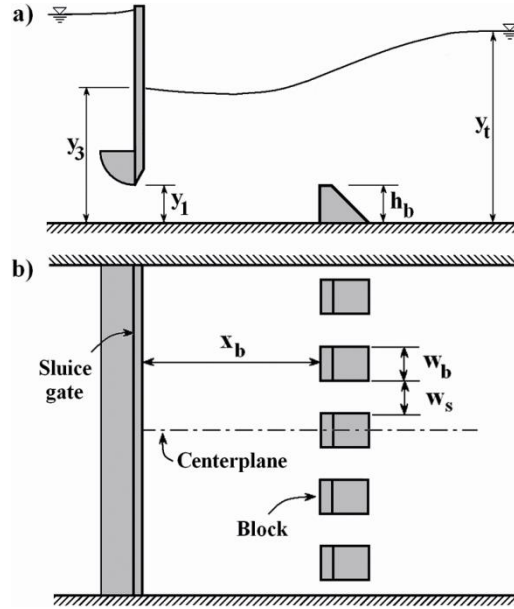


Figure 3.1 Schematic view of a submerged hydraulic jump with blocks; a) side view, b) top view.

The baffle blocks were made of PVC using the design guidelines for the standard USBR Basin III (Peterka 1984). Three different block heights of $h_b=1.9$, 3.8, and 5.1 cm with a width of $w_b=4.5$ cm were used. The top crest length of the block was set equal to $0.2 h_b$, the bottom length to $1.2 h_b$ and the downstream slope of the block was 1:1. The space between the blocks was set equal to their width $w_s=4.5$ cm and a total of five blocks were installed across the flume. Baffle blocks were mounted at different distances from the gate; $x_b=9.5$, 19.1, 28.6, 38.1, and 76.2 cm. For one of the block series ($h_b=3.8$ cm), a different width ($w_b=w_s=2.8$ cm corresponding to eight blocks across the flume) was also used to study the influence of this parameter. One case using two rows of staggered blocks was included in the experiments with block height of $h_b=3.8$ cm and with the second row placed at 9.5 cm downstream of the first row. A total of 334 experiments were conducted for which the range of the experimental parameters

is tabulated in Table 3-1. In the current paper, the submergence factor is defined as $S=(y_t - y_2)/y_2$; where y_t is the tailwater depth and y_2 is the subcritical sequent depth for a free jump corresponding to the supercritical depth of y_1 (calculated by the Belanger equation (Chow 1959)).

Table 3-1 The ranges of the experimental parameters.

Parameter	Symbol	Values
Froude Number	F_1	4.0, 5.0, 6.0, 7.0, 8.2
Submergence Factor	S	-0.2 ~ 3.0
Block Height	h_b/y_1	1.0, 2.0, 2.67
Block Width	w_b/y_1	1.47, 2.36
	w_b/h_b	0.73, 0.88, 1.18, 2.36
Block Location	x_b/y_1	5, 10, 15, 20, 40

Results and Discussion

Flow Observations

The dye injection method was used to visualize the flow around the blocks along with high speed videos recorded using a MotionScope® PCI 1000S camera that acquired 1000 frames per second. It was observed that at a given Froude number, as the tailwater depth increased the flow behavior changed and was similar to a submerged flow over a baffle wall (Wu and Rajaratnam 1995). A sketch of the centerplane flow pattern (i.e. flow pattern in the plane passing through the center of block) is shown in Figure 3.2. At small tailwater depths (low submergence factors), the supercritical jet, in the centerplane, was deflected by the blocks towards the water surface. The deflected jet created a bulge on the water surface at the boundary between the forward and backward flows and this flow is referred to as the Deflected Surface Jet (DSJ) regime following Wu and Rajaratnam (1995). The near-surface flow upstream of the blocks consisted of a small region of recirculating flow located between the gate and the blocks (see Figure 3.2a). A bulge was formed on the water surface right above the blocks, connecting the two flow depths upstream and downstream of the blocks. As the tailwater depth increased (higher submergence factors), the height of the jump decreased; i.e. the difference between the back-up depth and the tailwater depth

diminished. Water surface fluctuations were observed downstream of the jump in the DSJ regime which damped out as S increased. In the DSJ regime, there was some air entrainment occurring at the water surface but this was reduced as S increased.

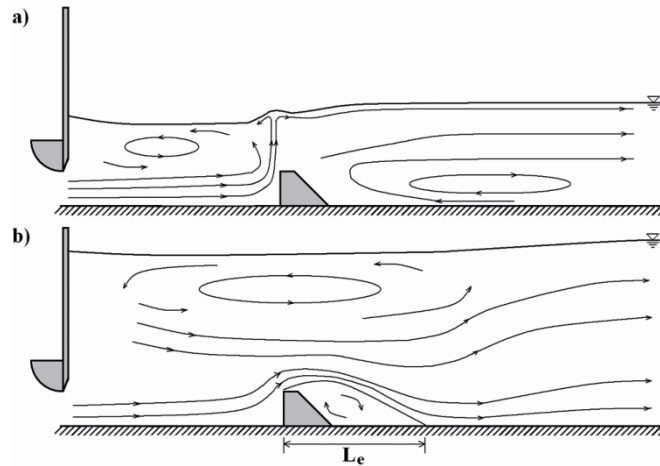


Figure 3.2 Sketch of the centerplane flow pattern for a) Deflected Surface Jet (DSJ) and b) Reattaching Wall Jet (RWJ).

For large submergences, the flow in the centerplane first separated from the bed just upstream of the block face then reattached to the bed just downstream of the blocks. The standard block shapes that are used in this study act like sharp-edged obstacles for which the flow separates at the upstream tip of the block. Further downstream of the reattachment point, the flow behaved similar to a wall jet. This flow is defined as the Reattaching Wall Jet (RWJ) regime following Wu and Rajaratnam (1995). The flow in this regime includes a large recirculating region near the water surface which extends further downstream of the blocks (see Figure 3.2b). The water surface profile was approximately horizontal; i.e. the height of the jump was negligible. The water surface downstream of the jump was free of water surface fluctuations unlike the DSJ regime.

The abovementioned flow regimes apply to the centerplane of the flow; i.e. the plane passing through the center of block (see Figure 3.1b). In both flow regimes, the flow between the blocks was observed to behave like a submerged

wall jet with a recirculating flow region (surface roller). In both flow regimes, the surface roller extended downstream of the blocks; however, the length of the surface roller was larger in the RWJ regime. In the DSJ regime, the surface roller in the plane between the blocks ended just downstream of the blocks; i.e. downstream of the surface bulge; while in the RWJ regime, the length of the surface roller was close to that of the submerged jump without blocks.

It can be shown that for submerged hydraulic jumps with blocks, dimensional analysis leads to the following equation,

$$f\left(C_D = \frac{F_D}{1/2 \lambda \rho h_b U_1^2}, F_1 = \frac{U_1}{\sqrt{g y_1}}, R_1 = \frac{U_1 y_1}{\nu}, \frac{y_t}{y_1}, \frac{h_b}{y_1}, \frac{x_b}{y_1}, \frac{w_b}{y_1}\right) = 0 \quad 3-1$$

where, C_D is the drag coefficient, F_D is the drag force, λ is the spacing parameter defined as the ratio of blocked width to the total flow width, ρ is the mass density of water, R_1 is the Reynolds number at the gate, U_1 is the velocity at the gate opening, g is the acceleration due to gravity, and ν is the kinematic viscosity of water. This equation is similar to the one for free hydraulic jump with baffle walls (Rajaratnam and Murahari 1970, Ohtsu et al. 1991) with additional terms for the back-up depth and the width of blocks; i.e. y_3/y_1 and w_b/y_1 . Large Reynolds numbers were encountered for the range of parameters in the current experimental work (i.e. R_1 was always greater than 30,000); hence, the effect of Reynolds number can be considered to be insignificant. The value of λ was kept constant at the recommended value of 0.5 and it can be shown that the back-up depth is a function of the tailwater depth (Habibzadeh et al., 2011). Therefore, Eq. (3-1) reduces to,

$$C_D \text{ or } S_{1,2} = f\left(F_1, S, \frac{h_b}{y_1}, \frac{x_b}{y_1}, \frac{w_b}{y_1}, \lambda\right) \quad 3-2$$

where, S_1 and S_2 are critical submergence factors which will be described in the following. As it was noted previously, the flow regime that was observed was found to be a function of the submergence factor, S . A separate series of 44

experiments was conducted for each block arrangement (set values of h_b/y_1 , x_b/y_1 and w_b/y_1) and Froude number to find the critical value of the submergence factor at which this change in flow regime occurred. It was observed that for each Froude number and block arrangement, the flow was always in the DSJ regime for submergence factors less than a critical value, defined as S_1 . Values of S_1 were found by starting at a large S value, with the flow in the RWJ regime, and decreasing the tailwater depth until the flow changed to the DSJ regime. The tailwater depth at which the flow changed from RWJ to DSJ was recorded and used to calculate S_1 . It was observed that for each Froude number and block arrangement, the flow was always in the RWJ regime when the submergence factor was greater than a critical value, defined as S_2 . Values of S_2 were determined by starting at a small S value, with the flow in the DSJ regime, and increasing the tailwater depth until the flow changed to the RWJ regime. The tailwater depth at which the flow changed from DSJ to RWJ was recorded and used to calculate S_2 . Note that S_1 is always smaller than (or equal to) S_2 and if $S < S_1$, the flow was always in the DSJ regime, and if $S > S_2$, the flow was always in the RWJ regime. If $S_1 < S < S_2$, the flow was in either of the regimes depending upon whether the tailwater depth was increasing or decreasing; i.e. hysteresis was observed. That is, for $S_1 < S < S_2$, if the tailwater depth is increasing, the flow continues to be in the DSJ regime until S_2 is reached but if the tailwater depth is decreasing, the flow continues to be in the RWJ regime until S_1 is reached.

Variations of S_1 and S_2 for the range of Froude numbers and block arrangements were studied in detail. It was observed that the hysteresis range narrows as F_1 increased; e.g. for $F_1=8.2$ the difference between the values of S_1 and S_2 was less than 0.1 while for $F_1=4.0$ it was approximately 0.5. The general trend for both S_1 and S_2 was that they decreased as F_1 increased but, this trend was more pronounced for larger blocks. This means that for each block arrangement, the regime change occurs at lower S values as F_1 increases and less hysteresis occurs. It was also found that there is a direct relation between the values of S_1

and S_2 and the distance between the blocks and the gate. At a given value of F_1 , as x_b increased, both S_1 and S_2 increased. S_1 and S_2 are also functions of the block height and width; i.e. as h_b or w_b increases, both S_1 and S_2 increase.

It should be noted that for the range of Froude numbers and submergence factors studied, the RWJ regimes did not occur for two cases; the two-row case and the case with $x_b=76.2$ cm ($x_b/y_1=40$). This is consistent with the above-mentioned conclusion; i.e. when the blocks are far away from the gate, the S_1 and S_2 values fall beyond the range which could be maintained in the laboratory flume. In general, both S_1 and S_2 were more sensitive to block height and location for small Froude numbers. Changing the block height, results in changes in both S_1 and S_2 values, with these variations being much less for large Froude numbers. At large Froude numbers the large momentum is the dominating factor that controls the flow behavior, resulting in lower levels of sensitivity to other external factors such as the block height.

The general trends for S_1 and S_2 were examined using multiple regression analysis. This was done using the Statistics Toolbox™ of MATLAB® which uses the Levenberg-Marquardt algorithm for nonlinear least squares regression (MATLAB Statistics Toolbox User's Guide, 2011). Using Eq. (3-2) and multiple regression analysis, the following two equations were derived,

$$S_1 = 0.44 F_1^{-2.1} \left(\frac{h_b}{y_1} \right)^{3.1} \left(\frac{w_b}{h_b} \right)^{1.9} \left(\frac{x_b}{y_1} \right)^{0.65} - 0.06 \quad 3-3$$

$$S_2 = 2.40 F_1^{-1.3} \left(\frac{h_b}{y_1} \right)^{1.7} \left(\frac{w_b}{h_b} \right)^{1.1} \left(\frac{x_b}{y_1} \right)^{0.17} - 0.50 \quad 3-4$$

These two empirical equations have correlation coefficients of $R^2=0.98$ and $R^2=0.93$, respectively. To determine the accuracy of these equations in predicting the flow regime, they were compared with all of the experimental data points. The comparison showed that predictions of the flow regime using Eqs. (3-3) and (3-4) were correct 85% of the time. Therefore, these equations can be used

with confidence to predict the flow regime within the range of the experimental data covered in this study.

In the RWJ regime a recirculating eddy exists downstream of each block inside a separated flow region (see Figure 3.2b). Due to the finite width of the blocks, the separated flow region is three-dimensional (3D). To approximately evaluate the length of the standing eddy (L_e), dye was injected on the bed behind the blocks. The length of this eddy was measured by injecting dye behind the blocks and observing the extent of the standing eddy. Due to the smaller velocities in that region, L_e could be measured with an accuracy of $\pm 5\%$. The dimensionless eddy length L_e/w_b had a mean value of approximately 2.0 with a standard deviation of 0.2 but the eddy length varied by less than 25% as the block height was varied by a factor of 2.67. Therefore, it was concluded that the length of the eddy is predominantly a function of block width.

Drag Coefficient

The drag force (F_D) acting on blocks in a submerged jump on a horizontal bed is equal to the difference in the sum of the pressure force and momentum fluxes between the supercritical and tailwater sections neglecting the bed shear stress (Habibzadeh et al. 2011). The drag force calculated by this method is typically scaled using the tailwater pressure force (P_t), because it is the most indicative scale (Harleman 1955, Basco and Adams 1971).

The dimensionless drag force (F_D/P_t) is plotted versus the submergence factor (S) in Figure 3.3 for selected block arrangements. The ratio F_D/P_t is a measure of the effectiveness of the blocks (Harleman 1955) and it can be seen that, this ratio decreases rapidly at small submergences and more slowly at larger submergences; while for larger Froude numbers and for large values of x_b/y_I , the ratio is approximately constant as S varies. That is, at small submergences, the effectiveness of the blocks is a strong function of S , and at large submergences, it

is only a weak function of S ; i.e. in the RWJ regime (for instance for $S > 1.5$ in Figure 3.3b).

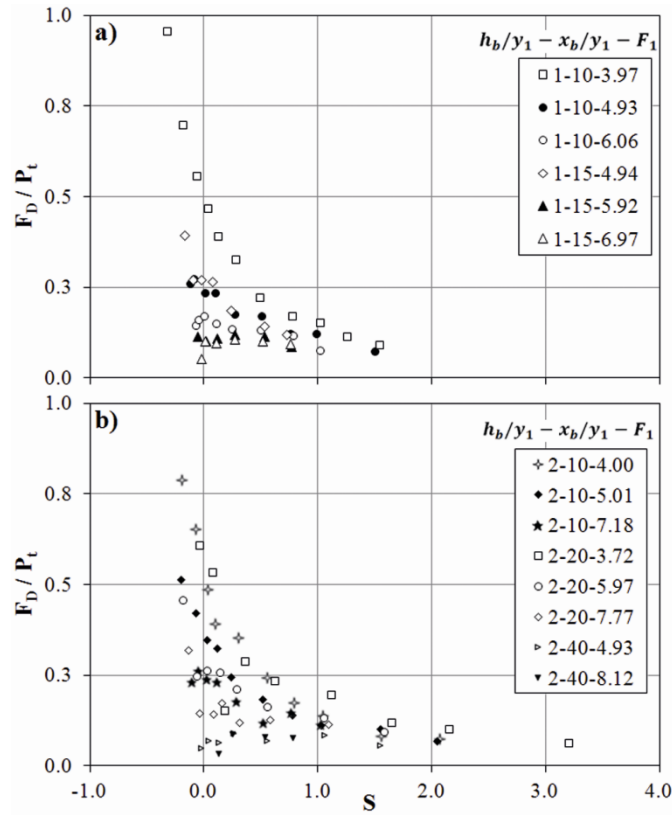


Figure 3.3 Dimensionless drag force (F_D/P_t) versus the submergence factor (S) with $w_b/y_1=2.36$ (the three numbers in the legend refer to $h_b/y_1, x_b/y_1$, and F_1 , respectively).

The experimental data series were individually studied to observe the effect of each variable. It was found that for each block arrangement for a given S value, the dimensionless drag force decreases as F_1 increases. The ratio F_D/P_t for each block arrangement changes with S ; for small F_1 values, this ratio rapidly decreases as S increases, while for large F_1 values, the ratio first slightly increases then gradually decreases as S increases. This is also the case for blocks furthest away from the gate (see Figure 3.3b). The effect of F_1 was minor for the largest value of x_b/y_1 of 40 (see Figure 3.3b). For every block height, increasing x_b resulted in a decrease in F_D/P_t (see Figure 3.3a and b), and, for each block

arrangement, increasing h_b increased F_D/P_t . The effect of the block width was found to be insignificant.

The drag force can also be represented by the drag coefficient (C_D) which is influenced by S , F_I and the block arrangement (see Eq. 3-2). Habibzadeh et al. (2011) presented an equation to evaluate C_D in terms of S , F_I , h_b and λ . It has been shown that the free jump is most efficient at dissipating energy when half of the flow is blocked; that is $\lambda=0.5$ (Blaisdell 1959, Rajaratnam 1964, Basco and Adams 1971, Peterka 1984). It was because of this that $\lambda=0.5$ was employed in all experiments in this study. Analysis of the large dataset obtained in this study demonstrated that at a constant Froude number C_D increased with S and decreased with block width. As the Froude number increased C_D decreased, which is in contrast to the free forced jump case where the effect of the Froude number was found to be negligible (Rajaratnam and Murahari 1971).

Habibzadeh et al. (2011) derived a theoretical equation for predicting C_D which includes all of the parameters that appear in Eq. (3-2), derived using dimensional analysis, except x_b/y_I . This is due to the fact that bed shear was neglected by Habibzadeh et al. (2011); therefore, the location of the blocks within the control volume was not considered. However, C_D in free jumps was found to be a function of the location of the baffle (Rajaratnam and Murahari 1971). The influence of all dimensionless parameters in Eq. (3-2) on C_D , except x_b/y_I , can be studied using the theoretical equation; its effect was studied experimentally by analyzing the data for which x_b/y_I varied from 10 to 40. In Figure 3.4 C_D is plotted versus x_b/y_I for selected Froude numbers of $F_I=6.0$ and 8.2 and a block height of $h_b/y_I=2.0$. It is evident that C_D decreases as the blocks are moved away from the gate or if F_I increases. In addition, at a given F_I , C_D increases with S . In this figure, the data for the free hydraulic jump with a 2D baffle wall are also shown (Rajaratnam and Murahari 1971) and this data is the lower limit for all submerged jump data in the figure.

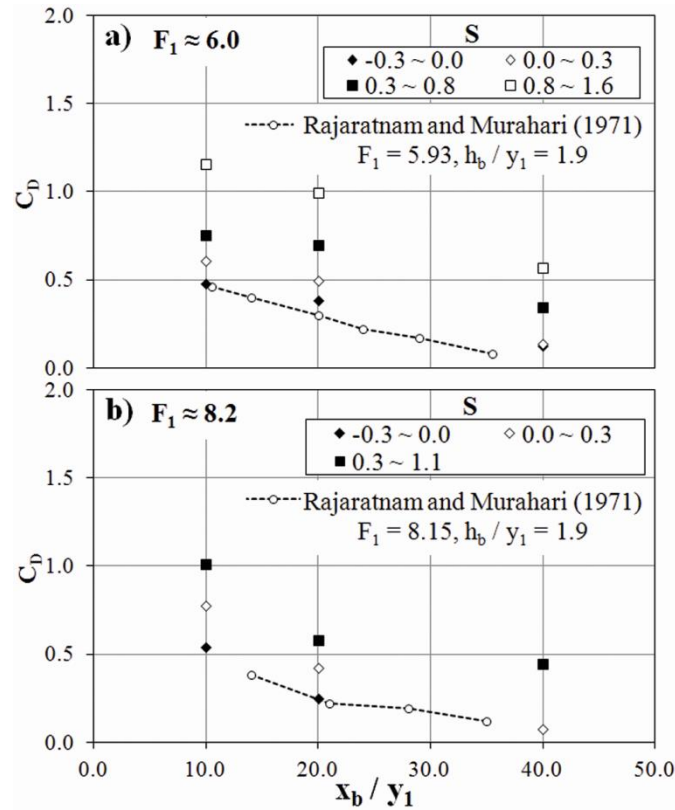


Figure 3.4 The drag coefficient (C_D) versus dimensionless distance (x_b/y_1) for $h_b/y_1=2.0$ and $w_b/y_1=2.36$.

Energy Dissipation

Habibzadeh et al. (2011) defined the energy dissipation efficiency ratio (η) as the ratio of the energy dissipation efficiency in a submerged jump with blocks to that in a free jump without blocks. The energy dissipation efficiency is defined as the ratio of the energy dissipated in the jump (E_L) to the specific energy of the supercritical stream (E_1) (i.e. E_L/E_1). In Figure 3.5 η is plotted versus S for selected block arrangements and F_1 values. A general trend in both Figure 3.5a and b is that as S increases from negative values, η increases reaching a maximum at $S \approx 0.0$, which corresponds to the tailwater depth being equal to the subcritical sequent depth. For $S > 0$, η decreases approximately linearly with S . This is consistent with the observations of Habibzadeh et al. (2011), who found that η first increased with dimensionless tailwater depth reaching a maximum then

gradually decreased. It was found that for each block arrangement, η is larger when the flow is in the DSJ regime compared to the RWJ regime.

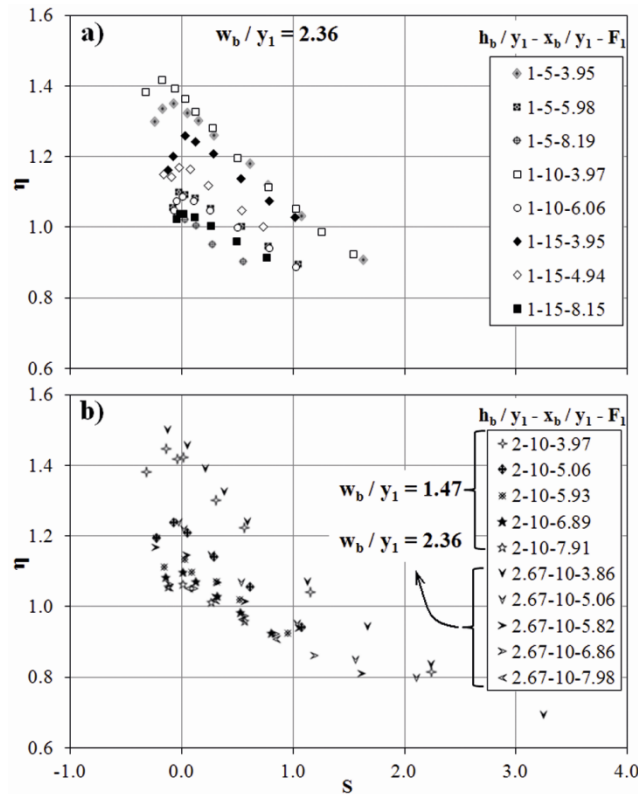


Figure 3.5 The energy dissipation efficiency ratio (η) versus the submergence factor (S) (the three numbers in the legend refer to h_b/y_1 , x_b/y_1 , and F_1 , respectively).

In Figure 3.5a and b the upper part of each data series, which corresponds to smaller values of S and larger values of η , coincides with the DSJ regime and includes the maximum value of η . It was also observed that for each block arrangement, at constant S , η decreases as F_1 increases. It is important to know how η varies with S because the goal is to ensure that the jump provides sufficient energy dissipation over the range of flow rates and tailwater depths expected to occur. The results from this study indicate that greater energy dissipation (i.e. large η values) will occur at lower submergences when the flow is in the DSJ regime.

The block height and width were found to have a negligible effect on the energy dissipation efficiency since the maximum variations in η were found to be approximately 5% for both flow regimes. Basco and Adams (1971) found that, in free jumps with blocks, the effect of increasing block height levels off after a certain height which was attributed to the fact that once the blocks protrude into the roller there is no further increase in the drag force. In the case of submerged jumps, the thickness of the supercritical jet is a function of S as well as Froude number. In the DSJ regime, the blocks primarily act as deflectors of the incoming jet, and therefore, the height of the blocks has a minor effect as long as they are equal to or greater in height than the jet thickness. In the RWJ regime, larger blocks result in a larger separated flow region behind the blocks and this is expected to increase mixing and energy dissipation. However, taller blocks require larger values of S to establish the RWJ regime, which in turn, results in a thicker jet at the location of the blocks. This means that in the RWJ regime, as the block height increases the energy dissipation tends to increase as a result of increasing eddy size but it also tends to decrease because the effectiveness of the blocks decreases as the blocks protrude into the thick incoming jet. These two opposing effects may be the reason that η does not vary at larger values of S .

Adding a second row of blocks increases the energy dissipation efficiency a small amount in free jumps (Peterka 1984). The effect of adding a second row of blocks on energy dissipation was studied and it was observed that this resulted in a statistically insignificant change in the energy dissipation efficiency (i.e. $\leq 4\%$). The main effect of a second row of blocks is to prevent the formation of the RWJ regime which is desirable because the risk of bed scour is higher in this regime.

The experimental data show that the energy dissipation is on average significantly greater in the DSJ regime compared to the RWJ regime and this may be related to differences in the how energy is dissipated in the two flows. Previous studies have shown that the mechanism of energy dissipation in hydraulic jumps

is dominated by the larger scales of the turbulence; e.g. the surface roller (Rouse et al. 1958, and Qingchao and Drewes 1994). The impingement of the deflected jet on the water surface in the DSJ regime produces a large-scale turbulent motion in the form of a surface roller between the gate and the blocks (see Figure 3.2a). This recirculating flow region may contribute to the large energy dissipation that occurs in the DSJ regime. Also, it is known that curvilinear jets entrain more fluid than straight jets which results in more mixing and more dissipation (Rajaratnam 1976). As a result, the deflected jet that curves sharply upwards in the DSJ regime may also contribute to the larger energy dissipation observed in the DSJ regime compared to the RWJ regime.

In free hydraulic jumps, the location of the blocks has an important effect on the performance of the jump. It influences the efficiency as well as the longitudinal profile of the jump (Murahari 1973). In the current study, it was observed that the effect of the block location was different in submerged jumps compared to free jumps. That is, the block location has a significant influence on which flow regime forms but it has only a minor effect on the energy dissipation efficiency. In both DSJ and RWJ regimes, the variations in the energy dissipation efficiency with x_b/y_1 were statistically insignificant (i.e. <5%). However, block location does play an important role in determining the flow regime.

Practical Considerations

In practice, hydraulic jump stilling basins are designed to increase energy dissipation and to confine the jump to the protected bed within the basin. Use of baffle blocks helps in achieving these objectives. If the jump becomes submerged, as is often the case in practice, the performance of the blocks is altered. In previous sections, it was demonstrated that the effectiveness of the blocks, in terms of the energy dissipation decreases as the submergence factor increases. The flow regime that occurs is, in turn, dependent on the block configuration. It was found that the block arrangement (i.e. block height, width and location) has a

negligible effect on the energy dissipation efficiency. The blocks were found to be most effective when the flow is in the DSJ regime and the bed shear stress downstream of the blocks is expected to be smaller in this regime similar to the baffle wall case (Wu and Rajaratnam 1995). As a result, it can be concluded that if a submerged jump is to be used as an energy dissipator, the design should ensure that the flow is in the DSJ regime. The criterion for formation of the DSJ regime was presented in Eq. (3-3) which gives the critical submergence factor (S_1) for this flow regime. An example is used to illustrate the practical implications of these results.

Consider a sluice gate, with an opening of $y_1=10$ cm that is being operated in an irrigation network. The USBR standards specify that a conventional type-III stilling basin (Peterka 1984) downstream of the gate be designed with $h_b=0.2$ m, $w_b=0.16$ m, $x_b=1.0$ m, and $\lambda=0.5$. For a design discharge of 0.77 m³/s, the gate Froude number is 5.16 and the flow depth in the downstream channel is equal to the subcritical sequent depth of the jump, 0.7 m. Eq. (3-3) predicts that $S_1=0.29$, therefore, as long as the tailwater depth is less than 0.88 m, the flow will always be in the DSJ regime and $\eta>1.17$ (see Figure 3.5). Eq. (3-4) predicts that $S_2=0.57$, therefore, for tailwater depths greater than 1.07 m, the flow will always be in the RWJ regime and $\eta<1.02$ (see Figure 3.5). If the tailwater depth increases to 1.2 m, for example, as a result of a backwater curve due to an obstacle or debris in the channel, the flow would be in the RWJ regime and the value of η would be 0.97. In this case the efficiency of the basin would be reduced and the risk of downstream scouring due to the higher bed shear stresses that occur in the RWJ regime would be high. If the block width and spacing are not changed but the height of the blocks was increased to $h_b=0.25$ m and the location to $x_b=1.5$ m, the new values of S_1 and S_2 predicted from Eqs. (3-3) and (3-4) would be 0.86 and 1.18, respectively, which correspond to tailwater depths of 1.26 m and 1.48 m, respectively. Under these conditions, the energy dissipation efficiency ratio

decreases slightly ($\eta > 1.0$ for $S < 0.86$, and $\eta < 0.93$ for $S > 1.18$, see Figure 3.5); but, the flow will remain in the DSJ regime for a wider range of tailwater depths.

Using the modified design (i.e. $h_b = 0.25$ m and $x_b = 1.5$ m), the flow will always be in the DSJ regime if the tailwater depth is less than 1.26 m and it will always be in the RWJ regime for tailwater depths greater than 1.48 m. In between these two depths the DSJ and RWJ regimes will occur if the tailwater depth is increasing or decreasing, respectively. The example demonstrates that minor modifications to the standard USBR design prevent the occurrence of the RWJ regime over a wider range of tailwater depths, under submerged conditions; while providing energy dissipation efficiencies that are comparable to a free jump without blocks.

Conclusions

The performance of baffle blocks in submerged hydraulic jumps was studied for a range of Froude numbers, submergence factors and block arrangements. In all cases, the flow was observed to be in either the Deflected Surface Jet (DSJ) or the Reattaching Wall Jet (RWJ) regime. It was observed that the performance of the blocks was different in these two flow regimes. Empirical equations were derived to estimate S_1 and S_2 the critical values of the submergence factor that predict which flow regime will occur. These empirical equations were found to predict the flow regime accurately 85% of the time. The DSJ regime, which occurred at smaller submergence factors, was found to be the more efficient in terms of energy dissipation than the RWJ regime; since the energy dissipation efficiency decreases as S increases. In both flow regimes, the effect of the height, width, location and number of rows of the blocks on energy dissipation efficiency was found to be insignificant. However, these parameters had a significant influence on the flow regime. When the blocks are further away from the gate; e.g. for $x_b/y_1 = 40.0$, the formation of the RWJ regime was prevented at all F_1 and S values within the studied range. Employing a second row of blocks

Chapter 3: Performance of Baffle Blocks in Submerged Hydraulic Jumps

or narrower blocks also increased the magnitude of the submergence factor required for the formation of the RWJ regime. In practice if a submerged jump with blocks is to be used as an energy dissipator, the designer should ensure that the flow is in the DSJ regime. The block characteristics should be specified so that for the design tailwater depth, the critical submergence factor for the DSJ regime (S_1), from Eq. (3-3), is greater than the design submergence factor.

References

- Basco, D. R., and Adams, J. R. (1971). "Drag forces on baffle blocks in hydraulic jumps." *J. Hyd. Div.*, 97(HY12), 2023-2035.
- Blaisdell, F.W. (1959). "The SAF stilling basin." *USDA Agriculture Handbook No. 156*.
- Chow, V. (1959). *Open-channel hydraulics*. McGraw-Hill, New York.
- Dey, S., and Sarkar, A. (2008). "Characteristics of Turbulent Flow in Submerged Jumps on Rough Beds." *J. Engrg. Mech.*, 134(1), 49-59.
- Gajusingh, S. T., Shaikh, N., and Siddiqui, K. (2010). "Influence of a rectangular baffle on the downstream flow structure." *Exp. Therm. Fluid Sci.*, 34(5), 590-602.
- Govinda Rao, N. S., and Rajaratnam, N. (1963). "The submerged hydraulic jump." *J. Hyd. Div.*, 89(HY1), 139-162.
- Habibzadeh, A., Wu S., Ade F., Rajaratnam, N., and Loewen, M. R. (2011). "An Exploratory Study on Submerged Hydraulic Jumps with Blocks." *ASCE J. Hydr. Engrg.*, 137(6), 706-710.
- Hager, W. H. (1992). *Energy Dissipators and Hydraulic Jump*. Kluwer, London.
- Harleman, D. R. F. (1955). "Effect of baffle piers on stilling basin performance." *J. Boston Soc. of Civil Engrs*, 42(2), 84-99.
- Jamshidnia, H., Takeda, Y., and Firoozabadi, B. (2010). "Effect of a standing baffle on the flow structure in a rectangular open channel." *J. Hydraul. Res.*, 48(3), 400-404.
- Long, D., Steffler, P. M., and Rajaratnam, N. (1990). "LDA study of flow structure in submerged hydraulic jump." *J. Hydraul. Res.*, 28(4), 437-460.

Chapter 3: Performance of Baffle Blocks in Submerged Hydraulic Jumps

MATLAB Statistics Toolbox™ User's Guide 7, (2011), The MathWorks Inc., Natick, MA.

Murahari, V. (1973). "Regimes of forced hydraulic jump." *Water Resources Bulletin*, American Water Resources Association, 9(3), June, 613-617.

Ohtsu, I., Yasuda, Y., and Yamanaka, Y. (1991). "Drag on vertical sill of forced jump." *J. Hydraul. Res.*, 29(1), 29-47.

Onyshko, P.R., Loewen, M.R., and Rajaratnam, N. (2002). "Particle image velocimetry applied to a deflected wall jet." *Proceedings of the ASCE Hydraulic Measurements and Experimental Methods Conference*, July 28-August 1, Estes Park, Colorado, USA.

Peterka, A. J. (1984). "Hydraulic design of stilling basins and energy dissipators." *Engineering Monograph No. 25*, 8th Ed. US Bureau of Reclamation, Denver, USA.

Qingchao, L., Drewes, U. (1994). "Turbulence characteristics in free and forced hydraulic jumps." *J. Hydraul. Res.*, 32(6), 877-898.

Rajaratnam, N. (1976). *Turbulent Jets*, Elsevier Publishing Co., Amsterdam and New York, 304 pages.

Rajaratnam, N. (1967). "Hydraulic Jumps." *Advances in Hydrosience Vol. 4*, Academic Press Inc., 197-280.

Rajaratnam, N. (1964a). "The forced hydraulic jump." *Water Power*, Part I – January, pp. 14-19.

Rajaratnam, N. (1964b). "The forced hydraulic jump." *Water Power*, Part II – February, pp. 61-65.

Rajaratnam, N., and Murahari, V. (1971). "A contribution to forced hydraulic jumps." *J. Hydraul. Res.*, 9(2), 217-240.

Rand, W. (1966). "Flow over a dentated sill in an open channel." *J. Hyd. Div.*, 92(HY5), 135-153.

Rouse, H., Siago, T.T., Nagaratnam, S. (1958). "Turbulence characteristics of the hydraulic jump." *J. Hyd. Div.*, 84(1), pp. 1-30.

Chapter 3: Performance of Baffle Blocks in Submerged Hydraulic Jumps

Thompson, P.L., and Kilgore, R.T. (2006). "Hydraulic Design of Energy Dissipators for Culverts and Channels." Hydraulic Engineering Circular Number 14 (HEC 14), Third Edition, Federal Highway Administration, FHWA-NHI-06-086.

Wu, S., and Rajaratnam, N. (1995). "Effect of Baffles on Submerged Flows." J. Hydr. Engrg., 121(9), 644-652.

Chapter 4: Mean Flow in a Submerged Hydraulic Jump with Baffle Blocks¹

Introduction

Supercritical flow often occurs downstream of hydraulic structures such as spillways and gates. Hydraulic jumps form when sufficient tailwater depth occurs in the downstream channel and the subcritical flow, that is established, can then be safely discharged into the natural channel. A *free hydraulic jump* forms when the tailwater depth is equal to the corresponding sequent depth of the supercritical flow. The sequent depths of free jumps are related by the well-known Belanger momentum equation (Chow 1959). In practice, stilling basins are constructed to confine this hydraulic jump and improve the dissipation of the excessive energy of the incoming supercritical stream. Stilling basins employ baffle blocks and sills to improve the energy dissipation efficiency and reduce the length of the jump (Peterka 1984). Such a jump, forcibly formed within a stilling basin is called a *forced hydraulic jump* (Rajaratnam 1967). For large tailwater depths, the hydraulic jump, and consequently, the stilling basin, is submerged and the resulting submerged flow has characteristics comparable to wall jets but with a recirculating region on top. In such a case a *submerged hydraulic jump* (with or without blocks) is formed (Rajaratnam 1967).

The free hydraulic jump was probably first studied by Leonardo Da Vinci in the sixteenth century (Rouse and Ince 1957) but it was not until 1820 that Giorgio Bidone experimentally studied the bulk properties (sequent depths ratio and length) of hydraulic jumps (Hager 1992). Bakhmeteff and Metzke (1935) were the first to study the global flow features including the dimensionless longitudinal surface profile and jump length, followed by many others (e.g. Rouse 1958, Rajaratnam 1965a). The internal flow properties of free hydraulic jumps,

¹ A version of this chapter has been accepted for publication (reused with permission from ASCE). Habibzadeh, A., Loewen, M.R., and Rajaratnam, N. "Mean Flow in a Submerged Hydraulic Jump with Baffle Blocks." *ASCE Journal of Engineering Mechanics*.

including the velocity distribution, were first studied by Rouse et al. (1958) in a wind tunnel and later by Rajaratnam (1965a) in a water channel. With the development of advanced measuring techniques, acoustic Doppler velocimetry (ADV) and particle image velocimetry (PIV), more detailed studies of the flow structure, including the turbulence characteristics, of free hydraulic jumps were undertaken (Svendsen et al. 2000, Liu et al. 2004, Misra et al. 2008). In a novel study Lin et al. (2012) investigated the turbulent flow field of, not only the water phase but also the bubble phase of a hydraulic jump. The unsteady periodic behavior of free hydraulic jumps has been investigated by Long et al. (1991) and Mossa (1999). Hydraulic jumps with baffles or sills; i.e. forced hydraulic jumps, generate high levels of turbulence and entrain significant volumes of air which make velocity measurements in these flows difficult (Hager 1992). As a result, there are very few velocity measurements reported for forced hydraulic jumps with sills (e.g. Hager and Li 1992) or blocks (e.g. Nettleton and McCorquodale 1989).

The properties of the flow in submerged hydraulic jumps have been studied by numerous researchers (Govinda Rao and Rajaratnam 1963; Rajaratnam 1965b; Rajaratnam and Mura Hari 1982; Long et al. 1990; Ead and Rajaratnam 2002 and 2004; Dey and Sarkar 2006 and 2008; Bhuiyan et al. 2011). Govinda Rao and Rajaratnam (1963) experimentally studied the bulk properties, including energy dissipation, surface profile and length of roller, in a submerged jump. Rajaratnam (1965b) compared the mean flow field of wall jets to submerged jumps. Long et al. (1990) studied the turbulent flow field in a submerged hydraulic jump using laser Doppler anemometry (LDA). Their experiments were conducted over a range of Froude numbers and submergence factors and the longitudinal and vertical variations of mean velocities, turbulent intensities and Reynolds stresses were investigated. Dey and Sarkar (2006 and 2008) studied the effects of bed roughness on the turbulent flow field in a submerged hydraulic jump. The response of the flow, as the bed roughness was varied from smooth to rough, was investigated.

Wu and Rajaratnam (1995a) were the first to study the mean flow in a submerged hydraulic jump forced with a two-dimensional baffle wall. Submerged hydraulic jumps were thought to be less efficient in dissipating energy (Rajaratnam 1967), but in the presence of baffle walls, their performance improved. As the baffle height and tailwater depth were varied they observed two regimes; the deflected surface jet and reattaching wall jet regimes. The decay of the maximum longitudinal velocity was studied for the two flow regimes and the deflected surface jet regime was found to be more efficient in reducing the maximum velocity. As a result, the deflected surface jet regime was recommended as a safe way of dissipating energy using a submerged jump. Their results regarding the mean flow field of the two flow regimes were later confirmed by Onyshko et al. (2002) using PIV measurements. They also measured the turbulence characteristics of the two flow regimes of a submerged jump with a baffle wall. The experimental results of Wu and Rajaratnam (1995a) were later used by Mehdizadeh et al. (2010) for a numerical study of the flow field and the drag on the baffle. A region of high bed shear stress was identified based on a particle trajectory study and bed protection was suggested for this region.

Submerged flow downstream of sluice gates has been studied in detail because of the significant effects of submergence on gate performance. A submerged hydraulic jump downstream of a sluice gate influences the discharge characteristics of the gate and produces a flow that is significantly different from the design flow; since stilling basins are typically designed to create free hydraulic jumps (Habibzadeh et al. 2011a and 2012). An exploratory study of the effects of 3D baffle blocks on submerged hydraulic jumps in stilling basins downstream of a sluice gate was conducted by Habibzadeh et al. (2011b). A theoretical equation for the drag coefficient based on a simplified form of the momentum equation and pressure force balance was derived. An empirical

equation for the back-up depth was presented and the effect of the blocks on energy dissipation was also studied.

Habibzadeh et al. (2012) conducted an extensive series of laboratory experiments investigating the performance of baffle blocks in submerged hydraulic jumps. The structure of the flow was studied and it was found that the flow could be classified into two regimes, the deflected surface jet (DSJ) and reattaching wall jet (RWJ) regimes following Wu and Rajaratnam (1995a). Using dimensional analysis and nonlinear regression methods, empirical equations for the critical values of the submergence factor required for the formation of each flow regime were derived. The flow regime that occurs was found to depend on the Froude number at the gate, the submergence factor and block properties (i.e. height, width and distance from the gate). The transition from one regime to another was sudden and no transition flow was observed. At submergences between the two critical submergence factors, the flow could be in either regime depending on whether the tailwater depth was increasing or decreasing. In this transition region, the flow could be made to switch from one regime to another by a finite disturbance; e.g. if the flow was in the RWJ regime, it would change to the DSJ regime if the flow was deflected upwards manually. That is, no transitional flow was observed, and instead a bi-stable flow region existed between the two critical submergence factors. A similar bi-stable flow region has been previously reported by Mossa (1999) for free hydraulic jumps where quasi-periodic oscillations of the flow caused the jump to switch back and forth from one type to another (e.g. between B and wave-type). Habibzadeh et al. (2012) concluded that the DSJ regime of a submerged jump with blocks was an effective way of dissipating energy that is as efficient as the free hydraulic jump. They recommended that for a given Froude number and submergence factor, the block arrangement should be designed such that the DSJ regime is maintained over the entire range of flow conditions, avoiding the bi-stable and the RWJ regimes.

In this study, the complex 3D mean flow field created by baffle blocks in a submerged hydraulic jump downstream of a sluice gate was investigated. The experiments were designed so that a practical range of Froude numbers and submergence factors were covered for the two flow regimes. Blocks with different heights and widths were mounted on the flume bed at various distances from the gate. For each run, the three-dimensional mean velocities were measured using an ADV. The deflection of the incoming jet by the blocks was studied for both flow regimes and the response of the mean velocity profiles to the presence of the blocks was investigated. The streamwise variation of the maximum longitudinal velocity was studied in detail and the effects of blocks and flow regime were assessed. This was achieved by analyzing the deflection and expansion of the incoming jet as well as decay of the velocity components in the two flow regimes.

Experimental Setup and Procedures

The experiments were conducted in the Hydraulics Laboratory of the Department of Civil and Environmental Engineering at the University of Alberta. A schematic view of the experimental setup including a longitudinal and plan view of the block arrangements is shown in Figure 4.1. Water was pumped by a Fairbanks-Morse KZKV pump from an underground sump into a head tank. The tank was equipped with a sluice gate with a streamlined edge which created a uniform supercritical stream with a depth equal to the gate opening; i.e. $y_f=19.1$ mm.

The discharge was measured with a magnetic flowmeter (Foxboro IMT25) installed in the supply pipe. The supply pipe was equipped with a valve which was used to control the flow rate. Downstream of the gate, there was a horizontal flume with an aluminum bed and glass walls with a width of 0.467 m, height of 0.60 m, and length of 7.5 m. A false bed made of 19.1mm-thick PVC sheet was mounted on the original bed of the flume to facilitate baffle block installation. This false bed extended 1.2 m upstream and 3.5 m downstream of the gate. A

tailgate located at the downstream end of the flume was used to control the tailwater depth. A point gauge with an accuracy of 0.1 mm was used to measure water depths.

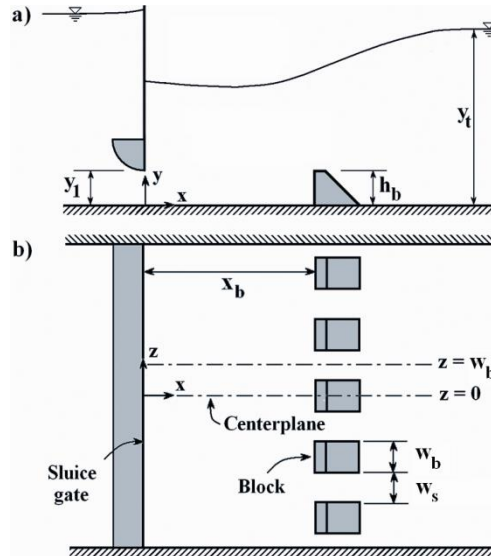


Figure 4.1 Schematic view of the experimental arrangement; a) side view, b) top view.

The baffle blocks were made of PVC using the design guidelines for the standard USBR Basin III (Peterka 1984). Block dimensions including height (h_b) and width (w_b) and block location (x_b) are listed in Table 4-1 for all the experiments. Based on the USBR guidelines, a top crest length of $0.2h_b$ and a downstream slope of 1:1 were used. The shape of the blocks influences their performance and the standard USBR shape is hydraulically efficient. The purpose of the wedged shape of the blocks is only to provide more structural stability and it has no effect on the hydraulic performance (Peterka 1984). Blocks designed following the USBR guidelines act as sharp-edged obstacles and, as a result, separation occurs at the upstream edges. Hence, under these conditions the height and width of the blocks are the only significant factors influencing the length of the standing eddy behind the blocks. In general, as long as the length of the blocks (top length and side lengths) is shorter than the recirculating eddy length, the blocks act as sharp obstacles and they can be considered ‘thin’. That is, the flow separates at the upstream top and side edges of the blocks and is not affected

by their longitudinal dimension due to their relatively short streamwise length. However, if the longitudinal dimension of the blocks is longer than the size of the standing eddy behind them, the separated flow may reattach onto the blocks and significantly change the geometry of the recirculating eddy (Lyn and Rodi 1994). In all cases, the space between the blocks (w_s) was kept equal to the block width; i.e. $w_b=w_s$. The number of blocks depended on their width; e.g. for $w_b=2.8$ cm and 4.5 cm, eight and five blocks were mounted on the bed, respectively.

Table 4-1 The range of the experimental parameters ($y_I=19.1$ mm for all runs).

Run	U_I	F_I	S	h_b	w_b	x_b	Flow Regime	L_e
	(m/s)			(cm)	(cm)	(cm)		(cm)
1	1.49	3.45	0.50	3.8	4.5	19.1	DSJ	
2	1.59	3.67	2.92	3.8	4.5	19.1	RWJ	8.1
3	2.00	4.63	0.25	3.8	4.5	19.1	DSJ	
4	1.98	4.59	0.52	3.8	4.5	19.1	DSJ	
5	1.93	4.46	1.25	3.8	4.5	19.1	DSJ	
6	2.00	4.63	1.73	3.8	4.5	19.1	RWJ	7.2
7	2.00	4.62	1.93	3.8	4.5	19.1	RWJ	8.6
8	2.00	4.62	2.39	3.8	4.5	19.1	RWJ	7.7
9	2.60	6.01	0.51	3.8	4.5	19.1	DSJ	
10	2.64	6.11	1.27	3.8	4.5	19.1	RWJ	7.1
11	2.50	5.79	0.55	3.8	4.5	76.2	RWJ	9.5
12	2.55	5.89	0.58	3.8	4.5	38.1	DSJ	
13	2.55	5.89	1.58	3.8	4.5	38.1	RWJ	8.4
14*	2.59	5.98	0.53	3.8	4.5	19.1	DSJ	
15	2.55	5.90	0.54	5.1	4.5	19.1	DSJ	
16	2.56	5.93	1.04	5.1	4.5	19.1	RWJ	8.6
17	2.48	5.73	0.51	3.8	2.8	19.1	RWJ	5.1
18	2.47	5.71	-0.01	3.8	2.8	19.1	DSJ	
19	2.20	5.10	0.12	1.9	4.5	19.1	DSJ	
20	2.23	5.15	0.70	1.9	4.5	19.1	RWJ	7.2

* Two-row block arrangement, second staggered row of blocks at $x_b=28.6$ cm.

The upstream face of the blocks was located at different distances from the gate ranging from $x_b=19.1$ cm to 76.2 cm, which corresponds to $x_b/y_I=10$ to 40. For the two-row case (Run #14), the first row of blocks was located at $x_b=19.1$ cm

and the second staggered row of blocks was placed at $x_b=28.6$ cm from the gate or 9.5 cm downstream of the first row. The distance between the two rows was set to a value of $2.5h_b$ (Hager 1992, Peterka 1984). A total of 20 experiments were conducted and the range of the experimental parameters is tabulated in Table 4-1. The Froude number at the gate opening defined as $F_1 = U_1/\sqrt{gy_1}$, where U_1 is the velocity at the gate opening, g is acceleration due to gravity, and S the submergence factor defined as $S=(y_t - y_2)/y_2$; where y_t is the tailwater depth and y_2 is the subcritical sequent depth of the corresponding free jump (computed from the Belanger equation, Chow 1959) are also listed in Table 4-1. The Reynolds number at the gate, defined as $R_I=U_1y_1/\nu$, where ν is the kinematic viscosity of water, was larger than 28,000 in all cases.

A Nortek Vectrino acoustic Doppler velocimeter (ADV) was used to measure the three velocity components. This ADV can measure instantaneous velocities at frequencies up to 200 Hz inside a cylindrical sampling volume with a diameter of 6 mm and a height of 2.5 to 15 mm (the height can be adjusted using the software) centered 5 cm below the transmitter. Based on preliminary tests, time series with frequencies over 100 Hz were found to have high noise levels. Hence, all measurements were conducted with a sampling frequency of 100 Hz. The ADV was mounted on a Velmex Bislid (model VXM-2) motorized traverse which was accurate to within $\pm 1.8 \mu\text{m/m}$ (Velmex Inc. 2002). This traverse was connected to a personal computer equipped with MATLAB[®] through the PC serial port. A Cartesian coordinate system with the origin located at the intersection of the bed and the gate centerlines was used (see Figure 4.1).

The ADV measures the Doppler shift between the transmitted and reflected acoustic waves and converts this into velocity. Along with velocity measurements, other parameters are computed by ADV software (Vectrino) including the correlation coefficient (COR) and signal-to-noise-ratio (SNR). The correlation is a data quality parameter and the SNR is a measure of signal strength compared to the background noise (SonTek 1997). For mean velocity

measurements, a minimum of 30% and 5 dB are recommended for COR and SNR, respectively (SonTek 1997). When the ADV is being used in clear water, seeding particles can be used to improve SNR. Such particles act as acoustic wave scattering targets and improve the acoustic reflections from water and increase SNR values. Spherical[®] (Potters Industries LLC, Valley Forge, PA, USA) was used as seeding particle. This seeding material consists of hollow glass spheres with a median diameter of 10 μm and a density of 1100 kg/m^3 . It was observed that without the seeding particles, the SNR values were not satisfactory; i.e. typically less than 10 dB. As a result, approximately 5 kg of Spherical[®] was added to the sump tank which had a volume of 300 m^3 , resulting in a seed concentration of 0.0167 kg/m^3 . Adding seed increased SNR values so that they were always larger than 10 dB.

Time-averaged velocity components were measured in two longitudinal planes; the centerplane ($z=0$) of the flume and the off-centerplane, the plane passing between the blocks at $z=w_b$ (see Figure 4.1). Measurements were gathered at different distances from the gate, starting from a section upstream of the blocks and ending at a section far downstream of the blocks. It was observed that the presence of the PVC sheet reduced the echo effects from the bed to a large extent compared to the original aluminum bed. It is known that the time-averaged quantities are less sensitive to bed echoes compared to turbulence ones (Dombroski and Crimaldi 2007). As a result, measurements of time-averaged velocities could be made as close as 5 mm from the bed. For near bed measurements, a sampling volume height of 2.5 mm was used to decrease the effect of bed proximity (Precht et al. 2006). For points further from the bed; i.e. for $y>2$ cm, the sampling volume height was increased to 7 mm. Measurements were conducted at increments of 2 mm near the bed and the increment was increased moving towards the water surface. The ADV probe was tilted upwards at a 60° angle with the water surface so that measurements near the water surface were possible (i.e. at distances less than 5 cm below the surface).

A sensitivity analysis was conducted to find the appropriate sampling duration. In this sensitivity analysis, 30-minute long time series of instantaneous velocities were gathered at a number of points located at various distances from the gate and heights from the bed. Time-averaged velocities were then computed using different lengths of the 30-minute time series. It was assumed that the 30-minute time-averaged value was free of any sensitivity to the sampling duration. The computed time-averaged velocities computed for shorter durations were compared with the values calculated using the entire 30-minute time series. It was found that the time-averaged velocities computed using time series with a duration of one minute or greater had magnitudes that were within 4% of the values computed using the 30-minute time series. As a result, a sampling duration of one minute was used and each resulting time series was comprised of 6,000 instantaneous velocity samples (i.e. one minute duration sampled at 100 Hz).

At each point, the measured time series was analyzed using a MATLAB[®] code to filter the time series and remove spikes in the data. The filtering procedure started with the removal of any point which had a low COR less than 60% and SNR less than 10 dB (Sadeque et al. 2009). The spikes in the ADV time series were removed using the Phase-Space Thresholding Method (PSTM) developed by Goring and Nikora (2002). The points removed from the time series by the despiking algorithm were not replaced since only time-averaged velocities were being computed.

As will be discussed later, the flow separated at the upstream crest edge of the blocks. This caused rapid changes to the three velocity components to occur in a small region adjacent to the blocks. These high velocity gradients degrade the ADV measurements resulting in low-quality data with low COR and SNR values. This has also been reported by Voulgaris and Trowbridge (1998) and McLelland and Nicholas (2000). As a result, the measurements in these regions (i.e. measurements just above the block crest) were discarded.

The experimental set-up used in this study was identical to the one used by Habibzadeh et al. (2012). They determined that the uncertainty, in terms of the standard deviation of repeated measurements, was ± 0.2 L/s, ± 0.05 cm and ± 0.10 cm for the discharge, tailwater (y_1) and back-up depth (y_3), respectively. The propagated error in the submergence factor (S) was calculated to be ± 0.02 and the uncertainty in the Froude number (F_1) was estimated to be less than 2%. The ADV measurements are accurate within $\pm 0.5\%$ of measured value ± 1 mm/s (Nortek 2004). The random errors in the mean velocity measurements were estimated by comparing mean velocities estimated using 1-minute time series with those computed from the 30-minute time series. This approach is reasonable because the random errors associated with the 30-minute estimates are negligible due to the large sample size (i.e. 180,000). Using this approach the random errors in mean velocity estimates computed from 1-minute time series were found to be less than 4%.

Results and Discussion

The flow pattern observed in the DSJ regime is shown in Figure 4.2 where two-dimensional velocity vectors in the two planes are plotted at each measurement station for Run #4.

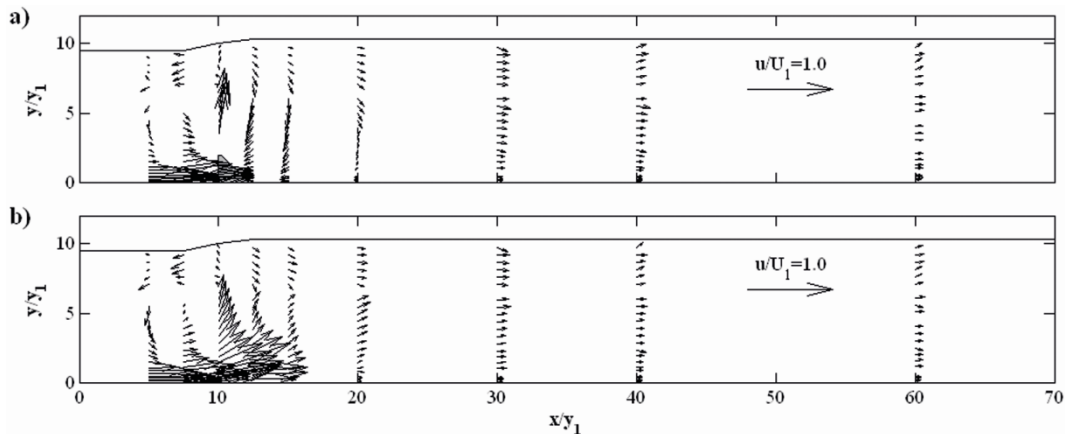


Figure 4.2 Normalized velocity vector plot for the DSJ regime (Run #4); a) centerplane, and b) off-centerplane (blocks are located at $x=19.1$ cm or $x/y_1=10$).

Upstream of the blocks in both planes, the velocity vectors are similar to a wall jet near the bed with a backward flow region near the water surface due to the finite tailwater depth. In the centerplane, the supercritical jet is deflected upwards towards the water surface at the block crest which results in a nearly vertical jet, with a deflection angle of approximately 85° , forming a submerged fountain (Baines et al. 1990). This deflected jet impinges on the water surface and then plunges back down towards the bed. This phenomenon results in the formation of two recirculating regions; i.e. a small recirculating region near the water surface between the gate and the blocks, and a backward flow region near the bed downstream of the blocks. These observations confirm the results obtained by Habibzadeh et al. (2012) on the main characteristics of the flow field in this flow regime. This flow behavior is similar to the one observed in the B-jump of a sill-controlled forced jump as reported by Hager and Li (1992). They observed that, in the B-jump, the main stream is first deflected towards the water surface and then plunges back into the downstream flow. However, the deflection angles observed in this study are much steeper, almost twice as large compared to theirs. In the off-centerplane, the supercritical jet continues to grow similar to a wall jet but with a faster rate of expansion; i.e. with larger vertical velocities. The deflection angle of the jet was approximately 12° at the blocks in the off-centerplane. A faster rate of expansion has also been reported in the case of a submerged hydraulic jump on a rough bed by Dey and Sarkar (2006 and 2008). They observed that when the bed changes from smooth to rough, the rate of velocity decay and expansion of the jet both increase. The phenomenon observed in the off-centerplane of the current experiments has a similar trend; but with larger rates of velocity decay and jet expansion compared to submerged jumps on smooth beds (Long et al. 1990) and rough beds (Dey and Sarkar 2006 and 2008). Note that low amplitude water surface fluctuations were observed at small submergences in the DSJ regime and it was assumed that these fluctuations or waves had a negligible effect on the mean flow.

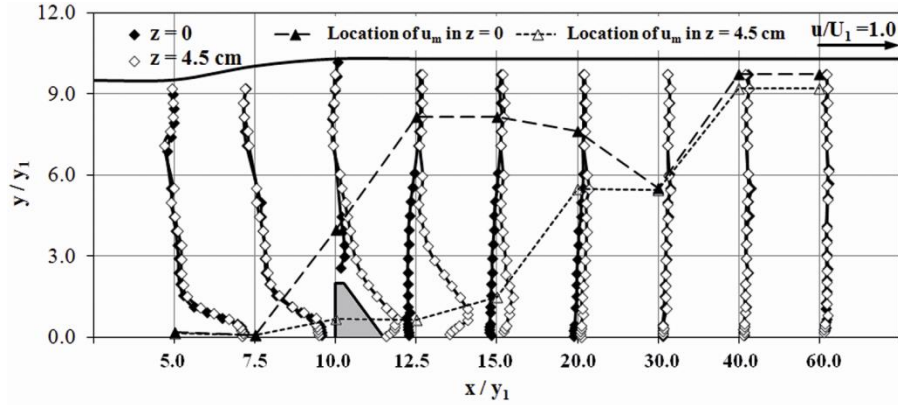


Figure 4.3 Normalized longitudinal velocity profiles for the DSJ regime (Run #4).

Longitudinal (streamwise) velocity profiles for Run #4 are shown in Figure 4.3. This figure shows the velocity distributions for the DSJ regime at nine stations in the centerplane at $z=0$ and the off-centerplane at $z=4.5$ cm. The velocity profiles upstream of the blocks are similar to those in wall jets, while the velocity distribution downstream of the blocks is greatly influenced by them. The velocity profiles upstream of the blocks have insignificant transverse variations; i.e. the profiles in the two planes collapse on each other at each station. The vertical location of the maximum longitudinal velocity, u_m , for the two planes is also shown in this figure. The location of u_m can be considered as an approximate representation of the jet deflection. It can be observed in this figure that the location of u_m rapidly approaches the water surface immediately downstream of the blocks in the centerplane. In the off-centerplane, however, the location of u_m gradually moves away from the bed, until at $x/y_1 \approx 30.0$, the location of u_m in the two planes occurs at an almost identical height.

It can be observed in Figure 4.3 that the velocity profiles at $x/y_1 \geq 10$ are altered by the blocks and that there are significant lateral (cross-stream) variations immediately downstream of the blocks. In the region $x/y_1 = 10$ to 20, the velocity profiles in the centerplane are significantly different from the profiles in the off-centerplane. The velocity profiles in the off-centerplane have a shape similar to a submerged wall jet up to $x/y_1 = 15$; but the maximum velocity rapidly decays and

the profile becomes more uniform for $x/y_I \geq 20$. The rapid decay of the maximum longitudinal velocity in the off-centerplane immediately downstream of the blocks is similar to that observed in submerged hydraulic jumps when the bed roughness increases (Dey and Sarkar 2008). However, the velocities in the centerplane show a different pattern. Above the block crest, at $x/y_I=10$, the longitudinal velocities are small due to the vertical deflection of the jet which produces large vertical velocities. Downstream of the blocks up to $x/y_I=20$, the velocities below a certain depth are negative (e.g. for $y/y_I < 7$ at $x/y_I=12.5$); for $x/y_I > 20$ the forward velocities are recovered. This corresponds to the backward flow in the recirculating region downstream of the block observed in the DSJ regime (Habibzadeh et al. 2012).

Vertical velocity component profiles in the two planes are plotted in Figure 4.4 for the DSJ regime. Complex 3D flow structures have been observed in the flow around 3D obstacles (Sadeque et al. 2008, Martinuzzi and Tropea 1993). These 3D vertical structures result in different 3D velocity patterns around the blocks.

It was observed that, in the centerplane upstream of the blocks, the vertical velocities were negligible near the bed and small vertical velocities develop near the water surface. This is due to the recirculating region near the gate which can be seen in Figure 4.2a. Upstream of the blocks at $x/y_I=5$, negative (downward) vertical velocities with approximate magnitudes of $-0.1 U_I$ are observed in both planes as a result of this recirculating flow region. Large positive (upwards) velocities ($v/U_I > 0.5$) occur at the block crest ($x_b/y_I=10$) and large negative (downward) velocities occur just downstream of the blocks, e.g. at $x/y_I=12.5$ and 15, negative vertical velocities with magnitudes of approximately $-0.2U_I$ are observed at mid-depth of flow between $y/y_I \approx 4$ and 8 (see Figure 4.4a). At all other points, the vertical velocity component is less than $0.1 U_I$.

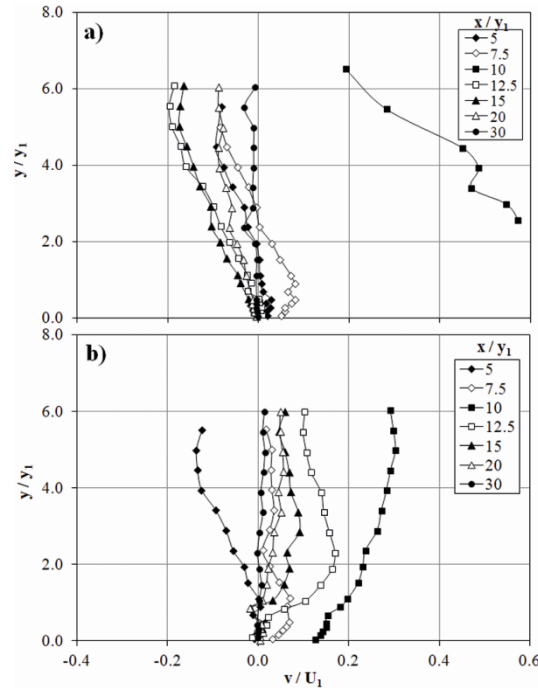


Figure 4.4 Normalized vertical velocity profiles for the DSJ regime (Run #4); a) centerplane, and b) off-centerplane.

The vertical velocity profiles in the off-centerplane are shown in Figure 4.4b. The flow upstream of the blocks has a similar pattern to the centerplane. Above the blocks and just downstream, i.e. for $x/y_1 \geq 10$, positive (upward) vertical velocities develop and their magnitude decreases with distance; e.g. maximum velocities are $v/U_1 \approx 0.3$ and 0.05 at $x/y_1 = 10$ and 20 , respectively. The extent and magnitude of the negative vertical velocities decrease at stations further downstream. The flow in the off-centerplane has negligible vertical velocities ($v/U_1 < 0.05$) further downstream; i.e. $x/y_1 \geq 30$. It can be observed in Figure 4.4 that there are negative vertical velocities in the centerplane for $x/y_1 = 12.5$ to 30 ; while, positive vertical velocities are observed in the off-centerplane for $x/y_1 = 10$ to 30 . That is, the whole flow field downstream of the blocks in the DSJ regime is greatly influenced by the blocks, resulting in large differences in the vertical velocities in the two measurement planes and large shear surfaces between the two planes.

Plots of the two-dimensional velocity vectors at each station are shown in Figure 4.5 for the two measurement planes for the RWJ flow regime for Run #6. In the centerplane, the jet is deflected upwards by the blocks at an angle of approximately 50° and large vertical velocity components are observed (see $x/y_1=10$ in Figure 4.5a). This flow pattern is similar to the C-jump of a sill-controlled free jump (Hager and Li 1992). As discussed by Hager and Li (1992), this type of flow regime is less efficient at dissipating energy and there is potential for scouring at the reattachment point.

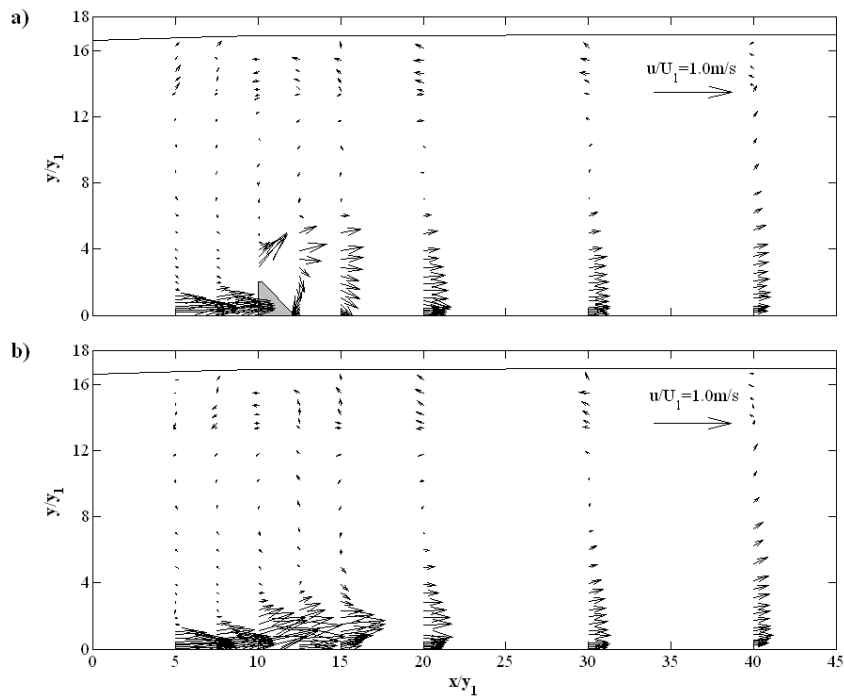


Figure 4.5 Normalized velocity vector plot for the RWJ regime (Run #6); a) centerplane, and b) off-centerplane (blocks are located at $x=19.1$ cm or $x/y_1=10$).

The flow in the off-centerplane is deflected upwards at approximately 12° at the blocks. There is a large recirculating flow region near the water surface, evident in both planes, which extends to approximately $x/y_1 \approx 50$ (found by injecting dye on the water surface). This is due to the finite tailwater depth which requires a recirculating flow to replenish the fluid that is entrained into the flow at the upstream stations. The similarities between the two planes in regions away

from the blocks demonstrates that for the deep flow in the RWJ regime, the effect of the blocks is limited to a small region just downstream of them; i.e. for $x/y_1=10$ to 15 and $y/y_1 \leq 5$. The overall flow pattern in the off-centerplane is comparable to that of a submerged jump on a rough bed (Dey and Sarkar 2008). The jet expansion rate is larger than a wall jet (Rajaratnam 1976), a submerged jump on a smooth bed (Long et al. 1990) and a submerged jump on a rough bed (Dey and Sarkar 2008); but smaller than in the DSJ regime.

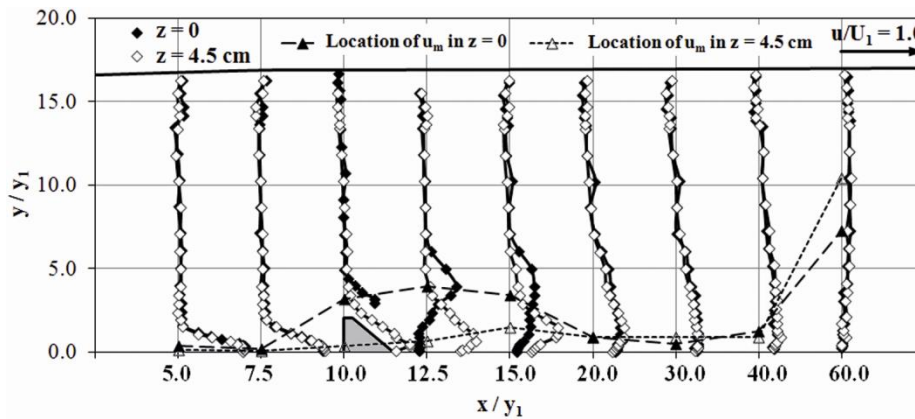


Figure 4.6 Normalized longitudinal velocity profiles for the RWJ regime (Run #6).

Variation of the longitudinal velocity profiles and the vertical location of u_m at each station are shown in Figure 4.6 for Run #6 in the RWJ regime. In the centerplane, the supercritical jet is deflected by the blocks but it reattaches to the bed at a short distance downstream. It is well known that the static pressure behind bluff bodies decreases due to boundary layer separation (Castro and Robins 1977). At the station just downstream of the blocks at $x/y_1=12.5$, the deflected jet curves downwards due to the low pressure inside the eddy behind the blocks producing the downward velocity components. Further downstream, the jet in the centerplane reattaches to the bed at $x/y_1 \approx 13.8$ and grows as a reattached wall jet downstream of this point. The location of the reattachment was defined as the station at which the longitudinal velocity changes its direction or $u_{bed}=0$. Hence, for each run, the two stations where the longitudinal velocity near the bed changed from negative (backward) to positive (forward) were identified and then

linear interpolation was used to estimate the location where $u_{bed}=0$. A standing eddy of length L_e exists in the region between the blocks and the reattachment point.

At the stations just downstream of the blocks; i.e. $x/y_I=12.5$ and 15 in Figure 4.6, the velocity profiles at each station show large variations in the magnitude of the longitudinal velocity; e.g. at $x/y_I=12.5$, u/U_I varies from -0.07 to 0.59. Further downstream starting at $x/y_I \geq 20$, the diffusion of the jet, due to both lateral and vertical expansion, causes these three-dimensional features to decay and, after jet reattachment in the centerplane, the flow has a pattern similar to a two-dimensional reattached wall jet (Rajaratnam and Subramanya 1968). The recirculating flow region upstream of the blocks was found to be similar in the two planes and, as a result, the two velocity profiles in each plane upstream of the blocks are identical and appear similar to a wall jet (see sections at $x/y_I=5$ and 7.5 in Figure 4.6).

The profiles at the block crest and just downstream of it show great variations in the velocity distribution between the two planes. The velocity profile in the off-centerplane at $x/y_I=12.5$ in Figure 4.6 is similar to a wall jet with a recirculating flow region near the water surface. The centerplane profile has a backward flow region near the bed, a detached jet and a backward flow region near the water surface. The negative velocities near the bed correspond to the small standing eddy behind the block which exists in the RWJ regime (Habibzadeh et al. 2012). The backward flow region near the water surface is caused by the finite tailwater depth.

Vertical velocity components for the RWJ regime are shown in Figure 4.7. It can be observed that the flow in regions close to the blocks is significantly affected by their presence. In the centerplane, large upward vertical velocities up to $v/U_I \approx 0.4$ are observed for $y/y_I < 4$ at $x/y_I=10$ (see Figure 4.7a). It is seen that there is an upward flow at $x/y_I=10$ at the crests of the blocks followed by downward flow just behind the blocks at $x/y_I=12.5$ and 15 with negative vertical

velocities of $-0.25 U_1$ and $-0.15 U_1$, respectively, for $y/y_1 < 4$. This feature of the flow is an indication of the separation that occurs at the block crest edge and formation of the standing eddy behind the block. The maximum vertical velocity in the off-centerplane occurred at $y/y_1 \approx 1$ and $x/y_1 = 10$ and had a magnitude of $v/U_1 \approx 0.2$ (see Figure 4.7b). It is interesting to note that for $y/y_1 < 4$ just downstream of the blocks at $x/y_1 = 12.5$ and 15 , the vertical velocity component switches from negative in the centerplane to positive in the off-centerplane; e.g. at $x/y_1 = 12.5$ for $y/y_1 \approx 2$, $v/U_1 \approx -0.25$ in the centerplane and $v/U_1 \approx 0.1$ in the off-centerplane. These large lateral variations in the vertical velocity indicate that a shear layer exists in this region.

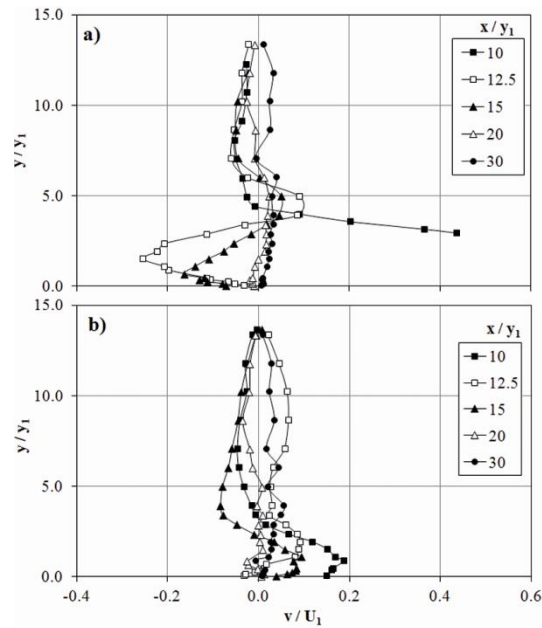


Figure 4.7 Normalized vertical velocity profiles for the RWJ regime (Run #6); a) centerplane, and b) off-centerplane.

For both flow regimes, the lateral velocity component was insignificant throughout the entire flow except near the bed at the station just downstream of the blocks; i.e. at $x/y_1 = 12.5$ for $y/y_1 < 4$ ($y/h_b < 2$). The lateral velocity component in the centerplane of both flow regimes has a magnitude of less than $0.1U_1$ at all points. In the off-centerplane of both flow regimes, however, the lateral velocity component has a magnitude of approximately $0.2U_1$ at $x/y_1 = 12.5$ for $y/y_1 < 4$

($y/h_b < 2$) and, at all other points, it does not exceed $0.1U_1$. That is, the lateral velocity component is least affected by the blocks and the flow field could be assumed to be two-dimensional away from the blocks. However, in both flow regimes, the lateral variations in the flow field disappeared completely at approximately $x/y_1=30$.

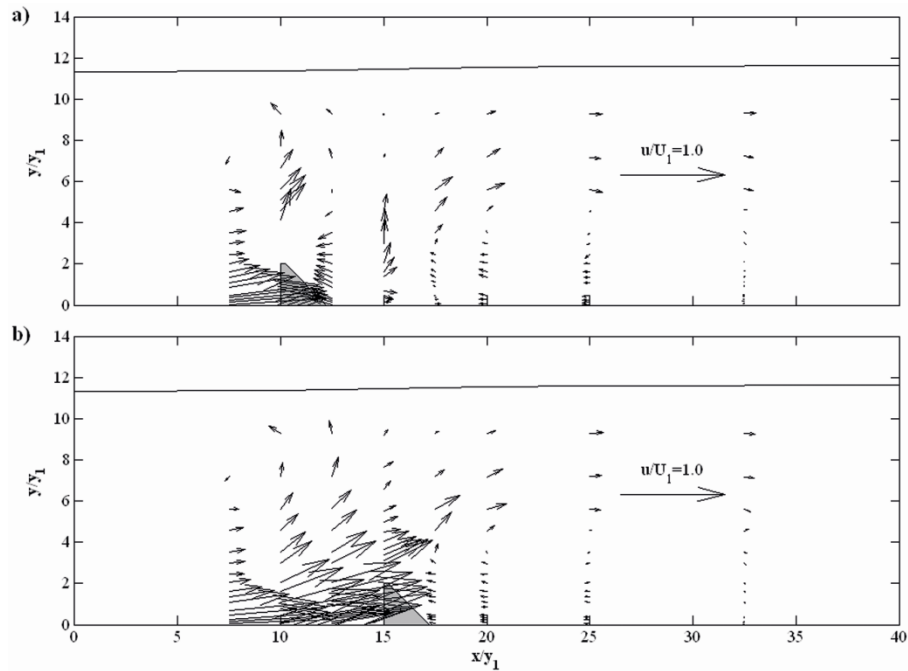


Figure 4.8 Normalized velocity vector plot for the two-row block arrangement (Run #14); a) centerplane, and b) off-centerplane (first row of blocks is located at $x=19.1$ cm or $x/y_1=10$ and the second row at $x=28.6$ cm or $x/y_1=15$).

The 2D velocity vector field for Run #14 of the experiments which had a two-row block arrangement is shown in Figure 4.8 for the two planes. In the centerplane, the flow is deflected by the first row of the blocks with a maximum deflection angle of approximately 50° , which is smaller than the one-row case. At $x/y_1=15$, the flow in the off-centerplane is deflected upwards by the second row of the blocks at an approximate angle of 25° ; while the centerplane flow at this station is almost vertical although there are no blocks at this station of the centerplane to deflect the flow (see Figure 4.8a and b). It is seen in Figure 4.8 that

the flow downstream of the second row of blocks; i.e. $x/y_1 \geq 17.5$, is similar in the two planes with a large recirculating region near the bed and a surface jet on top.

The longitudinal velocity profiles for Run #14 are plotted in Figure 4.9. The location of the maximum velocity u_m , which illustrates the jet deflection, is also shown in this figure. In the region between the two rows (i.e. for $x/y_1 \approx 10$ to 15) the largest variations in velocities are observed between the two planes. For instance, at $x/y_1 = 12.5$, backward velocities are observed over the entire depth in the centerplane with a minimum velocity of $u/U_1 \approx -0.2$ while in the off-centerplane the velocities are positive for $y/y_1 < 8$ with a maximum velocity of $u/U_1 \approx 0.96$. The flow in the centerplane consists of a reverse flow near the bed which extends up to a height of $5y_1$ while the flow in the off-centerplane is similar to a submerged wall jet.

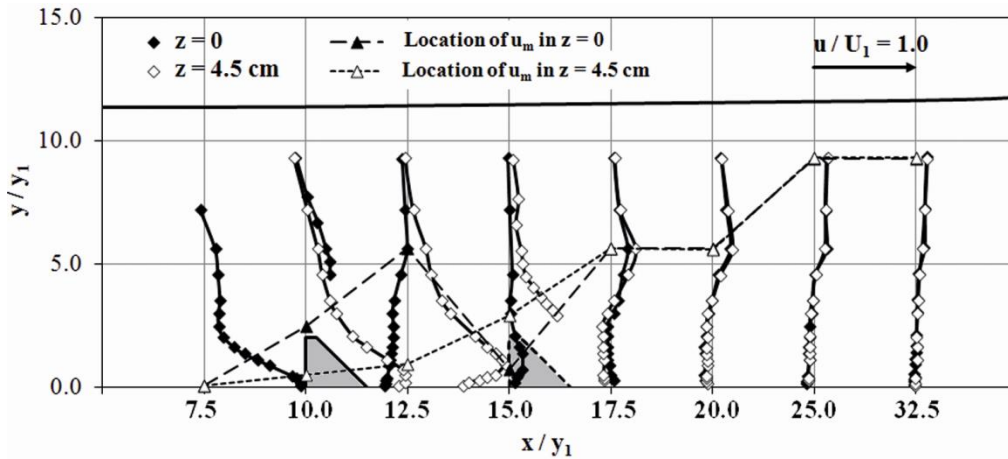


Figure 4.9 Normalized longitudinal velocity profiles for the two-row block arrangement (Run #14).

After reaching the second row of blocks, the flow in the off-centerplane is deflected upwards. The curves for the location of u_m in Figure 4.9 show that the centerplane flow is deflected by the first row and then it drops back down close to the bed and is then deflected up again by the second row. While in the off-centerplane the flow is deflected slightly by the first row and then continues upwards and is deflected further upwards by the second row and the two curves

join at $x/y_I=17.5$. At the first row of blocks in the centerplane some of the flow in the jet is deflected upwards by the blocks and some of it flows around the sides of the block and joins the flow in the off-centerplane (see Figure 4.8b). At $x/y_I=12.5$ and 15.0 the differences in the velocity between the two planes is particularly large (Figure 4.8b) indicating that a very strong shear layer exists in this region. The energetic mixing and rapid momentum transfer that occurs in this region produces velocity profiles in the two planes that are virtually identical at $x/y_I \geq 20$.

The two-row block arrangement has been found to prevent the formation of the RWJ flow regime which is considered a beneficial feature of this arrangement (Habibzadeh et al. 2012). In Figure 4.9, the flow in the centerplane is seen to be deflected by the first row of blocks while the flow in the off-centerplane is not significantly affected by the first row of blocks but is deflected by the second row. This behavior is due to the fact that the second row of blocks is staggered.

Downstream of the blocks at $x/y_I \geq 20$, there are no significant variations between the velocity profiles. A short distance downstream of the second row of blocks; i.e. at $x/y_I=20$, the velocity profiles consist of a weak backward flow near the bed, extending up to $3y_I (=1.5h_b)$ above the blocks, and above this, there is a deflected surface jet. Further downstream, the backward flow near the bed diminishes and the velocity profiles start to develop a more uniform shape (see $x/y_I=32.5$ in Figure 4.9).

It is well-known that the longitudinal velocity profiles in wall jets and submerged jumps are self-similar; that is, velocity profiles at different stations have a similar distribution if the maximum velocity and the jet half-width are used as scaling parameters for velocity and height, respectively (Rajaratnam 1976, Wu and Rajaratnam 1995b). The jet half-width b is defined as the height y at which $u=1/2u_m$ and the velocity gradient is negative (i.e. $\partial u/\partial y < 0$).

The dimensionless longitudinal velocity profiles upstream of the blocks are plotted in Figure 4.10 for the current study, also plotted are the equations for a wall jet and free jump. These velocity profiles are similar in shape to the non-dimensional velocity distribution of a wall jet near the bed; i.e. they are self-similar, which is in agreement with previous studies on hydraulic jumps (e.g. Lin et al. 2012, Dey and Sarkar 2006, Long et al. 1990, Rajaratnam 1965a). It is well-established in the literature that a boundary layer does exist between the location of the maximum velocity and the bed; that is, the velocity goes to zero at the bed due to the no-slip boundary condition (e.g. Rajaratnam 1965, Long et al. 1990, Dey and Sarkar 2006, Lin et al. 2012). However, no measurements could be made in the boundary layer because the ADV's measuring volume is too large. The velocity distributions deviated from the wall jet curve for $y/b \geq 1.8$. This is because the conventional scales used in wall jets; i.e. the maximum velocity and half width, are not the suitable scales in the surface roller region (Rajaratnam 1965b).

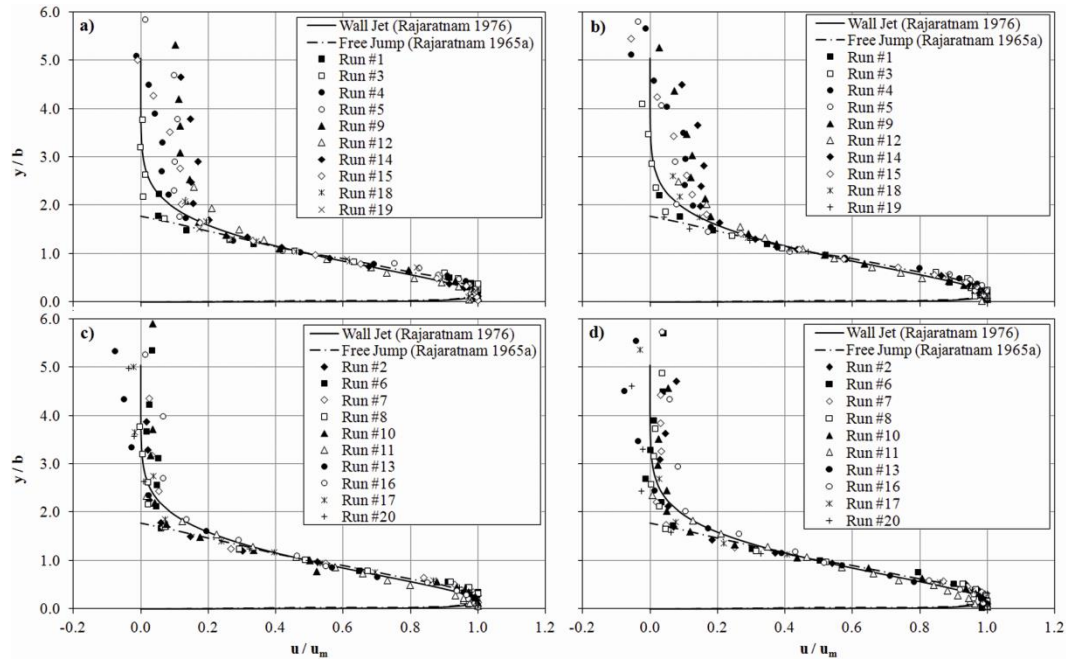


Figure 4.10 Normalized longitudinal velocity profiles upstream of the blocks ($x/y_1 < 10$) for the DSJ (a and b) and RWJ (c and d) regimes in the centerplane (a and c) and off-centerplane (b and d).

It was observed that, downstream of the blocks; e.g. for $x/y_I \geq 10$, the velocities did not follow the wall jet curve due to the effect of the blocks on the flow. This effect is related to the decay of the flow momentum and the start of the process of transition to an open channel flow (i.e. gravity driven flow). Wu and Rajaratnam (1996) found that the transition from a hydraulic jump to a fully developed open channel flow requires a length equal to 10 times the tailwater depth. This length was later confirmed by the turbulence measurements of Zobeyer et al. (2010). It should be noted that the furthest downstream station located at $x/y_I = 60$ is less than 10 tailwater depths downstream. This length was not enough for the flow to fully transition to gravity driven flow; however, the presence of the blocks increases the decay rate of the momentum of the incoming jet and results in velocity profiles which are more uniform compared to submerged jumps without blocks. However, the full transition to an open channel flow requires a longer distance than was studied in the current research.

In the RWJ regime, a small region of recirculating flow is formed behind each block as a result of separation and reattachment of the incoming jet (Habibzadeh et al. 2012). The length of this standing eddy (L_e), as discussed earlier, was defined to be equal to the distance between the upstream face of the blocks and the reattachment point. This length (L_e) is tabulated in Table 4-1 for the RWJ runs. In general, the length of the recirculating region has been found to be shorter for 3D objects compared to 2D ones (Lacey and Rennie 2012, Sadeque et al. 2009, Hussein and Martinuzzi 1996). This is because the lateral extent of the object controls the horseshoe vortices which are swept downstream of the object and outline the recirculating region (Martinuzzi and Tropea 1993). As a result the size of the recirculating region is largely influenced by the cross-stream dimension of the object. This was confirmed in this study because the smallest eddy length of $L_e = 5.1$ cm, occurred for Run #17 where the block width was smallest.

The dimensionless maximum longitudinal velocity (u_m/U_1) is plotted as a function of the dimensional longitudinal distance (x/y_1) in Figure 4.11 for the DSJ regime and in Figure 4.12 for the RWJ regime. The curves representing the wall jet and free hydraulic jump case are also plotted in these figures. In Figure 4.11a, it is seen that the maximum velocity in the centerplane rapidly decreases at the blocks. Just downstream of the blocks, at $x/y_1=12.5$, the maximum velocities are negligible compared to the wall jet or free jump cases; i.e. $u_m/U_1 \approx 0.1$ compared to 0.95 and 0.8 for the wall jet and free jump, respectively. In Figure 4.11b, the maximum velocity in the off-centerplane persists for a longer distance but at $x/y_1 \approx 20$, the maximum velocities are also much smaller than the wall jet and free jump velocities. Further downstream, a constant ratio of $u_m/U_1 \approx 0.1$ is reached in both planes.

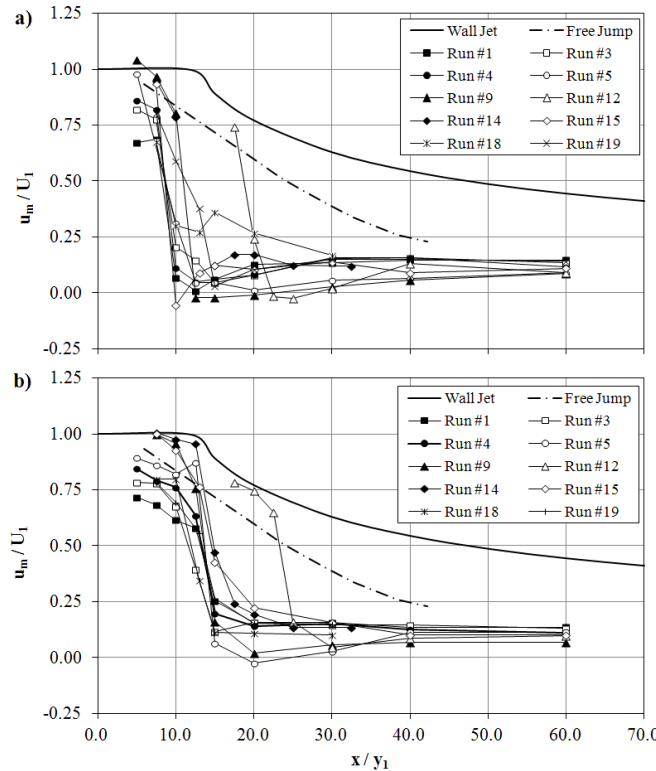


Figure 4.11 The maximum normalized longitudinal velocity versus the normalized longitudinal distance for the DSJ regime; a) centerplane, and b) off-centerplane (wall jet curve from Rajaratnam 1976 and free jump curve from Rajaratnam 1965a).

A similar trend was observed in a radial forced free hydraulic jump by Nettleton and McCorquodale (1989). They observed that the maximum longitudinal velocity in a radial jump rapidly decreases at the blocks and reaches an approximately constant magnitude further downstream. This means that in the DSJ flow regime of a submerged hydraulic jump the maximum longitudinal velocity is reduced by the baffle blocks similar to forced jumps.

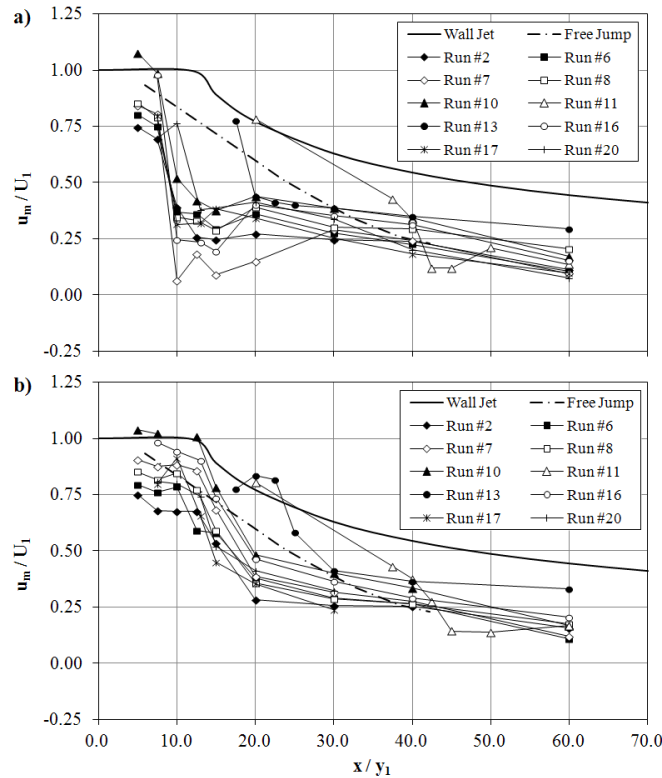


Figure 4.12 The maximum normalized longitudinal velocity versus the normalized longitudinal distance for the RWJ regime; a) centerplane, and b) off-centerplane (wall jet curve from Rajaratnam 1976 and free jump curve from Rajaratnam 1965a).

In Figure 4.12 it is observed that the centerplane velocities in the RWJ regime have a similar pattern to the DSJ regime but with slightly larger velocities; e.g. at $x/y_1=20$, average $u_m/U_1 \approx 0.1$ and 0.35 in Figure 4.11a and Figure 4.12a, respectively. The velocities in the off-centerplane are significantly larger and persist for a longer distance downstream of the blocks compared to the DSJ regime. In general, the maximum velocities in the off-centerplane are slightly

smaller than the free jump case but follow a similar pattern. Further downstream, i.e. at $x/y_1 \approx 60$, the maximum velocity in both planes approaches $u_m/U_1 \approx 0.2$. For a given Froude number, the maximum velocity is larger in the RWJ regime than the DSJ regime. This illustrates the advantage of the DSJ regime over the RWJ regime in terms of reducing the maximum velocities particularly near the bed. This is clear evidence that the DSJ regime is preferable to the RWJ regime when considering the design of stilling basins containing submerged hydraulic jumps (Habibzadeh et al. 2012).

A condensed version of the data from Figure 4.11 and Figure 4.12 for the runs with $x_b/y_1=10$ is shown in Figure 4.13. In this figure, each curve represents the average of the data from runs with $x_b/y_1=10$. The error bars in this figure represent the standard error of the mean associated with each point. The maximum standard error associated with the average curves was 12.1%. It can be observed in Figure 4.13 that u_m sharply decreases at the blocks. Just downstream of the blocks at $x/y_1 \approx 15$, u_m/U_1 in the centerplane and off-centerplane of the DSJ regime drops to approximately 0.05 and 0.4, respectively. At $x/y_1 \approx 15$, u_m/U_1 in the centerplane and off-centerplane of the RWJ regime decreases to 0.3 and 0.7, respectively. It is clear in this figure that u_m/U_1 decreases much faster in the x-direction in the DSJ regime compared to the RWJ regime. It is also seen that the reduction of u_m/U_1 occurs further downstream in the off-centerplane compared to the centerplane. But, the difference between the two planes diminishes at $x/y_1 \approx 20$ in both regimes. It can be observed in Figure 4.13 that the average DSJ curves fall below the average RWJ curves downstream of the blocks which demonstrates that the velocities are always smaller in the DSJ regime. One interesting feature observed in Figure 4.13 is that, in both flow regimes, the off-centerplane curve is shifted to the right. That is, the reduction of u_m in the off-centerplane flow is delayed, for a length of approximately 5 times x/y_1 , compared to the centerplane flow. This shift is caused by the eddy that occurs behind the blocks and, it also highlights the highly three-dimensional flow in that region.

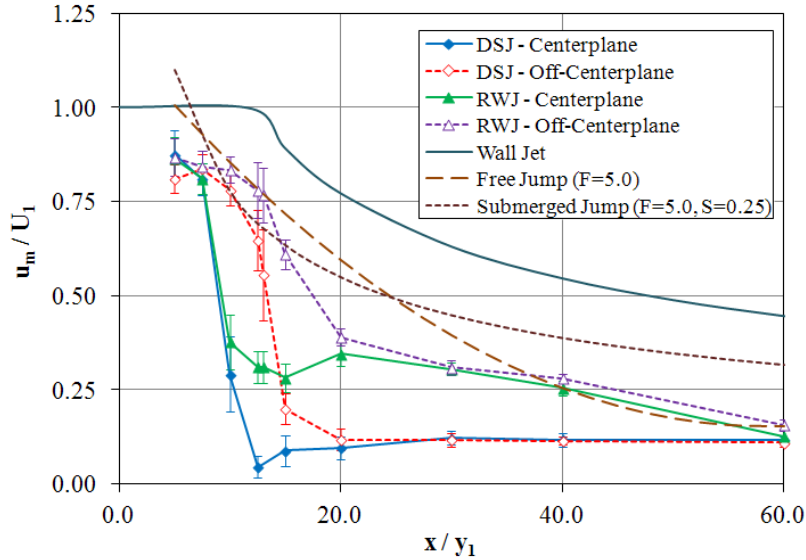


Figure 4.13 Average curves of the maximum normalized longitudinal velocity versus the normalized longitudinal distance for runs with $x_b/y_1=10$ (wall jet curve from Rajaratnam 1976; free and submerged jump curves from Wu and Rajaratnam 1995).

Long et al. (1990) introduced a longitudinal length scale (λ) for submerged jumps without blocks. The scale λ was defined as the distance x from the efflux at which $u_m=1/2U_1$ and an empirical equation was presented for λ/y_1 as a function of F_1 and S . They showed that, using λ , major flow characteristics could be grouped together. In the current study, the maximum longitudinal velocity is sharply reduced at the blocks in the centerplane for both flow regimes. That is, u_m in the centerplane decreased to approximately $0.5 U_1$ just upstream of the blocks; e.g. $\lambda/y_1 \approx 8.0$ for runs with $x_b/y_1=10$ (see Figure 4.13). However, the decay of u_m in the off-centerplane is delayed in both flow regimes and for the DSJ and RWJ regimes, respectively; $\lambda/y_1 \approx 12.5$ and 17.5 (see Figure 4.13). In submerged hydraulic jumps with blocks, the decay of the maximum longitudinal velocity is significantly enhanced by the blocks; this results in a shorter characteristic length scale λ . The reduction of u_m with distance is mainly influenced by the blocks and, as a result, λ is dependent on only the block location x_b rather than F_1 or S .

The jet half-width b was used to study the jet growth rate in the off-centerplane. The average dimensionless jet half-width b/y_1 for all runs with

$x_b/y_I=10$ at each station in the off-centerplane is plotted in Figure 4.14a for both flow regimes. The curve for the DSJ regime was cut off at $x/y_I \approx 20$ because, the jet half-width definition is not valid for $x/y_I > 20$. Also, no curves are presented for the centerplane because of the same reason. This is because of the fact that, as discussed earlier, the centerplane flow in both flow regimes is significantly influenced by the blocks and the velocity profiles rapidly deviate from the jet-shaped velocity profiles. In the DSJ flow regime, the off-centerplane flow also follows a similar trend for $x/y_I > 20$. The use of the jet half-width is only logical when the observed velocity profiles are jet-like in shape and therefore, the use of this parameter for the centerplane flow of the two flow regimes and also the off-centerplane flow of the DSJ flow regime for $x/y_I > 20$ is not justified. It has been observed that the incoming jet grows faster in the free and submerged jumps compared to the wall jet (Rajaratnam 1967). That is, the growth rate of the jet is inversely related to the submergence factor (Rajaratnam 1965b). It can be seen in Figure 4.14a that in the DSJ regime all the data downstream of the blocks (i.e. $x/y_I \geq 10$) are above the wall jet case. As the flow approaches the blocks (i.e. going from $x/y_I=7.5$ to $x/y_I=10$) the jet half-width increases at a rate of 0.381 in the off-centerplane which is 5.8 times larger than the growth rate of a wall jet or submerged jumps.

For the RWJ cases, it was also evident that the blocks increase the half-width of the jet to a large extent. In the region from $x/y_I=7.5$ to $x/y_I=10$, the jet half-width increases at a rate of 0.278 in the off-centerplane which is 4.3 times larger than the growth rate of a wall jet or submerged jumps. This, in turn, results in the maximum velocity occurring at a higher location from the bed and, thus, this effect is beneficial in terms of protecting the bed against shear stress.

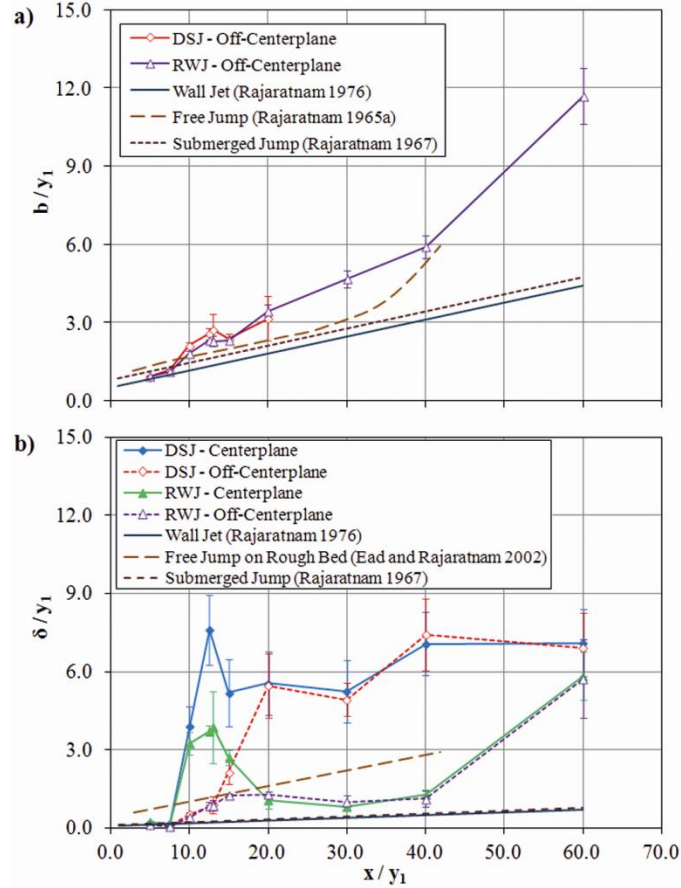


Figure 4.14 Average curves showing the variation of the a) normalized jet half-width and b) normalized location of u_m versus the normalized longitudinal distance for runs with $x_b/y_1=10$.

The location δ of maximum longitudinal velocity, defined as the height y at which $u=u_m$ at each station was also calculated and the average δ/y_1 for all runs with $x_b/y_1=10$ was computed. The resulting average curves are shown in Figure 4.14b. It is seen in Figure 4.14b that δ/y_1 for the RWJ regime is always smaller than that of the DSJ regime in the same planes. The δ/y_1 curve for the off-centerplane of the RWJ regime falls between the free and submerged jump curves but the centerplane curve, rapidly increases to $\delta/y_1 \approx 4$ at $x/y_1 \approx 12.5$ and then decreases and joins the off-centerplane curve for $x/y_1 > 20$. In the DSJ regime, δ/y_1 in the centerplane sharply increases to approximately 8 at $x/y_1 \approx 10$ and, similar to the RWJ regime joins with the off-centerplane curve at $x/y_1 \geq 20$. The DSJ curves level off for $x/y_1 \geq 40$, indicating that the maximum velocity occurs near the water

surface (see Figure 4.3) and the flow is recovering to an open channel flow. In Figure 4.14b it is evident that for the RWJ regime δ/y_1 is still increasing for $x/y_1 \geq 40$ showing that the location of the maximum velocity is still approaching the water surface (see Figure 4.6) and that it takes longer for the transition to an open channel flow to occur. It can be observed in Figure 4.14b that δ/y_1 for the DSJ regime is larger than that of the RWJ regime; e.g. at $x/y_1 \approx 20$, δ/y_1 is approximately 5.5 and 1.0 for the DSJ and RWJ flow regimes, respectively.

Summary and Conclusion

The mean flow fields for the DSJ and RWJ flow regimes in a submerged hydraulic jump with baffle blocks were studied in detail experimentally. Vector plots of the flow field, for the two flow regimes; i.e. the deflected surface jet (DSJ) and reattaching wall jet (RWJ) flow regimes, confirm the general flow patterns and significant flow features deduced by Habibzadeh et al. (2012) using only flow visualization methods. It was found that, in the centerplane, the deflection of the incoming supercritical stream at the blocks occurs at a sharper angle in the DSJ flow regime compared to the RWJ regime. In the DSJ flow regime, the deflection of the jet in the centerplane approaches 85° ; while the deflection angle in the RWJ flow regime, with the same Froude number, did not exceed 50° . The deflection angle of the flow in the off-centerplane at the same station was approximately 12° in both flow regimes. The difference between the deflection angles of the flow in the centerplane and the off-centerplane results in a large shear interface between the two planes. The maximum longitudinal velocity in the centerplane in both flow regimes is rapidly reduced at the blocks. In the DSJ regime, it takes a distance of about five block heights for the maximum velocity to drop by approximately 80%. This reduction of the maximum velocity is gradual in the RWJ regime; e.g. at $x/y_1 = 20$ the dimensionless maximum velocity u_m/U_1 in the DSJ regime is approximately 30% less than that in the RWJ regime. It was observed that the reduction of u_m in the off-centerplane flow in both flow regimes follows a similar pattern to the centerplane but the reduction is

delayed; i.e. the reduction of u_m in the off-centerplane is both shifted and at a slower rate compared to the centerplane. However, further downstream for $x/y_l \geq 20$, the reduction of u_m in both shows has a similar pattern. The width of the submerged jet was studied in terms of the jet half-width and it was observed that, in both flow regimes, the jet width is comparable to that of the wall jet upstream of the blocks. At the blocks, however, the width in the off-center plane increases sharply and reaches magnitudes which are larger than those in the corresponding free hydraulic jumps. In the centerplane of both flow regimes the flow is deflected upwards by the blocks and does not behave like a wall jet. The blocks cause the jet-like flow in the off-centerplane to expand 5.8 and 4.3 times faster than a wall jet or submerged jump, in the DSJ and RWJ flow regimes, respectively.

In summary, this experimental study of submerged hydraulic jumps with baffle blocks showed that the flow in the DSJ regime is more effective in reducing the longitudinal component of the velocity than the RWJ regime. This DSJ flow regime was also found to have a shorter streamwise length; i.e. a shorter recirculating region. This supports the conclusion that a submerged hydraulic jump with baffle blocks is an efficient method of dissipating the excess kinetic energy of the incoming supercritical jet as long as the DSJ flow regime is maintained. Hydraulic jump stilling basins can operate effectively under submerged conditions, if they are designed such that the DSJ regime occurs over the entire range of tailwater depths that are likely to occur.

References

Baines, W. D., Turner, J. S., and Campbell, I. H., (1990). "Turbulent fountains in an open chamber." *J. Fluid Mech.*, Vol. 212, pp. 557-592.

Bakhmeteff, B. A., and Metzke, A. E. (1935). "The hydraulic jump in terms of dynamic similarity." *Transactions of the ASCE*, 101, pp. 630-680.

Chapter 4: Mean Flow in a Submerged Hydraulic Jump with Baffle Blocks

Bhuiyan, F., Habibzadeh, A., Rajaratnam, N., and Zhu, D. Z., (2011). "Reattached Turbulent Submerged Offset Jets on Rough Beds with Shallow Tailwater." *ASCE J. Hydr. Engrg.*, 137(12), 1636-1648.

Castro, I. P., and Robins, A. G. (1977). "The flow around a surface-mounted cube in uniform and turbulent streams." *J. Fluid Mech.*, Vol. 79, Part 2, pp. 307-335.

Chow, V. (1959). *Open-channel hydraulics*. McGraw-Hill, New York.

Dey, S., and Sarkar, A. (2008). "Characteristics of Turbulent Flow in Submerged Jumps on Rough Beds." *ASCE J. Engrg. Mech.*, 134(1), 49-59.

Dombroski D. E. and Crimaldi, J. P. (2007). "The accuracy of acoustic Doppler velocimetry measurements in turbulent boundary layer flows over a smooth bed." *Limnol. Oceanogr. Methods* 5, pp. 23–33.

Ead, S. A., and Rajaratnam, N. (2004). "Plane turbulent wall jets on rough boundaries with limited tailwater." *ASCE Journal of Engineering Mechanics*, 130(10), pp. 1245-1250.

Ead, S. A., and Rajaratnam, N. (2002). "Plane turbulent wall jets in shallow tailwater." *ASCE Journal of Engineering Mechanics*, 128(2), pp. 143-155.

Goring, D. G., and Nikora, V. I. (2002). "Despiking Acoustic Doppler Velocimeter Data." *ASCE Journal of Hydraulic Engineering*, 128(1), pp. 117-126.

Govinda Rao, N. S., and Rajaratnam, N. (1963). "The submerged hydraulic jump." *J. Hyd. Div.*, 89(HY1), 139-162.

Habibzadeh, A., Loewen, M. R., and Rajaratnam, N. (2012). "Performance of Baffle Blocks in Submerged Hydraulic Jumps." *ASCE J. Hydr. Engrg.*, 138(10), 902-908.

Habibzadeh, A., Vatankhah, A. R., and Rajaratnam, N. (2011a). "Role of Energy Loss on Discharge Characteristics of Sluice Gates." *ASCE J. Hydr. Engrg.*, 137(9), 1079-1084.

Habibzadeh, A., Wu S., Ade F., Rajaratnam, N., and Loewen, M. R. (2011b). "An Exploratory Study on Submerged Hydraulic Jumps with Blocks." *ASCE J. Hydr. Engrg.*, 137(6), 706-710.

Chapter 4: Mean Flow in a Submerged Hydraulic Jump with Baffle Blocks

Hager, W. H. (1992). *Energy Dissipators and Hydraulic Jump*. Kluwer, London.

Hager, W. H., and Li, D. (1992). "Sill-controlled energy dissipator." *J. Hydraul. Res.*, 30(2), 165-181.

Hussein, H. J., and Martinuzzi, R. J. (1996). "Energy balance for turbulent flow around a surface mounted cube placed in a channel." *AIP Physics of Fluids*, 8(3), 764-780.

Lacey, R. W. J., and Rennie, C. D. (2012). "Laboratory investigation of turbulent flow structure around a bed-mounted cube at multiple flow stages." *ASCE Journal of Hydraulic Engineering*, 138(1), 71-84.

Lin, C., Hsieh, S. C., Lin, I. J., Chang, K. A., and Raikar, R. V. (2012). "Flow property and self-similarity in steady hydraulic jumps." *Exp. Fluids*, 53, pp. 1591-1616.

Liu, M., Zhu, D. Z., and Rajaratnam, N. (2004). "Turbulence structure of hydraulic jumps of low Froude numbers." *ASCE Journal of Hydraulic Engineering*, 130(6), 511-520.

Long, D., Rajaratnam, N., and Steffler, P. M. (1991). "Structure of flow in hydraulic jumps." *IAHR Journal of Hydraulic Research*, 29(2), pp. 207-218.

Long, D., Steffler, P. M., and Rajaratnam, N. (1990). "LDA study of flow structure in submerged hydraulic jump." *J. Hydraul. Res.*, 28(4), 437-460.

Martinuzzi, R., and Tropea, C. (1993). "The flow around surface-mounted, prismatic obstacles placed in a fully developed channel flow." *ASME Journal of Fluids Engineering*, 115(1), 85-92.

McLelland, S. J. and Nicholas, A. P. (2000). "A new method for evaluating errors in high-frequency ADV measurements." *Hydrol. Process.* 14(2), pp. 351-366.

Mehdizadeh, A., Firoozabadi, B., and Sherif, S. A. (2010). "Particle Trajectory Study in Submerged Flows With Baffles Using v2-f and k- ϵ Turbulence Models." *J.Fluids Eng.*, 132(5), 051105.

Chapter 4: Mean Flow in a Submerged Hydraulic Jump with Baffle Blocks

Misra, S. K., Kirby, J. T., Brocchini, M., Veron, F., Thomas, M., and Kambhamettu, C. (2008). "The mean and turbulent flow structure of a weak hydraulic jump." *Physics of Fluids*, 20(3), 035106.

Mossa, M. (1999). "On the oscillating characteristics of hydraulic jumps." *IAHR Journal of Hydraulic Research*, 37(4), pp. 541-558.

Nettleton, P. C., and McCorquodale, J. A. (1989). "Radial flow stilling basins with baffle blocks." *Canadian Journal of Civil Engineering*, 16(4), 489-497.

Nortek, (2004). *Vectrino Velocimeter User Guide*.

Onyshko, P.R., Loewen, M.R., and Rajaratnam, N. (2002). "Particle image velocimetry applied to a deflected wall jet." *Proceedings of the ASCE Hydraulic Measurements and Experimental Methods Conference*, July 28-August 1, Estes Park, Colorado, USA.

Peterka, A. J. (1984). "Hydraulic design of stilling basins and energy dissipators." *Engineering Monograph No. 25*, 8th Ed. US Bureau of Reclamation, Denver, USA.

Precht E., Janssen, F., and Huettel, M. (2006). "Near-bottom performance of the Acoustic Doppler Velocimeter (ADV) – a comparative study." *Aquatic Ecology* 40, pp. 481–492.

Rajaratnam, N. (1976). *Turbulent Jets*, Elsevier Publishing Co., Amsterdam and New York, 304 pages.

Rajaratnam, N. (1967). "Hydraulic Jumps." *Advances in Hydrosience Vol. 4*, Academic Press Inc., 197-280.

Rajaratnam, N. (1965a). "The hydraulic jump as a wall jet." *J. Hyd. Div.*, 91(HY5), 107-132.

Rajaratnam, N. (1965b). "Submerged hydraulic jump." *J. Hyd. Div.*, 91(HY4), 71-96.

Rajaratnam, N., and Mura Hari, V. (1982). "Plane turbulent wall jets with finite submergence." *Water Power and Dam Construction*, 34, 43-8.

Chapter 4: Mean Flow in a Submerged Hydraulic Jump with Baffle Blocks

- Rajaratnam, N., and Subramanya, K. (1968). "Plane turbulent reattached wall jets." *J. Hyd. Div.*, 94(HY1), 95-112.
- Rouse, H., and Ince, S. (1957). *History of Hydraulics*. Iowa Institute of Hydraulic Research, University of Iowa, Iowa City, IA.
- Rouse, H., Siago, T.T., Nagaratnam, S. (1958). "Turbulence characteristics of the hydraulic jump." *J. Hyd. Div.*, 84(1), pp. 1-30.
- Sadeque, M. F., Rajaratnam, N., and Loewen, M. R. (2009). "Shallow turbulent wakes behind bed-mounted cylinders in open channels." *IAHR Journal of Hydraulic Research*, 47(6), 727-743.
- Sadeque, M. F., Rajaratnam, N., and Loewen, M. R. (2008). "Flow around Cylinders in Open Channels." *ASCE Journal of Engineering Mechanics*, 134(1), pp. 60-71.
- SonTek Technical Notes, (1997). "Pulse Coherent Doppler Processing and the ADV Correlation Coefficient." 6837 Nancy Ridge Drive, Suite A, San Diego, CA 92121. 5 pp.
- Svendsen, IB A., Veeramony, J., Bakunin, J., and Kirby, J. T. (2000). "The flow in weak turbulent hydraulic jumps." *J. Fluid Mech.*, Vol. 418, pp. 25-57.
- Velmex Inc. (2002). *VXM Stepping Motor Controller User's Manual*, Bloomfield, NY, USA.
- Voulgaris, G. and Trowbridge, J. H. (1998). "Evaluation of the Acoustic Doppler Velocimeter (ADV) for Turbulence Measurements." *J. Atmos. Ocean. Technol.*, Vol. 15(1), pp. 272-289.
- Wu, S., and Rajaratnam, N. (1996). "Transition from hydraulic jump to open channel flow." *J. Hydr. Engrg.*, 122(9), 526-528.
- Wu, S., and Rajaratnam, N. (1995a). "Effect of Baffles on Submerged Flows." *J. Hydr. Engrg.*, 121(9), 644-652.
- Wu, S., and Rajaratnam, N. (1995b). "Free jumps, submerged jumps and wall jets." *J. Hydraul. Res.*, 33(2), 197-212.

Chapter 4: Mean Flow in a Submerged Hydraulic Jump with Baffle Blocks

Zobeyer, A.T.M.H., Jahan, N., Islam, Z., Singh, G., and Rajaratnam, N. (2010).
“Turbulence characteristics of the transition region from hydraulic jump to open
channel flow.” *J. Hydraul. Res.*, 48(3), 395-399.

Chapter 5: Turbulence Characteristics of Submerged Hydraulic Jumps with Baffle Blocks

Introduction

Hydraulic jumps are often used to dissipate energy downstream of hydraulic structures such as spillways, sluice gates and drops. The structures are typically designed to operate with a free jump but when tailwater depths increase the jump becomes submerged. In the past submerged hydraulic jumps were generally believed to be less efficient in dissipating energy and thus less effective at reducing the downstream velocity compared to free jumps (Rajaratnam 1967). Recent studies have shown that the use of baffle walls (Wu and Rajaratnam 1995) or baffle blocks (Habibzadeh et al. 2012 and 2013) significantly increases the amount of energy dissipated in a submerged jump. However, these studies only included observations of mean flow properties and time-averaged velocities and as a result the role baffle walls or blocks play in the generation and subsequent dissipation of turbulent kinetic energy is poorly understood.

The turbulent flow field in free hydraulic jumps has been studied by numerous researchers. Rouse et al. (1958) were the first to conduct detailed measurements of turbulence in a hydraulic jump. Their experiments were carried out in an air duct having a profile similar to that of a hydraulic jump. The structure of the turbulence in free hydraulic jumps was studied more recently using Particle Image Velocimetry (PIV) (Lin et al. 2012, Misra et al. 2008, Lennon and Hill 2006), Laser Doppler Anemometer (LDA) (Svendsen et al. 2000) and Acoustic Doppler Velocimeter (ADV) (Mignot and Cienfuegos 2010 and 2011, Liu et al. 2004). The turbulent flow field in free hydraulic jumps with low Froude numbers (2.0, 2.5, and 3.2) was studied by Liu et al. (2004). They observed that the maximum turbulence intensities and Reynolds stress rapidly decreased in the streamwise direction. The energy dissipation rate was found to be larger in the surface roller compared to the flow beneath the surface roller and it

gradually decayed with distance downstream. The flow downstream of a hydraulic jump has also been studied experimentally to identify the required length for the transition to open channel flow (Zobeyer et al. 2010, Wu and Rajaratnam 1996). It was found by Wu and Rajaratnam (1996) that a length equal to 10 times the subcritical sequent depth was required for the momentum dominated flow in the jump to make the transition to a fully turbulent boundary layer or open channel flow. Zobeyer et al. (2010) showed that this same distance was required for the turbulence characteristics to attain magnitudes comparable to those typically observed in open channel flows.

Long et al. (1990) were the first to study the turbulence properties in submerged hydraulic jumps using an LDA. They found that the profile of the longitudinal velocity was similar to that of a wall jet and that the turbulence intensities and Reynolds stress were self-similar. The decay of the turbulence intensities and Reynolds stress in the streamwise direction were found to be faster than a wall jet. Dey and Sarkar (2006 and 2008) studied the effect of bed roughness on the turbulence properties in a submerged jump. They observed that a rough bed causes the turbulence intensities and Reynolds stress to decay more rapidly, but preserves the self-similarity. Dey et al. (2011) studied the near-wake flow region behind a submerged sphere placed on a rough bed. They found that, within the near-wake, the vorticity effects dominate, while further downstream, the mixing effects created by the shear layers are predominant. The presence of an obstacle was observed to create a shear layer along which the turbulence production attains a maximum.

The mean flow in a submerged jump with a baffle wall was studied by Wu and Rajaratnam (1995). They found that, depending on the flow properties and the baffle wall height and location, that the flow could either be deflected towards the water surface or reattach to the bed just downstream of the baffle. These two flow patterns were called the deflected surface jet (DSJ) and the reattaching wall jet (RWJ) flow regimes, respectively. The time-averaged flow characteristics were

studied and it was observed that in the DSJ flow regime, the maximum longitudinal velocity component decayed more rapidly. As a result, they concluded that the DSJ flow regime could potentially be used as an energy dissipator downstream of submerged outlets.

A study of the submerged hydraulic jump with 3D baffle blocks downstream of a sluice gate was conducted by Habibzadeh et al. (2012). The flow patterns were studied and they found that the flow classification proposed by Wu and Rajaratnam (1995) was also valid for submerged jumps with baffle blocks. Therefore, following Wu and Rajaratnam (1995), they classified the flow into two regimes, the deflected surface jet (DSJ) and reattaching wall jet (RWJ) regimes. Habibzadeh et al. (2012) concluded, that the DSJ regime is safer and more efficient than the RWJ regime and that a submerged jump with blocks operating in the DSJ regime dissipates energy as efficiently as the corresponding free jump. A detailed study of the two flow regimes in submerged hydraulic jumps with blocks was carried out by Habibzadeh et al. (2013). The mean flow field, decay of the maximum longitudinal velocity and energy dissipation were compared and the DSJ regime was found to be more effective than the RWJ regime in reducing the longitudinal component of the velocity and dissipating the excess energy of the incoming flow.

In this study, the complex 3D turbulent flow field created in a submerged hydraulic jump with baffle blocks is investigated experimentally. The experiments were designed to cover practical ranges of the Froude number and submergence factor and to encompass both flow regimes. The turbulence properties of the flow field and the effects of the blocks on turbulence intensity, Reynolds stress, kinetic energy, and energy dissipation rate were investigated in detail. The longitudinal variations of the maximum turbulence intensities, turbulence kinetic energy and Reynolds stresses along the jump were also studied. The effect of the blocks on the dissipation of turbulent kinetic energy was of particular interest because the

primary purpose of a submerged hydraulic jump with baffle blocks is to dissipate energy.

Experimental Setup and Procedures

The experiments were conducted in the Hydraulics Laboratory of the Department of Civil and Environmental Engineering at the University of Alberta. A schematic view of the experimental setup including a longitudinal and plan view of the block arrangements is shown in Figure 5.1. Water was pumped by a Fairbanks-Morse KZKV pump from an underground sump into a head tank. The tank was equipped with a sluice gate with a streamlined edge which created a uniform supercritical stream with a depth equal to the gate opening; i.e. $y_1=19.1$ mm. The discharge was measured with a magnetic flowmeter (Foxboro IMT25) installed in the supply pipe. The supply pipe was equipped with a valve which was used to control the flow rate. Downstream of the gate, there was a horizontal flume with an aluminum bed and glass walls and a width of 0.467 m, height of 0.60 m, and length of 7.5 m. A false bed made of 19.1 mm-thick PVC sheet was mounted on the original bed of the flume to facilitate baffle block installation. This false bed extended 1.2 m upstream and 3.5 m downstream of the gate. A tailgate located at the downstream end of the flume was used to control the tailwater depth. A point gauge with an accuracy of 0.1 mm was used to measure water depths.

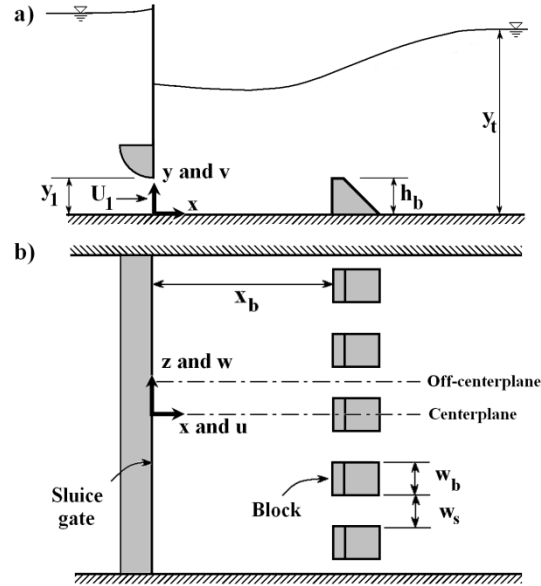


Figure 5.1 Schematic view of the experimental arrangement; a) side view, b) top view.

Two different experimental series were conducted; i.e. submerged jumps with baffle blocks (BB series), and submerged jumps without any baffles (NB series). The experimental parameters for all runs are tabulated in Table 5-1. In this table, U_1 and F_1 refer to the velocity and Froude number at the gate opening, respectively, and S refers to the submergence factor. Here, the Froude number at the gate opening is defined as $F_1 = U_1 / \sqrt{gy_1}$, where g is acceleration due to gravity, and S the submergence factor is defined as $S = (y_t - y_2) / y_2$; where y_t is the tailwater depth and y_2 is the subcritical sequent depth of the corresponding free jump (computed from the Belanger equation, Chow 1959). The flow regime for each run is also listed in the table; i.e. DSJ and RWJ flow regimes for the BB series; and submerged jump (SJ) for the NB series.

The experimental set-up used in this study was identical to the one used by Habibzadeh et al. (2012). In that study the uncertainty, in terms of the standard deviation of repeated measurements was estimated to be, ± 0.2 L/s, ± 0.05 cm and ± 0.10 cm for the discharge, tailwater (y_t) and back-up depth (y_3), respectively. The propagated error in the submergence factor (S) was calculated to be ± 0.02 and the uncertainty in the Froude number (F_1) was estimated to be less than 2%.

Table 5-1 Range of the experimental parameters ($y_1=19.1$ mm for all runs).

Run	U_1 m/s	F_1	S	Flow Regime	ε_{ave} m^2/s^3
BB1	1.44	3.34	0.87	DSJ	0.43
BB2	1.47	3.41	2.61	RWJ	0.45
BB3	2.30	5.32	0.54	DSJ	1.04
BB4	2.27	5.25	1.55	RWJ	1.02
BB5	3.01	6.97	0.20	DSJ	1.59
BB6	3.00	6.94	0.79	RWJ	1.58
NB1	1.51	3.48	0.76	SJ	0.47
NB2	1.48	3.43	2.67	SJ	0.45
NB3	2.30	5.33	0.49	SJ	1.04
NB4	2.28	5.28	1.53	SJ	1.03
NB5	3.00	6.94	0.20	SJ	1.58
NB6	2.99	6.92	0.82	SJ	1.57

For the BB series, the baffle blocks were made of PVC using the design guidelines for the standard USBR Basin III (Peterka 1984). The blocks had a height of $h_b=3.8$ cm ($h_b/y_1=2.0$) and a width of $w_b=4.5$ cm. Based on the USBR guidelines, a top crest length of $0.2h_b$ and a downstream slope of 1:1 were used. In all cases, the space between the blocks (w_s) was kept equal to the block width; i.e. $w_b=w_s=4.5$ cm. There were five blocks mounted on the bed with their upstream face located at $x_b=19.1$ cm from the gate, which corresponds to $x_b/y_1=10$. The Reynolds number at the gate, defined as $R_1=U_1y_1/\nu$, where ν is the kinematic viscosity of water, was larger than 27,000 in all cases.

A Nortek Vectrino acoustic Doppler velocimeter (ADV) was used to measure the three velocity components. This ADV can measure instantaneous velocities at frequencies up to 200 Hz inside a sampling volume, centered 5 cm below the transmitter, and cylindrical in shape with a diameter of 6 mm and a user adjustable height of 2.5 to 15 mm. Based on preliminary tests, time series sampled at frequencies over 100 Hz were found to have high noise levels. Hence, all measurements were conducted using a sampling frequency of 100 Hz. The ADV was mounted on a Velmex Bslide (model VXM-2) motorized traverse which was

accurate to within $\pm 1.8 \mu\text{m/m}$ (Velmex Inc. 2002). This traverse was connected to a personal computer equipped with Matlab[®] through the PC serial port. A Cartesian coordinate system with the origin located at the intersection of the bed and the gate centerlines was used (see Figure 5.1).

The ADV measures the Doppler shift between the transmitted and reflected acoustic waves and converts this into velocity. Along with velocity measurements, other parameters are computed by ADV software (Vectrino) including the correlation coefficient (COR) and signal-to-noise-ratio (SNR). The correlation is a data quality parameter and the SNR is a measure of signal strength compared to the background noise (SonTek 1997). It has been shown that in turbulent flows, low correlation is not necessarily an indication of bad data; i.e. good data can be present even when correlations are low (Cea et al. 2007; Wahl 2000). If the ADV is being used in clear water, seeding particles can be used to increase the SNR. The particles act as acoustic wave scattering targets increasing the acoustic reflections and hence the SNR. Spherical[®] (Potters Industries LLC, Valley Forge, PA, USA) particles which are hollow glass spheres with a median diameter of $10 \mu\text{m}$ and a density of 1100 kg/m^3 were used as seed particles. It was observed that without the seeding particles, the SNR values were not satisfactory; i.e. typically less than 10 dB. Adding approximately 5 kg of Spherical[®] to the sump tank which had a volume of 300 m^3 , resulted in SNR that were always larger than 10 dB.

Instantaneous velocity components were measured in two longitudinal planes; the centerplane at $z=0$ of the flume and the off-centerplane, the plane passing between the blocks at $z=w_b$ (see Figure 5.1). Measurements were gathered at different distances from the gate, starting from a section upstream of the blocks at $x/y_I=5$ and ending at a section far downstream of the blocks at $x/y_I=60$. For all measurements, a sampling volume height of 2.5 mm was used to decrease the effect of bed proximity (Precht et al. 2006). Measurements were conducted at

vertical increments of 2 mm starting from 3 mm from the bed and the increment was increased moving towards the water surface.

A sensitivity analysis was conducted to find the appropriate sampling duration. In this sensitivity analysis, 30-minute long time series of instantaneous velocities were gathered at a number of points located at various distances from the gate and heights from the bed. Time-averaged quantities; including the three-dimensional mean velocities and turbulence intensities and Reynolds stresses, were then computed using different lengths of the 30-minute time series. It was assumed that the 30-minute time-averaged values were free of any sensitivity to the sampling duration. The computed time-averaged quantities computed for shorter durations were compared with the values calculated using the entire 30-minute time series. It was found that the time-averaged parameters computed using time series with durations of five minutes or greater had magnitudes that were within 4% of the values computed using the 30-minute time series. As a result, a sampling duration of five minutes was used and each resulting time series was comprised of 30,000 instantaneous velocity samples (i.e. five minutes duration sampled at 100 Hz).

At each point, the measured time series was analyzed using a MATLAB[®] code to filter the time series and remove spikes in the data. There are numerous methods of removing spikes from the time series (e.g. Goring and Nikora 2002, Wahl 2003, Cea et al. 2007, Parsheh et al. 2010) but an iteration-free method recently developed by Islam and Zhu (2013) was used in this study. In this method, in each space domain defined by each velocity component and its time derivative, the distribution of the data cluster is evaluated using a bivariate kernel density function and the outliers are detected as spikes and removed from the time series. They tested their algorithm using wall jet data and showed that, even when more than 40% of the times series was comprised of spikes that their algorithm produced fewer outliers compared to previous methods. After removing the

spikes, this algorithm uses a linear interpolation to reconstruct the time series. This algorithm was applied to all the ADV time series data.

The time series for each point was, then, corrected for Doppler noise and filtering effects, using the method developed by Romagnoli et al. (2012). In this method, the power spectrum was computed for each velocity component using the Welch method; in this case the time series was split into blocks of 512 points with 50% overlap. The Doppler noise energy level was estimated from the tail of the spectrum (Voulgaris and Trowbridge 1998) using spectral density values at frequencies in the 49-50 Hz range. The corrected power spectra were obtained by subtracting the Doppler noise energy level from the power spectra of the despiked time series. Corrected variances for each velocity component were then estimated by integrating the corrected power spectrum. Finally, the variances were corrected for ADV spatial and temporal averaging effects using the performance curves presented by Garcia et al. (2005). Note that no correction for noise is required for the Reynolds stresses since they are not influenced by the Doppler noise (Khorsandi et al. 2012, Voulgaris and Trowbridge 1998).

In the presence of a 3D obstacle, the flow field is disturbed such that the turbulence field is inhomogeneous and highly anisotropic and estimates of the dissipation rate typically require the measurement of a number of component gradients (Hussein and Martinuzzi 1996). The spatial resolution constraints due to the ADV limitations make such direct measurement unattainable (the ADV makes point measurements so even if its measuring volume was much smaller it could not measure instantaneous gradients). Hence, the energy dissipation rate per unit mass (ϵ) was estimated using a method based on dimensional analysis which was developed for highly turbulent mixing flows (Wu and Patterson 1989, Kresta and Wood 1993, Wernersson and Tragardh 2000, Pearson et al. 2002). In this method, energy dissipation is related to a characteristic turbulent velocity (V_t) and length scale (L_t) as follows,

$$\varepsilon = A \frac{V_t^3}{L_t} \quad 5-1$$

where, A=0.85 is a constant. The characteristic velocity is taken as the square root of the turbulent kinetic energy as shown in Eq. (5-2).

$$V_t = \sqrt{k} = \sqrt{\frac{1}{2}(\overline{u'^2} + \overline{v'^2} + \overline{w'^2})} \quad 5-2$$

The characteristic length is also shown in Eq. (5-3).

$$L_t = \sqrt{\frac{1}{2}(L_x^2 + L_y^2 + L_z^2)} \quad 5-3$$

where, L_x , L_y , and L_z are the turbulence integral length scales in the longitudinal, vertical, and transverse directions, respectively. The integral time scale is defined as the area under the autocorrelation function up to the first zero crossing (Pope 2000). First, the autocorrelation function was computed as the inverse fast Fourier transform of the corrected power spectrum. Taylor's frozen turbulence hypothesis (Taylor 1938) was used to transform from the temporal domain (time scale) to the spatial domain (length scale).

A source of error in ADV measurements is the statistical error in sampling a random signal. The estimation of this sampling error provides a good approximation of the total error when the other error components are relatively small (Garcia et al. 2006). To evaluate the significance of this error, uncertainty analysis is used. The uncertainty analysis provides a data range for the measured parameter within which the true value, for the selected confidence limit, is located. If the parameter being analyzed has a normal probability distribution, standard methods are available to approximate the confidence intervals (Moffat 1988). These methods require the standard error of the parameter to be known which can be estimated for uncorrelated data with any arbitrary probability distribution using the equations available in the literature (Benedict and Gould 1996). For correlated data such as velocity time series, however, equations for the

standard error of the mean and variance are only available (Bendat and Piersol 2010). No equations are available to compute the standard error of parameters such as turbulence time and length scales or the rate of dissipation of turbulent kinetic energy which are dependent on the correlation structure of the turbulent velocity field (Garcia et al. 2006). The alternative method for such complicated parameters is the bootstrap technique introduced by Efron (1979).

The standard bootstrap method can be used to evaluate the confidence intervals for uncorrelated data with any complex structure (Efron and Tibshirani 1993). However, Kusch (1989) introduced the moving block bootstrap method which preserves the correlation structure and, hence, can be used for correlated data. This method is based on randomly re-sampling the signal using blocks with a certain length (Zoubir and Iskander 2004). This procedure is repeated and the error and confidence intervals are estimated using the repeated re-sampled values. It is recommended that 200 and 1000 replications be used for estimating the error variance and confidence interval, respectively (Efron and Tibshirani 1993). An optimum block length must be used so that the structure of the time series is preserved. Therefore, the moving block bootstrap method with an optimum block length provided by Politis and White (2004) with 1000 repetitions was used to evaluate the confidence intervals of all turbulence parameters.

Results and Discussion

Typical plots of time-averaged velocity vectors for the DSJ and RWJ flow regimes are presented in Figure 5.2 and Figure 5.3, respectively. Also included in these figures, is the corresponding plot for the flow field in a submerged hydraulic jump without blocks. As described by Habibzadeh et al. (2013), the flow in the centerplane of the DSJ regime is deflected by the blocks at a sharp angle ($x/y_I=10$ in Figure 5.2a), while the flow in the off-centerplane grows similar to a wall jet but with a faster rate of expansion (Figure 5.2b). Comparing DSJ velocity fields plotted Figure 5.2a and b with the NB series in Figure 5.2c, it is obvious that the

blocks significantly reduce the velocity magnitude; e.g. compare the velocity vectors located at $x/y_1=20$ to 40 in Figure 5.2a, b and c.

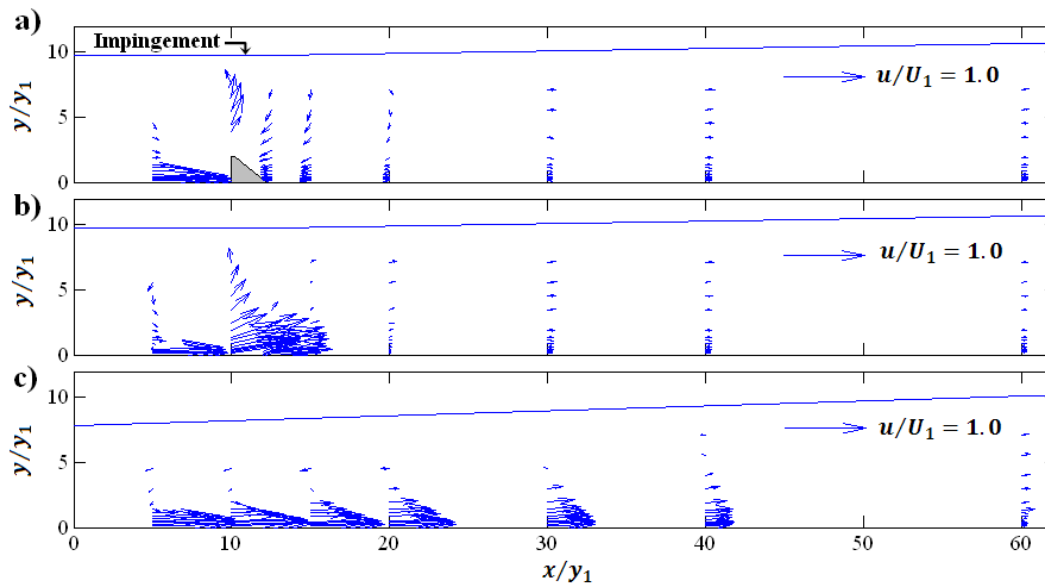


Figure 5.2 Vector plots of the mean flow field in (a) the centerplane and (b) off-centerplane of the DSJ flow regime (run BB3, $F_1=5.32$ and $S=0.54$) and (c) the submerged jump without blocks (run NB3, $F_1=5.33$ and $S=0.49$).

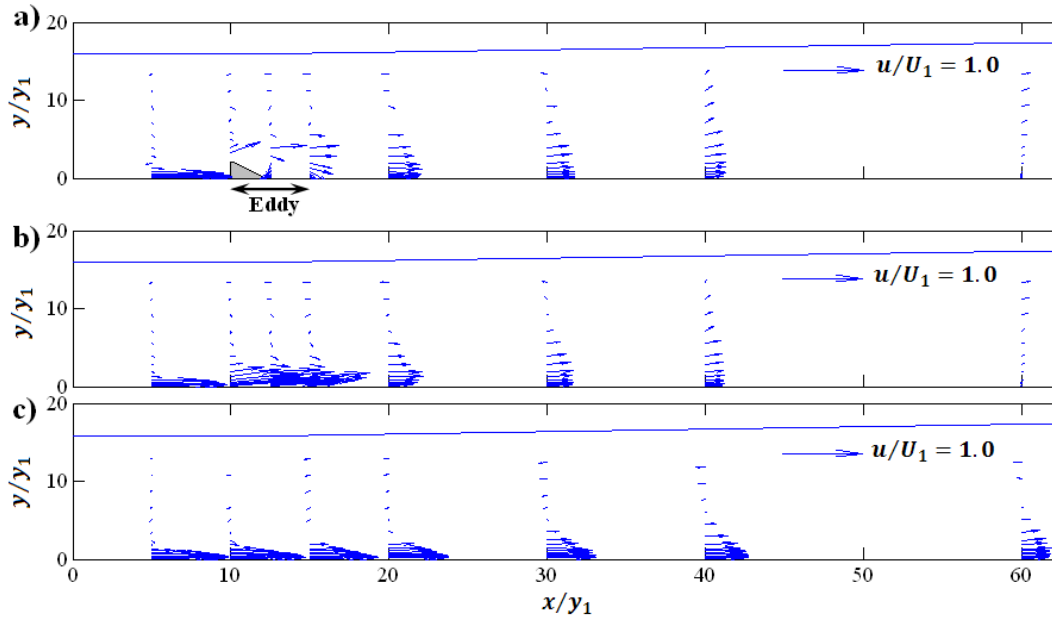


Figure 5.3 Vector plots of the mean flow field in the centerplane (a) and off-centerplane (b) of the RWJ flow regime (run BB4, $F_I=5.25$ and $S=1.55$) and the submerged jump without blocks (run NB4, $F_I=5.28$ and $S=1.53$).

In the RWJ regime, however, the flow pattern is considerably different (see Figure 5.3). The flow in the centerplane of the RWJ regime reattaches to the bed a short distance downstream of the blocks (Figure 5.3a). The off-centerplane flow has a pattern similar to the flow in the off-centerplane of the DSJ regime but with a slower rate of growth (Figure 5.2b and Figure 5.3b). This flow regime, also, has lower velocities compared to the NB case; although larger velocities are observed downstream of the blocks compared to the DSJ regime (e.g., compare velocities at $x/y_I=30$ in Figure 5.3a, b and c with those in Figure 5.2a, b and c).

The distinction between the DSJ and RWJ flow regimes lies in the separation-reattachment pattern at the blocks as mentioned by Habibzadeh et al. (2013). In both flow regimes, the incoming stream is separated at the leading edge of the block. In the DSJ regime, however, the deflected flow deflects upwards towards the water surface, while in the RWJ regime, the deflected jet reattaches to the bed just downstream of the block. In the latter, a separation bubble is formed which is bounded by the sharp leading edge of the block and the reattachment

point downstream of the blocks, which is similar to flow around a cube observed by Lyn and Rodi (1994). It has been observed that, in flow around bed-mounted square cylinders, the characteristics of the reattachment phenomenon is largely dependent on the upstream flow conditions including the upstream turbulent kinetic energy, shear and boundary layer thickness (Castro and Robins 1977). In the current study, however, the occurrence of reattachment; i.e. the occurrence of either flow regime for a given F_1 and block arrangement, is determined by the submergence factor (S), that is, the surrounding pressure (Habibzadeh et al. 2012). As S increases, the free stream pressure increases, and, as a result, for a constant pressure coefficient (as defined by Castro and Robins 1977), smaller surface pressures are expected. In the DSJ regime, with smaller tailwater, the pressure deficit around the block is not sufficiently strong to force the separated high-momentum jet to reattach to the bed. In the RWJ regime, however, the suction behind the block is adequate to cause the deflected jet to reattach and form the eddy behind the block. The dimension of this eddy was found by Habibzadeh et al. (2013) to be mainly influenced by the width of the block. The observation that the longitudinal extension of this cavity is only controlled by the lateral dimension of the obstacle, is an indication of the existence of the prolonged axial vorticity originated by the upstream boundary layer at the side edges of the block while the axial vorticity generated by the leading edge is rapidly destroyed by the wake turbulence and shear (Hussein and Martinuzzi 1996, Castro and Robins 1977). This process explains the mechanism which causes the mean flow patterns to be different in the flow regimes. Following a similar judgment, it is expected that the turbulence characteristics of the two flow regimes is influenced by the occurrence of either flow regime. This will be examined in detail in the following.

An example of vertical profiles of the longitudinal turbulence intensities in the centerplane and off-centerplane and the corresponding submerged jump without baffles (NB series) are shown in Figure 5.4a and b for the DSJ and RWJ

flow regimes, respectively. The longitudinal and vertical turbulence intensities (I_x and I_y) are defined in Eq. (5-4).

$$I_x = \frac{\sqrt{u'^2}}{U_1}, \quad I_y = \frac{\sqrt{v'^2}}{U_1} \quad 5-4$$

Here, u' and v' are the fluctuating velocity components in the longitudinal (streamwise) and vertical directions, respectively. The random error associated with the measured I_x was estimated to be less than 4% based on the moving block bootstrap technique (error bars are not shown on the figure for simplicity). At the blocks ($x/y_1=10$), the measured time series just above the blocks in the centerplane consisted of a large percentage of spikes (more than 60%). This can be attributed to the large velocity gradients created by the deflected jet in this region. As a result, the measurements at this station in the the centerplane were not included in the analysis. Also, the data sampled furthest from the bed for the NB series at stations $x/y_1=15, 20,$ and 30 were also not included because of the presence of spikes due to the shear layer formed at the lower edge of the recirculating surface roller. This is why the vertical profiles at these stations are shorter.

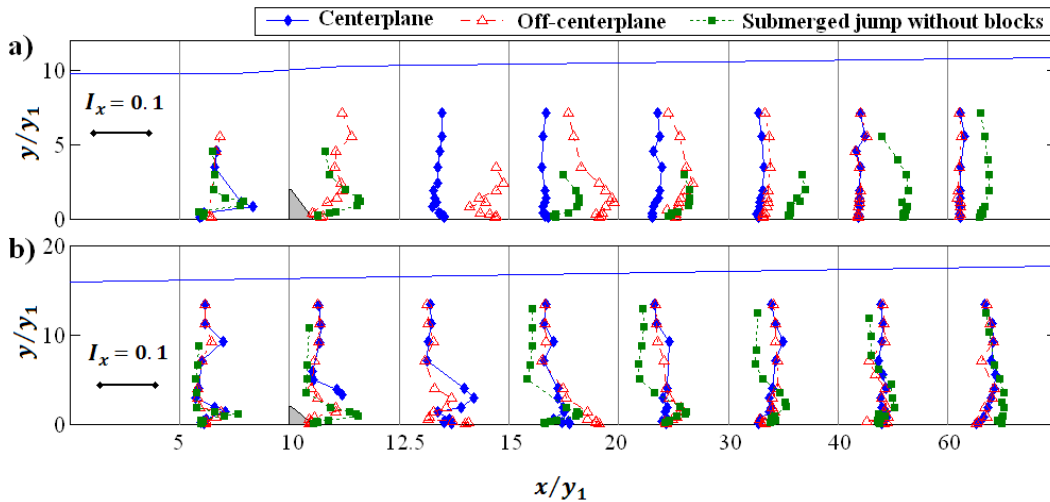


Figure 5.4 Typical streamwise variation of the longitudinal turbulence intensity (I_x) for a) the DSJ regime (run BB3, $F_1=5.32$, $S=0.54$) and b) the RWJ regime (run BB4, $F_1=5.25$, $S=1.55$) and the corresponding submerged jump without blocks.

It can be observed in Figure 5.4a that the magnitudes of I_x upstream of the blocks at $x/y_I=5$ in the centerplane, off-centerplane and the submerged jump without blocks follow a similar trend. In all three cases there is a maximum at upper edge of the expanding jet at approximately $y/y_I \approx 1.0$ caused by the shear layer that occurs at this location. Downstream of the blocks for $x/y_I \geq 15$, I_x values in the centerplane reach an almost constant magnitude throughout the entire depth. This magnitude is smaller than that for the series without blocks and gradually decreases with distance from the gate (I_x in the centerplane is smaller compared to the off-centerplane at $12.5 \leq x/y_I \leq 40$ and smaller than NB for $x/y_I \geq 12.5$). The values of I_x in the off-centerplane are comparable to the case without blocks at the blocks (i.e. $x/y_I=10$). Just downstream of the blocks at $x/y_I=12.5$, the intensities in the off-centerplane are approximately twice those in the centerplane. Further downstream, at $x/y_I=15$, the intensities in the off-centerplane are on average 37% larger than those in the series without blocks. At $x/y_I=20$, the intensities in the off-centerplane are comparable to those of the submerged jump without blocks. Moving downstream, the intensities in the off-centerplane decrease and for $x/y_I \geq 30$, the intensities are almost identical in the two planes. In this region; i.e. for $x/y_I \geq 30$, the intensities are approximately 65% less than those of submerged jumps without blocks. It is clear in Figure 5.4a that downstream of the blocks; i.e. for $x/y_I \geq 12.5$, the I_x magnitudes in the centerplane gradually decrease with distance, while the intensities in the off-centerplane first increase (for $10 \leq x/y_I \leq 15$) and then quickly decrease (for $x/y_I > 15$).

Example profiles of the longitudinal turbulence intensities are shown in Figure 5.4b for the RWJ flow regime. It is observed that, in general there are only minor differences between the intensities in the two planes, except near the blocks at $10 \leq x/y_I \leq 15$ and $y/y_I < 5.0$. In this region, the intensities in the centerplane have a maximum at $y/y_I \approx 3.0$, which coincides with the shear interface created by flow separation at the leading top edge of the block. The location of the maximum I_x behind bluff bodies such as spheres has been reported to occur at the shear

interface (e.g. Dey et al. 2011). At $x/y_I=15$ for $y/y_I \leq 3.0$, the intensities are largest in the off-centerplane and for $y/y_I > 3.0$, the intensities are comparable in the two planes and larger than in the submerged jump without blocks. At $x/y_I=20$, the intensities in the off-centerplane are almost identical to the submerged jump without blocks for $y/y_I \leq 2.0$, and for $y/y_I > 2.0$, the intensities in the centerplane and off-centerplane are comparable and larger in the submerged jump without blocks. For $x/y_I \geq 30$, the intensities in the two planes are identical.

Typical variations of the vertical turbulence intensities I_y , defined in Eq. (5-4), are shown in Figure 5.5 for the two flow regimes. It can be observed in Figure 5.5a that the vertical turbulence intensities in the DSJ regime are similar in magnitude to those in the submerged jump without blocks upstream of the blocks. At $x/y_I=10$, the intensities in the off-centerplane continually increase towards the water surface while the intensities in the submerged jump without blocks have a peak at the interface of the expanding jet as expected. It should be reminded that in the centerplane at blocks, the measured time series consisted of a large percentage of spikes (more than 60%) and were not included in the analysis. At $x/y_I=12.5$, the turbulence intensities in the centerplane are smaller than those in the off-centerplane by 18% to 53%. At $x/y_I=15$, the intensities are smaller in the centerplane and the intensities in the submerged jump without blocks fall between the curves for the centerplane and off-centerplane. Further downstream, the intensities are virtually identical in the centerplane and off-centerplane at $x/y_I \geq 30$, and both are approximately 45% near the bed and 60% away from the bed less than those in the submerged jump without blocks.

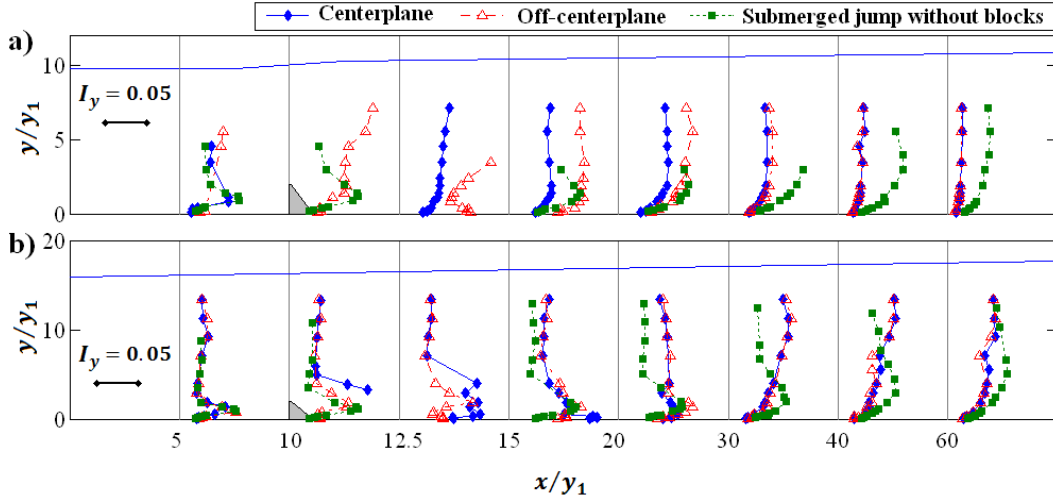


Figure 5.5 Typical streamwise variation of the vertical turbulence intensity (I_y) for a) the DSJ regime (run BB3, $F_I=5.32$, $S=0.54$) and b) the RWJ regime (run BB4, $F_I=5.25$, $S=1.55$) and the corresponding submerged jump without blocks.

Profiles of I_y for the RWJ flow regime are shown in Figure 5.5b. It can be seen in this figure that, upstream of the blocks at $x/y_1=5$, all three profiles representing the two planes of the RWJ regime and the submerged jump without blocks coincide. As the flow approaches the blocks, the I_y intensities are disturbed. But, this effect is different in the two planes of the RWJ regime only in the regions near the blocks. That is, the vertical turbulence intensities in the centerplane and off-centerplane are significantly different only in the flow region bounded by $y/y_1 \leq 6.0$ and $10 \leq x/y_1 \leq 20$. For $x/y_1 \geq 30$, the I_y profiles of the two planes coincide. At $x/y_1=30$ and 40, I_y in the RWJ regime is approximately 35% smaller than the corresponding submerged jump without blocks for $y/y_1 \leq 4.0$ and 7.6, respectively and larger for the rest of the depth. At $x/y_1=60$, I_y is smaller than the corresponding submerged jump without blocks for the entire depth and this difference first increase to about 30% at $y/y_1 \approx 5.5$ and then decreases as moving upwards. In summary, the differences between the vertical intensities between the RWJ and NB series are significant for $x/y_1 \geq 15$, where larger intensities are observed in the NB series near the bed while intensities in the RWJ regime are larger away from the bed. The region, in which the intensities are significantly

different between the two planes, approximately coincides with location of the standing eddy behind the block.

Vertical profiles of the normalized Reynolds stresses ($\hat{\tau}_R$), defined in Eq. (5-5), are plotted in Figure 5.6a and b for the DSJ and RWJ regimes, respectively. Also plotted for comparison in these figures are profiles for the corresponding submerged jumps without blocks (NB series).

$$\hat{\tau}_R = \frac{-\overline{u'v'}}{U_1^2} \quad 5-5$$

It can be observed in Figure 5.6a that three profiles of the $\hat{\tau}_R$ upstream of the blocks at $x/y_I=5$, are all similar with a peak at the shear interface which is typical in submerged jumps (Dey and Sarkar 2008, Long et al. 1990). At the blocks station ($x/y_I=10$), the $\hat{\tau}_R$ values are smaller in the off-centerplane for $y/y_I \leq 2.0$ compared to the NB series. Downstream of the blocks for $x/y_I \geq 12.5$, the Reynolds stresses in the centerplane are negligible. In the off-centerplane, however, the Reynolds stresses are significantly larger than the centerplane. The largest $\hat{\tau}_R$ magnitudes are observed in the off-centerplane at $x/y_I=12.5$. No measurements were made at this station in the corresponding submerged jumps without blocks (NB series); however, observing the trend of the $\hat{\tau}_R$ profiles of the submerged jumps without blocks between stations $x/y_I=10$ and 15, it appears that the RS magnitudes at $x/y_I=12.5$ in the off-centerplane of the DSJ regime are larger than those in the submerged jumps without blocks. For $x/y_I \geq 30$, the Reynolds stresses in the centerplane and off-centerplane are similar with magnitudes that are negligible compared to the NB series.

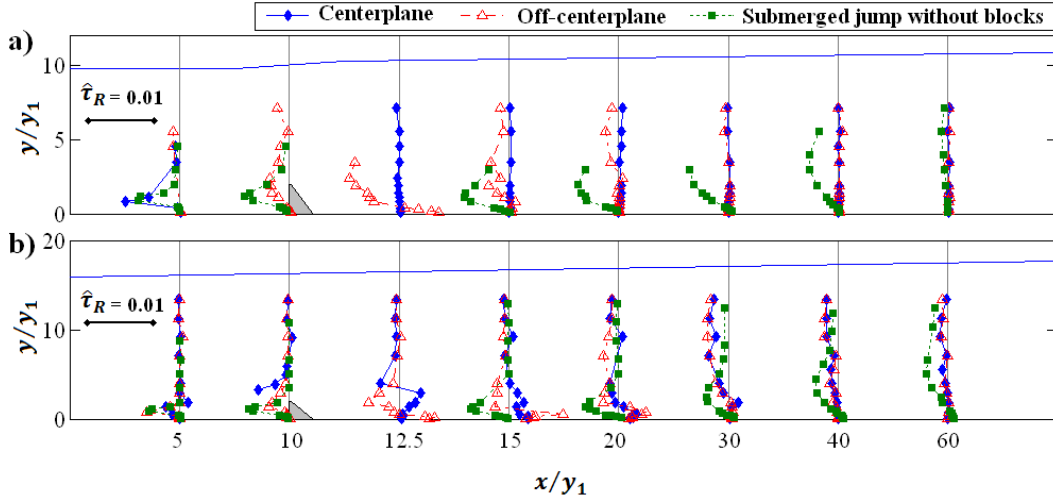


Figure 5.6 Typical streamwise variation of the normalized Reynolds stress for a) the DSJ regime (run BB3, $F_I=5.32$, $S=0.54$) and b) the RWJ regime (run BB4, $F_I=5.25$, $S=1.55$) and the corresponding submerged jump without blocks.

In Figure 5.6b for the RWJ regime, it can be seen that for $x/y_1 \leq 15$, the differences in the Reynolds stresses between the centerplane and off-centerplane and NB series are only significant for $y/y_1 \leq 5.0$ (except at $x/y_1=20$ where the differences extend to $y/y_1 \leq 11.0$). Further downstream at $x/y_1 \geq 30$, however, the magnitudes in the centerplane and off-centerplane are negligible compared to the NB series. Just downstream of the blocks at $x/y_1=12.5$, the Reynolds stresses are considerably different in the two planes. At this station, at a height of $y/y_1 \approx 3.0$ (corresponding to $y/h_b \approx 1.5$), maximum positive and minimum negative Reynolds stresses are observed in the centerplane and off-centerplane, respectively. This region of high Reynolds stress coincides with the boundary of the eddy formed downstream of due to flow separation. Further downstream, the maximum Reynolds stress in the centerplane moves towards the bed, showing the reattachment of the flow, and diminishes at $x/y_1=30$. The peak in the off-centerplane Reynolds stress, also, moves towards the bed and follows a similar trend to that in the centerplane at $x/y_1=20$. This indicates that the axial vortices from the sides of the block meet at $x/y_1 \approx 20$, corresponding to an eddy length of

$L_e \approx 5h_b$, which is consistent with the observations in previous studies (Habibzadeh et al. 2013, Castro and Robins 1977).

Note that, the Reynolds stress decays rapidly further downstream in the off-centerplane in the RWJ regime (for example, see $x/y_I=30$ Figure 5.6b). Rapid decay of the Reynolds stresses downstream of reattachment points has been observed in earlier studies (Bradshaw and Wong 1972, Song and Eaton 2004). This behavior was attributed by Song and Eaton (2004) to the stretching of vortices due to a streamwise gradient in the longitudinal velocity. This vortex stretching increases the vertical and transverse turbulence intensities and decreases the streamwise turbulence intensity. They also hypothesize that the presence of the wall redistributes some energy and increases energy dissipation.

The turbulent kinetic energy (k) is defined as the mean kinetic energy per unit mass in the fluctuating velocity field (Pope 2000). The magnitude of k is a measure of turbulence intensity and its rate of reduction is an indication of energy dissipation. In Figure 5.7, typical profiles of the normalized turbulent kinetic energy (\hat{k}) are plotted for the two flow regimes and the corresponding submerged jump without blocks. Here, \hat{k} is given by Eq. (5-6).

$$\hat{k} = \frac{k}{\frac{1}{2}U_1^2} = \frac{\frac{1}{2}(\overline{u'^2} + \overline{v'^2} + \overline{w'^2})}{\frac{1}{2}U_1^2} \quad 5-6$$

where, w' is the fluctuating turbulent velocity in the transverse direction. In Figure 5.7a and b, it can be observed that \hat{k} at $x/y_I=5$ in both flow regimes, reaches a maximum upstream of the blocks at $y/y_I \approx 1.0$ which is again due to the presence of the shear layer. In Figure 5.7a, it can be seen that at the location of the blocks $x/y_I=10$, \hat{k} in the off-centerplane of the DSJ regime is smaller in magnitude than the NB series near the bed for $y/y_I \leq 2.0$ and the peak occurs at a higher distance from the bed. Immediately downstream of the blocks at $x/y_I=12.5$, the magnitudes of \hat{k} observed in the centerplane are much smaller than in the off-centerplane. The magnitude of \hat{k} at $x/y_I=12.5$ in the off-centerplane, first decreases (moving up

from the bed) to reach its minimum of $\hat{k} \approx 0.02$ at $y/y_1 \approx 1.0$, then increases to its maximum of $\hat{k} \approx 0.06$ at $y/y_1 \approx 3.5$. Further downstream, \hat{k} in the off-centerplane decreases and for $x/y_1 \geq 30$, there are no significant differences between \hat{k} in the centerplane and off-centerplane and the magnitudes of \hat{k} in the submerged jump without blocks are considerably larger (by approximately 60-85%).

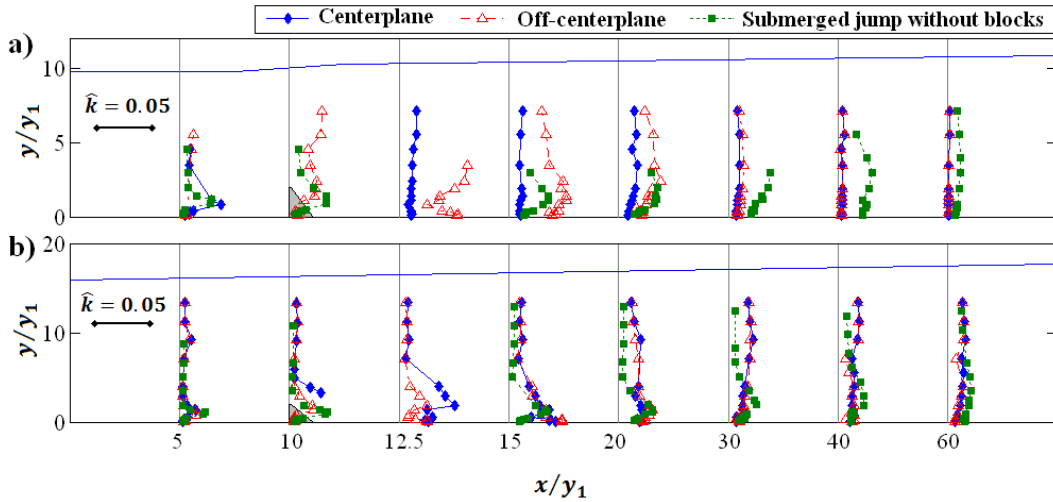


Figure 5.7 Typical streamwise variation of the normalized turbulence kinetic energy for a) the DSJ regime (run BB3, $F_1=5.32$, $S=0.54$) and b) the RWJ regime (run BB4, $F_1=5.25$, $S=1.55$) and the corresponding submerged jump without blocks.

Typical vertical profiles of \hat{k} for the RWJ regime are plotted in Figure 5.7b. At the blocks ($x/y_1=10$) a peak magnitude of $\hat{k} \approx 0.05$ are observed above the blocks in the centerplane. At this station, the peak magnitudes of $\hat{k} \approx 0.22$ and 0.035 respectively in the off-centerplane and the submerged jump without blocks are observed at $y/y_1 \approx 1.3$ and 1.1 , respectively. Downstream of the blocks at $x/y_1=12.5$, a maximum magnitude of $\hat{k} \approx 0.05$ is observed in the centerplane at $y/y_1 \approx 1.8$. At this station, the magnitudes of \hat{k} in the off-centerplane are smaller than the centerplane for $y/y_1 \leq 7.0$, but are similar for the rest of the flow depth. For $x/y_1=15$ and 20 , the \hat{k} profiles in the two planes are slightly different (with a maximum deviation of 20%) near the bed (for $y/y_1 < 4.0$) and are identical for $y/y_1 \geq 4.0$. At $x/y_1=30$ the magnitude of \hat{k} decreases, and the curves in the

centerplane and off-centerplane coincide as a result of mixing between the two planes.

Comparing Figure 5.4 to Figure 5.7, it is evident that the turbulence characteristics are significantly different in the centerplane and off-centerplane of the DSJ flow regime. Downstream of the blocks, the turbulence intensities and turbulent kinetic energy are smaller in the centerplane and larger in the off-centerplane compared to the submerged jump without blocks. But, this difference rapidly diminishes and for $x/y_I \geq 30$, the magnitudes in the two planes are approximately equal and less than those of the submerged jump without blocks. This rapid recovery of the flow is similar to that observed in wall-wakes behind spherical obstacles (Dey et al. 2011). In the RWJ flow regime, however, the difference between the two planes is only noticeable in the vicinity of the blocks. The difference between the RWJ flow regime and the submerged jump without blocks decreases as moving further downstream.

Vertical profiles of the dimensionless turbulent kinetic energy dissipation rate per unit mass, $\varepsilon/\varepsilon_{ave}$, are plotted in Figure 5.8 where ε_{ave} is the average dissipation rate per unit mass of the corresponding free jump computed using Eq. (5-7) (Liu et al. 2004) and tabulated in Table 5-1 for each run.

$$\varepsilon_{ave} = \frac{\rho g Q \Delta h}{\rho L_j B (y_1 + y_2) / 2} \quad 5-7$$

where, Q is the discharge, Δh is the head loss in the jump, L_j is the length of the jump being equal to approximately $6y_2$ (Peterka 1984), and $B=0.467$ m is the width of the channel.

It can be observed in Figure 5.8 that the maximum energy dissipation rate in the DSJ regime, $\varepsilon/\varepsilon_{ave} \approx 4$, in the off-centerplane occurs at $x/y_I = 12.5$ and 15. In the RWJ regime, however, the maximum value of $\varepsilon/\varepsilon_{ave} \approx 4$ occurs in the centerplane just downstream of the blocks at $x/y_I = 12.5$ at a height of $y/y_I \approx 2.0$. Comparing the two flow regimes in Figure 5.8a and b, it is clear that, in the DSJ

flow regime, the maximum dissipation occurs in the off-centerplane and persists for a longer distance downstream compared to the RWJ regime. In the RWJ flow regime the location of the maximum dissipation rate in the centerplane at $x/y_I=12.5$ coincides with the upper boundary of the reattaching jet. At $x/y_I=15$ near the reattachment point, high values of $\varepsilon/\varepsilon_{ave}$ are observed.

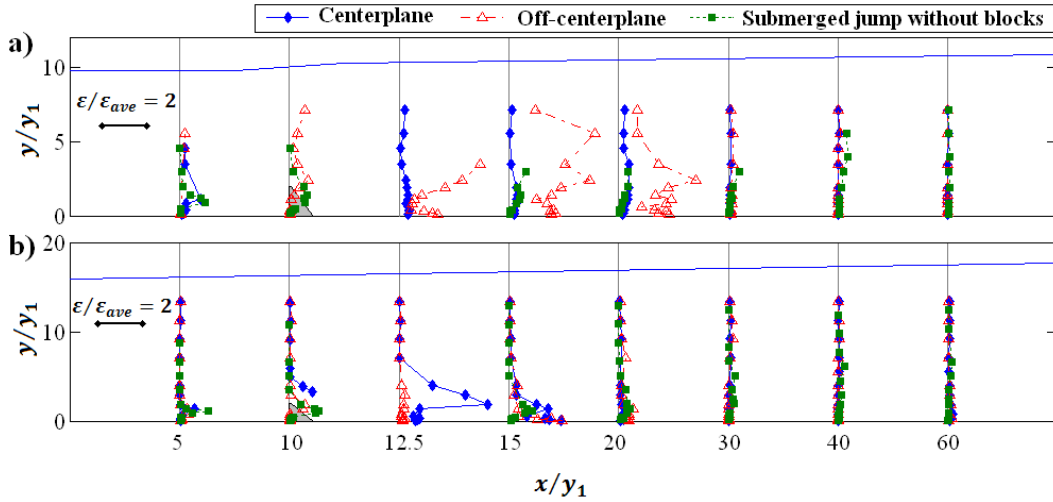


Figure 5.8 Typical streamwise variation of the dimensionless energy dissipation rate for a) the DSJ regime (run BB3, $F_I=5.32$, $S=0.54$) and b) the RWJ regime (run BB4, $F_I=5.25$, $S=1.55$) and the corresponding submerged jump without blocks.

The streamwise variations of the maximum (at a given x/y_I) longitudinal turbulence intensity $(I_x)_{max}$ and the maximum Reynolds stress $(\hat{\tau}_R)_{max}$ are plotted in Figure 5.9a and b, respectively. ADV measurements in free hydraulic jumps without blocks by Zobeyer et al. (2010) and Liu et al. (2004) are also shown in these figures.

In Figure 5.9a, it can be seen that the maximum longitudinal intensity in the centerplane of the DSJ flow regime, rapidly reduces to less than 0.09 just downstream of the blocks (at $x/y_I=12.5$) and gradually decreases with distance. It should be reminded that due to large percentage of spikes in the time series measured in the centerplane of the DSJ regime at the blocks, this station was removed from the analysis and the data were plotted starting at $x/y_I=12.5$. In the off-centerplane of the DSJ regime, the intensities increase from approximately 0.1

at the blocks to 0.19 just downstream at $x/y_I=12.5$ then decrease moving downstream. For $x/y_I \geq 15$, the maximum intensity in the off-centerplane closely follows the curves for free jumps without blocks but with slightly smaller magnitudes. For $x/y_I \geq 30$, the curves for the two planes of the DSJ regime coincide and further downstream, the maximum intensity gradually decreases to obtain a magnitude of approximately 0.03 at $x/y_I=60$, which is smaller than the magnitude in free jumps.

The maximum intensities in the RWJ regime in the two planes follow a similar trend with a peak at $x/y_I=12.5$ and 15 in the centerplane and off-centerplane, respectively. For $x/y_I \geq 20$, the curves in the two planes of the RWJ regime coincide and gradually decrease with distance downstream. At $x/y_I=20$, the maximum intensities in the two planes of this flow regime has a magnitude of about 0.12 and at $x/y_I=60$, the magnitude is approximately 0.09. For $x/y_I \geq 30$, the maximum intensities are larger in the RWJ regime compared to free jumps. The maximum intensities in the submerged jump without blocks first increase with distance and reach a peak at $x/y_I=15$ and remain approximately constant for $15 \leq x/y_I \leq 30$ followed by a gradual decrease. At $x/y_I=60$, the maximum intensities in the RWJ regime and the submerged jumps without blocks are approximately 0.09.

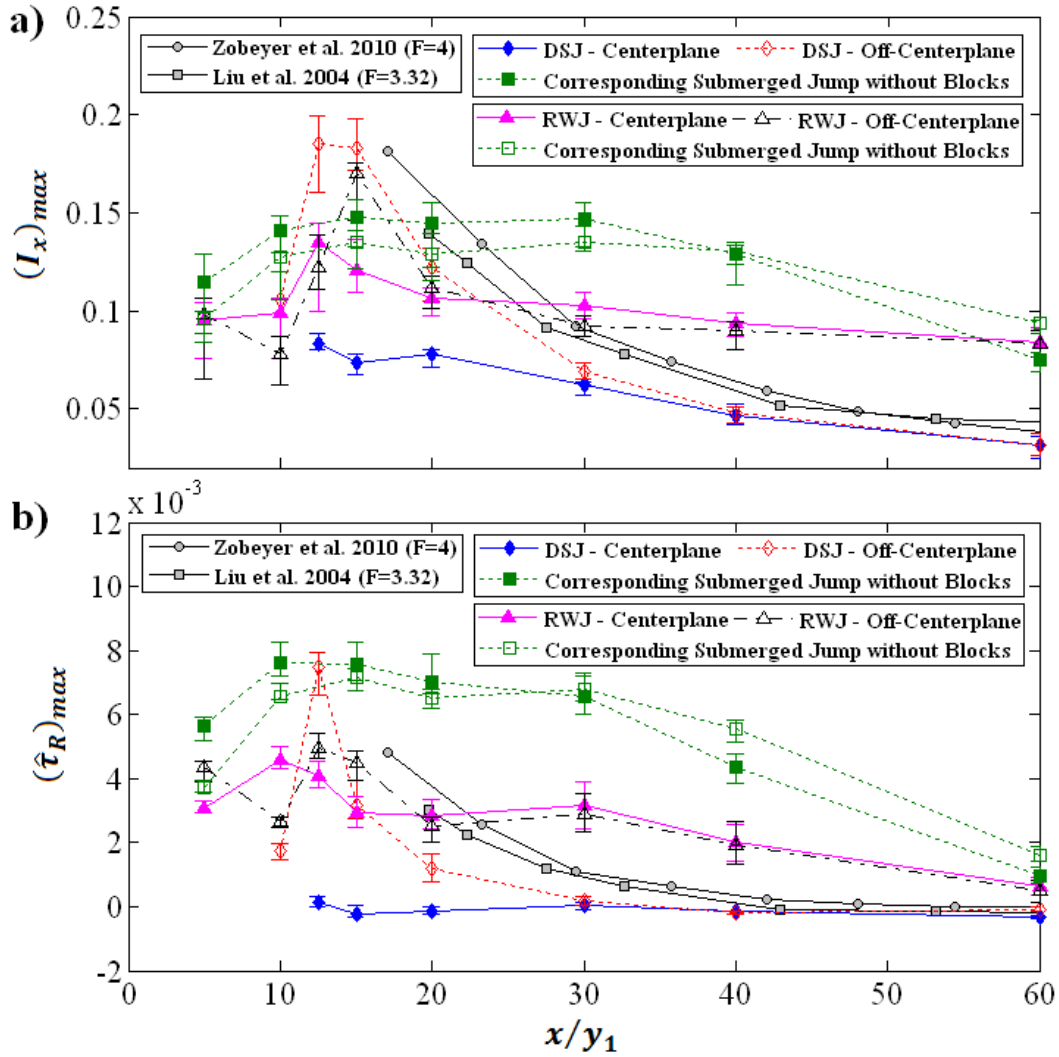


Figure 5.9 Average curves for the streamwise variation of a) the maximum longitudinal turbulence intensity $(I_x)_{max}$ and b) maximum Reynolds stress. (Error bars represent the range of the computed 95% confidence limits of the runs used in the averaging.)

The streamwise variation of the maximum normalized Reynolds stress $(\hat{\tau}_R)_{max}$ is plotted in Figure 5.9b. A similar trend to that of the maximum intensity exists for the Reynolds stress. The maximum Reynolds stress in the centerplane of the DSJ flow regime is small just downstream of the blocks; i.e. at $x/y_1=12.5$, and stays approximately constant with distance. In the off-centerplane of this flow regime, however, a peak occurs at $x/y_1=12.5$, followed by a decreasing trend. The maximum Reynolds stress in the RWJ regime reaches its

peak values in the centerplane and off-centerplane at $x/y_I=12.5$ and 15, respectively. The magnitude of $(\hat{\tau}_R)_{max}$ slightly decrease and, then, remains approximately constant for $15 \leq x/y_I \leq 30$ in the centerplane, and $20 \leq x/y_I \leq 30$ in the off-centerplane. This is followed by a gradual decrease for $x/y_I > 30$. The maximum Reynolds stress in the submerged jump without blocks first increases to its peak at $x/y_I=12.5$ and then gradually decreases with distance downstream. For $x/y_I \geq 30$, both the maximum intensity and maximum Reynolds stress are smallest in the DSJ regime, and largest for the submerged jump without blocks. In this region, the RWJ flow regime has large magnitudes of the maximum intensity and maximum Reynolds stress compared to free jumps while in the DSJ regime the magnitudes are less than or equal to the free jump.

The normalized vertically-averaged turbulent kinetic energy \hat{k}_0 is defined as,

$$\hat{k}_0 = \frac{1}{\frac{1}{2}U_1^2} \left[\frac{1}{y_0} \int_0^{y_0} k \, dy \right] \quad 5-8$$

where y_0 is the height of the highest point at which velocity measurements were conducted. The longitudinal variations of \hat{k}_0 are plotted in Figure 5.10 as average curves for the DSJ and RWJ flow regimes. Each curve is the result of averaging over the three experimental runs for each flow regime. The error bars in this figure represent the range of observed values at each location. It can be observed in Figure 5.10 that the magnitudes \hat{k}_0 in the centerplane of the DSJ regime increase slightly at $x/y_I \approx 20$ and then steadily decrease moving downstream. The peak of \hat{k}_0 in the off-centerplane of the DSJ regime occurs at $x/y_I=12.5$, followed by a rapid reduction for $12.5 \leq x/y_I \leq 30$ and a gradual decreasing trend for $x/y_I > 30$. At $x/y_I \approx 30$, the \hat{k}_0 values in the two planes are approximately equal and gradually decrease with distance. At $x/y_I=60$ the magnitude of \hat{k}_0 in the two planes approaches an approximately value of $\hat{k}_0 \approx 0.002$. For $x/y_I < 30$, \hat{k}_0 magnitudes are

considerably different between the two planes of the DSJ flow regime but this difference diminishes moving in the streamwise direction. The maximum difference between the two planes occurs at $x/y_I=12.5$, where \hat{k}_0 is approximately five times larger in the off-centerplane compared to the centerplane.

In Figure 5.10, it is also observed that the magnitudes of \hat{k}_0 in the two planes of the RWJ regime follow a similar trend, unlike the DSJ regime. In the RWJ regime, the \hat{k}_0 values in the centerplane follow a gradual decreasing trend. The \hat{k}_0 values in the off-centerplane, however, first increase to a peak at $x/y_I \approx 20$, and then gradually decrease. In both planes of the RWJ regime, the \hat{k}_0 magnitudes are larger than those of the corresponding submerged jump without blocks (except at $x/y_I=60$). At the furthest station; i.e. $x/y_I=60$, \hat{k}_0 magnitudes in the two planes of the RWJ regime are ~ 0.015 , which is comparable to the value observed in the submerged jump without blocks and approximately 9 times larger than the values observed in both planes of the DSJ regime.

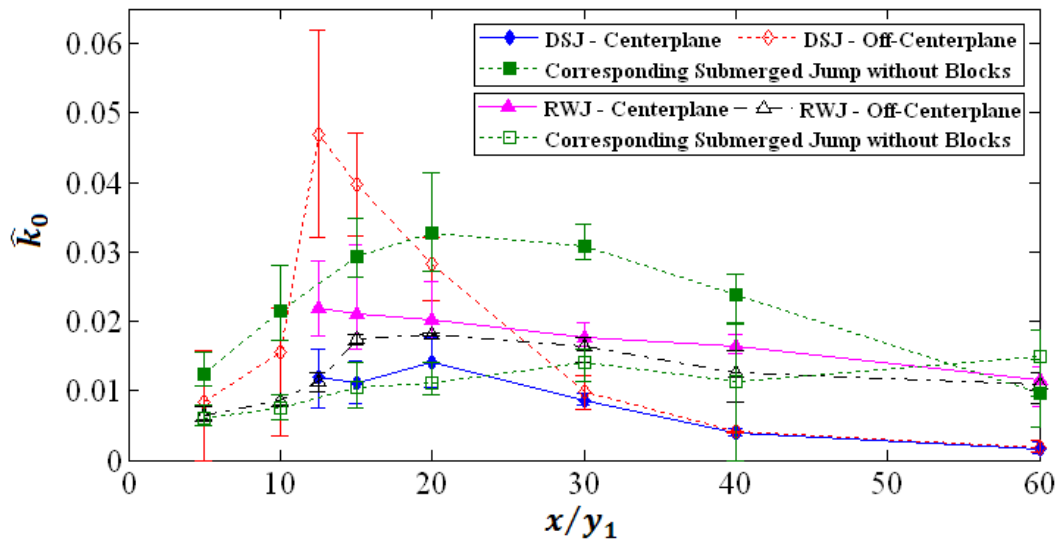


Figure 5.10 Average curves for the streamwise variation of the vertically-averaged turbulence kinetic energy. (Error bars represent the range of the computed 95% confidence limits of the runs used in the averaging.)

The pattern of \hat{k}_0 reduction in the DSJ regime indicates the presence of a large shear interface in the off-centerplane of this regime which creates strong mixing. As a result, in a short distance; i.e. $12.5 \leq x/y_I \leq 30$, the kinetic energy is decayed and the two planes attain an identical kinetic energy which is appreciably less than that of the RWJ regime and the submerged jump without blocks; e.g. \hat{k}_0 magnitudes at $x/y_I=40$ of the DSJ regime are approximately 4 and 7 times smaller than the RWJ and submerged jump without blocks.

The dimensionless vertically-averaged turbulence kinetic energy dissipation rate per unit mass $\hat{\varepsilon}_0$ is defined as,

$$\hat{\varepsilon}_0 = \frac{1}{\varepsilon_{ave}} \left[\frac{1}{y_0} \int_0^{y_0} \varepsilon dy \right] \quad 5-9$$

Average curves are presented in Figure 5.11 for the vertically-averaged turbulence kinetic energy dissipation rate per unit mass $\hat{\varepsilon}_0$ in the DSJ and RWJ regimes and the corresponding submerged jump without blocks data. The vertical average was calculated in the same manner as described previously, and similarly, the error bars in Figure 5.11 represent the range of values at each point. The magnitudes of $\hat{\varepsilon}_0$ in the centerplane of the DSJ flow regime are seen to be relatively small in Figure 5.11 ($\hat{\varepsilon}_0 < 0.33$) at all locations. In the off-centerplane, however, the magnitude of $\hat{\varepsilon}_0$ is significantly larger just downstream of the blocks; for i.e. $12.5 \leq x/y_I \leq 20$, with a peak value of $\hat{\varepsilon}_0 \approx 2.5$ at $x/y_I=15$. The dissipation rate in the corresponding submerged jump without blocks reaches a maximum value of $\hat{\varepsilon}_0 \approx 0.68$ at $x/y_I=15$ and then gradually decreases downstream. In the range $10 \leq x/y_I \leq 30$, the dissipation rate in the off-centerplane is significantly larger compared to the corresponding submerged jump without blocks. Figure 5.11 also shows that the dissipation rate in the off-centerplane of the RWJ regime and the corresponding submerged jump without blocks closely follow a similar trend with magnitudes of $\hat{\varepsilon}_0$ not exceeding 0.2. The dissipation rate in the centerplane of this flow regime also follows a similar trend except at $x/y_I=12.5$

and 15 (approximately coinciding with the location of the eddy behind the blocks) where the dissipation rate is higher, $\hat{\epsilon}_0 \approx 0.65$ and 0.38 , respectively.

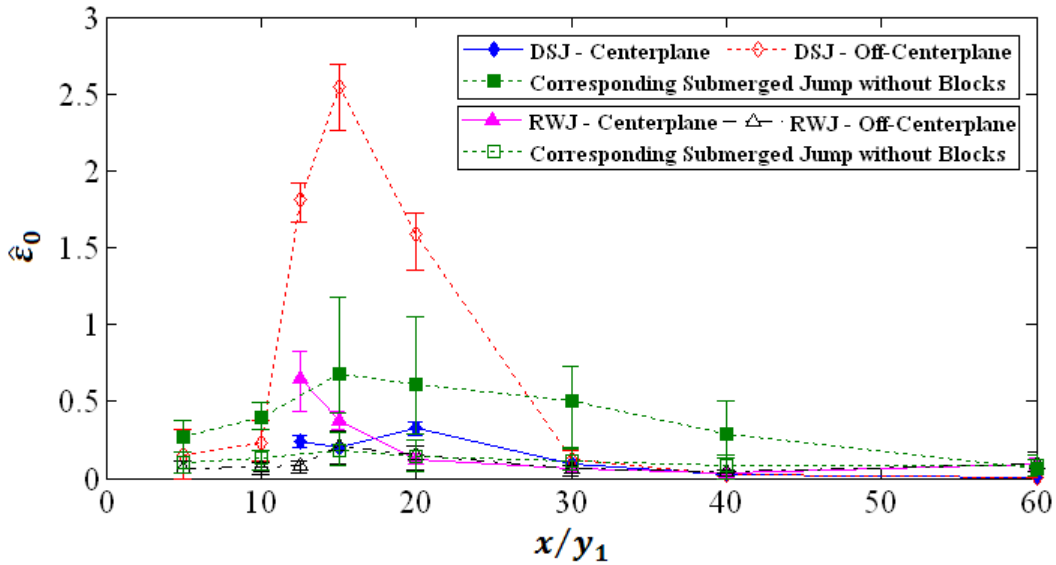


Figure 5.11 Average curves for the streamwise variation of the vertically-averaged turbulence dissipation rate. (Error bars represent the range of the computed 95% confidence limits of the runs used in the averaging.)

The difference between the two flow regimes can be clearly observed by comparing the intensities downstream of the blocks; i.e. $x/y_1 > 10$. In the DSJ flow regime, the intensities are, on average, 50% larger in the off-centerplane compared to the centerplane for $12.5 \leq x/y_1 \leq 20$. This difference between the two planes is because of a shear interface between the two which, in turn, is an indication of mixing. That is, in the centerplane, the flow deflects sharply upwards and in the off-centerplane it deflects at a smaller angle. This leads to large mean velocity differences between the two planes hence a shear layer/interface). As a result of this mixing, the difference in the intensities in the two planes becomes negligible in a short distance; i.e. for $x/y_1 \geq 30$, with magnitudes being less than the submerged jump without blocks. In the RWJ flow regime, however, the turbulence intensities are on the same order in the two planes and comparable to the submerged jump without blocks even at the furthest

station at $x/y_I=60$. This shows that a stronger mixing is created by the blocks in the DSJ flow regime compared to the RWJ regime.

Habibzadeh et al. (2013) found that, in the presence of the blocks in a submerged jump, the flow in the off-centerplane is influenced by the blocks, as well as the flow in the centerplane. They found that the maximum longitudinal mean velocity decayed more rapidly and that the jet thickness increased faster in both planes in the presence of the blocks in the DSJ regime. They also reported that the effect of the blocks on the mean flow field was more pronounced in the DSJ regime and concluded that this flow regime was more efficient at dissipating the kinetic energy of the mean flow. Based on the aforementioned results, it can be concluded that the turbulent flow field is affected by the blocks in both planes similar to the mean flow. Figure 5.9a and b clearly showed that the turbulence intensity and Reynolds stress are significantly affected by the blocks and this effect is noticeably different in the two planes. The effect of the blocks on the turbulence is concentrated in the region immediately downstream of the blocks and the difference between the two planes is larger in the DSJ regime. A similar trend was observed in the vertically-averaged turbulent kinetic energy (see Figure 5.10). That is, just downstream of the blocks in the off-centerplane of the DSJ flow regime, the turbulent kinetic energy reaches its maximum magnitude. The kinetic energy of the mean flow supplies energy of the fluctuating flow components in the form of the turbulent kinetic energy (Pope 2000). That is, if the turbulent kinetic energy increases dramatically, the mean kinetic energy is expected to decrease and if the longitudinal velocity component is the dominant velocity component, then, this velocity component (and the mean kinetic energy) would be expected to decrease significantly. This is consistent with the observations of Habibzadeh et al. (2013).

It is known that the mean flow field in the two planes of both flow regimes is disturbed by the presence of the blocks (Habibzadeh et al. 2013). The observations in Figure 5.9, Figure 5.10, and Figure 5.11 confirm that the turbulent

flow field is also disturbed by the blocks in the two planes of both flow regimes. It was found that the two planes of the RWJ flow regime have only slight differences; whereas the two planes of the DSJ flow regime exhibit considerable disparity. The energy dissipation rates are also largest in the off-centerplane of the DSJ flow regime with longer streamwise persistence. These observations explain the role of the blocks in the two flow regimes and the reason for their different behavior. That is, the turbulent kinetic energy in the DSJ regime is mostly concentrated in the off-centerplane with negligible magnitudes in the centerplane. This results in a gradient and major mixing between the two planes of this flow regime. As a result of the mixing shear interface created between the two planes, in a short distance downstream of the blocks, the kinetic energy of the flow is dissipated. The dissipation process is mainly occurring in the off-centerplane over a distance just downstream of the blocks. In the RWJ flow regime, however, the difference between the two planes is insignificant and the dissipation rate is smaller (in both magnitude and streamwise extent) compared to the DSJ flow regime. As a result, the kinetic energy of the flow persists for a longer distance with a larger magnitude compared to the DSJ flow regime.

Conclusions

The turbulent flow field in a submerged hydraulic jump with and without baffle blocks downstream of a sluice gate was experimentally studied using an ADV. It is known from an earlier study (Habibzadeh et al. 2012) that the presence of the blocks, results in the formation of two distinct flow regimes; i.e. the deflected surface jet (DSJ) and reattaching wall jet (RWJ). In addition, Habibzadeh et al. (2013) found that the mean flow in each regime is significantly influenced by the blocks and that the flow field in the centerplane and off-centerplane is significantly different due to the presence of the blocks. In this study the turbulence properties, including the longitudinal and vertical turbulence intensities, Reynolds stress, turbulent kinetic energy and energy dissipation rate per unit mass, were investigated in the two planes of both flow regimes and

compared with the corresponding submerged jump without blocks. It was observed that the turbulence in both planes was influenced by the blocks in both flow regimes. In the RWJ regime, the magnitudes of the turbulence properties were slightly different in the two planes but in the DSJ regime the differences were significant. The turbulence intensities, Reynolds stress and turbulent kinetic energy rapidly decreased just downstream of the blocks in the centerplane of the DSJ regime, which is similar to the trend observed in the mean velocities as reported by Habibzadeh et al. (2013). The turbulent kinetic energy in the off-centerplane of the DSJ regime reached its peak value just downstream of the blocks and then rapidly decreased with distance. The largest energy dissipation rates were observed in the off-centerplane of the DSJ regime with considerable magnitudes over a distance downstream of the blocks. This is coincident with the location of rapid reduction of the turbulent kinetic energy.

The significant difference in the strength of the turbulence observed between the two planes of the DSJ regime is a direct result of the blocks. In the centerplane the blocks deflect the flow sharply upwards at an angle of 85° ; while in the off-centerplane the flow is deflected upwards at a much smaller angle of 12° , and this creates large gradients in the mean velocity between the two planes. The interaction of these large mean velocity gradients with the large Reynolds stresses observed in the off-centerplane (see Figure 5.9b) results in the generation of significant amounts of turbulent kinetic energy via shear production (see Figure 5.10). Generation of turbulent kinetic energy by shear production should coincide with a decrease in the mean kinetic energy because turbulent shear production extracts energy from the mean flow (Pope 2000). In addition if the transport and buoyant production terms in the turbulent kinetic energy equation are negligible compared to the production and dissipation terms then large shear production of turbulent kinetic energy will be associated with large dissipation rates. This is what is observed downstream of the blocks in the Reynolds stress (Figure 5.9b), turbulent kinetic energy (Figure 5.10) and the dissipation rate (Figure 5.11) data

in the off-centerplane of the DSJ regime. The conclusion is that in the DSJ regime the presence of baffle blocks results in the conversion of large quantities of mean flow energy into turbulent energy followed by the dissipation of large quantities of turbulent kinetic energy. In the RWJ these processes occur but because the flow is not deflected sharply upward the mean velocity gradients and Reynolds stresses (Figure 5.9b) are smaller in magnitude resulting in less shear production (Figure 5.10) and dissipation (Figure 5.11) of turbulent kinetic energy.

In the absence of blocks, very large Reynolds stresses occur near the bed in the shear layer created by the wall-jet and these are associated with the production of significant turbulent kinetic energy and its subsequent dissipation. However, the difference is that in this case the high levels persist much further downstream compared to the DSJ regime. That is, the turbulent kinetic energy levels in the DSJ regime rapidly drop downstream of the blocks and the magnitude becomes insignificant at $x/y_I=30$. In the RWJ regime and the submerged jump without blocks, however, considerable turbulence levels persist for $x/y_I>30$ (Figure 5.9).

The results of this study demonstrate the process of energy dissipation and velocity decay in the DSJ flow regime, which has been previously reported to be more efficient than the RWJ flow regime. The longitudinal velocity in the DSJ regime rapidly drops at the blocks in the centerplane and slightly downstream of the blocks in the off-centerplane. The turbulent kinetic energy follows a similar trend and quickly decreases at the blocks. The sharp deflection of the centerplane flow associated with a mild deflection of the flow in the off-centerplane creates large velocity gradients, which result in the formation of a shear interface in the off-centerplane. As a result, large energy dissipation rates were observed in the off-centerplane of the DSJ regime. The results of this study demonstrate the efficiency of the DSJ regime in dissipating the energy of the incoming flow. That is, it is shown that, by introducing blocks to submerged jumps, the shear interface created in the DSJ regime is sufficiently strong to significantly enhance the

energy dissipation. As a result, the DSJ flow regime provides an efficient method of energy dissipation which is as effective as a free jump and can be used in practice.

References

- Abrahamsson, H., Johansson B., and Loöfdahl, L. (1997) "The turbulence field of a fully developed three-dimensional wall jet." Internal Report 97/1, Department of Thermo and Fluid Dynamics, Chalmers University of Technology, Goteborg, Sweden.
- Bendat, J. S., and Piersol, A. G. (2010). *Random Data: Analysis and Measurement Procedures*, Fourth Edition, John Wiley & Sons.
- Benedict, L. H., and Gould, R. D. (1996). "Towards better uncertainty estimates for turbulence statistics." *Experiments in Fluids*, 22, pp. 129-136
- Bhuiyan, F., Habibzadeh, A., Rajaratnam, N., and Zhu, D. Z., (2011). "Reattached Turbulent Submerged Offset Jets on Rough Beds with Shallow Tailwater." *ASCE J. Hydr. Engrg.*, 137(12), 1636-1648.
- Bradshaw, P., and Wong, F.Y.F. (1972). "The reattachment and relaxation of a turbulent shear layer." *J. Fluid Mech.*, Vol. 52, Part 1, pp. 113-135.
- Castro, I. P., and Robins, A. G. (1977). "The flow around a surface-mounted cube in uniform and turbulent streams." *J. Fluid Mech.*, Vol. 79, Part 2, pp. 307-335.
- Cea, L., Puerta, J., and Pena, L. (2007). "Velocity measurements on highly turbulent free surface flow using ADV." *Exp. Fluids*, Vol. 42, pp. 333-348.
- Chow, V. (1959). *Open-channel hydraulics*. McGraw-Hill, New York.
- Dey, S., Nath, T. K., and Bose, S. K. (2010). "Fully rough submerged plane wall-jets." *Journal of Hydro-environment Research*, 4, pp. 301-316.
- Dey, S., and Sarkar, A. (2008). "Characteristics of Turbulent Flow in Submerged Jumps on Rough Beds." *ASCE J. Engrg. Mech.*, 134(1), 49-59.
- Dey, S., and Sarkar, A. (2006). "Response of velocity and turbulence in submerged wall jets to abrupt changes from smooth to rough beds and its

application to scour downstream of an apron.” *J. Fluid Mech.*, Vol. 556, pp. 387-419.

Dey, S., Sarkar, S., Bose, S. K., Tait, S., and Castro-Orgaz, O. (2011). “Wall-Wake Flows Downstream of a Sphere Placed on a Plane Rough Wall.” *ASCE Journal of Hydraulic Engineering*, 137(10), pp. 1173-1189.

Ead, S. A., and Rajaratnam, N. (2004). “Plane turbulent wall jets on rough boundaries with limited tailwater.” *ASCE Journal of Engineering Mechanics*, 130(10), pp. 1245-1250.

Ead, S. A., and Rajaratnam, N. (2002). “Plane turbulent wall jets in shallow tailwater.” *ASCE Journal of Engineering Mechanics*, 128(2), pp. 143-155.

Efron, B. (1979). “Bootstrap Methods: Another Look at the Jackknife.” *The Annals of Statistics*, Vol. 7, No. 1, 1-26.

Efron, B., and Tibshirani, R. J. (1993). “An Introduction to the Bootstrap.” *Monographs on Statistics and Applied Probability 57*, Chapman and Hall Inc. New York.

Garcia, C. M., Jackson, P. R., and Garcia, M. H. (2006). “Confidence intervals in the determination of turbulence parameters.” *Experiments in Fluids*, 40, pp. 514-522.

Garcia, C. M., Cantero, M., Nino, Y., and Garcia, M. H. (2005). “Turbulence measurements with acoustic Doppler velocimeters.” *ASCE Journal of Hydraulic Engineering*, 131(12), pp. 1062-1073.

Goring, D. G., and Nikora, V. I. (2002). “Despiking Acoustic Doppler Velocimeter Data.” *ASCE Journal of Hydraulic Engineering*, 128(1), pp. 117-126.

Habibzadeh, A., Loewen, M. R., and Rajaratnam, N. (2013). “Mean Flow in a Submerged Hydraulic Jump with Baffle Blocks.” Accepted for publication in the *ASCE J. Engrg. Mech.*

Habibzadeh, A., Loewen, M. R., and Rajaratnam, N. (2012). “Performance of Baffle Blocks in Submerged Hydraulic Jumps.” *ASCE J. Hydr. Engrg.*, 138(10), 902-908.

Chapter 5: Turbulence Characteristics of Submerged Hydraulic Jumps with Baffle Blocks

Habibzadeh, A., Wu S., Ade F., Rajaratnam, N., and Loewen, M. R. (2011). "An Exploratory Study on Submerged Hydraulic Jumps with Blocks." *ASCE J. Hydr. Engrg.*, 137(6), 706-710.

Hager, W. H. (1992). *Energy Dissipators and Hydraulic Jump*. Kluwer, London.

Hussein, H. J., and Martinuzzi, R. J. (1996). "Energy balance for turbulent flow around a surface mounted cube placed in a channel." *AIP Phys. Fluids* 8(3), pp. 764-780.

Islam, M. and Zhu, D. (2013). "Kernel Density-Based Algorithm for Despiking ADV Data." *J. Hydraul. Eng.*, 139(7), 785-793.

Khorsandi, B., Mydlarski, L., and Gaskin, S. (2012). "Noise in turbulence measurements using acoustic Doppler velocimetry." *ASCE Journal of Hydraulic Engineering*, 138(10), 829-838.

Kresta, S., and Wood, P. (1993). "The flow field produced by a pitched blade turbine: Characterization of the turbulence and estimation of the dissipation rate.", *Chemical Engineering Science*, 48(10), pp. 1761-1774.

Kunsch, H. R. (1989). "The Jackknife and the Bootstrap for General Stationary Observations." *The Annals of Statistics*, Vol. 17, No. 3, pp. 1217-1241.

Lennon, J. M., and Hill, D. F. (2006). "Particle image velocity measurements of undular and hydraulic jumps." *ASCE Journal of Hydraulic Engineering*, 132(12), 1283-1294.

Lin, C., Hsieh, S. C., Lin, I. J., Chang, K. A., and Raikar, R. V. (2012). "Flow property and self-similarity in steady hydraulic jumps." *Exp. Fluids*, 53, pp. 1591-1616.

Liu, M., Zhu, D. Z., and Rajaratnam, N. (2004). "Turbulence structure of hydraulic jumps of low Froude numbers." *ASCE Journal of Hydraulic Engineering*, 130(6), 511-520.

Long, D., Steffler, P. M., and Rajaratnam, N. (1990). "LDA study of flow structure in submerged hydraulic jump." *J. Hydraul. Res.*, 28(4), 437-460.

Lyn, D. A., and Rodi, W. (1994). "The flapping shear layer formed by flow separation from the forward corner of a square cylinder." *J. Fluid Mech.*, Vol. 267, pp. 353-376.

Meroney, R. N., and Yang, B. T. (1971). "Wind tunnel study on gaseous mixing due to various stack heights and injection rates above and isolated structure." Fluid Dynamics and Diffusion Laboratory, Colorado State University, Fort Collins, Colorado, AEC Report No. C00-2053-6.

Mignot, E., and Cienfuegos, R. (2011). "Spatial evolution of turbulence characteristics in weak hydraulic jumps." *J. Hydraul. Res.*, 49(2), 222-230.

Mignot, E., and Cienfuegos, R. (2010). "Energy dissipation and turbulence production in weak hydraulic jumps." *ASCE Journal of Hydraulic Engineering*, 136(2), 116-121.

Misra, S. K., Kirby, J. T., Brocchini, M., Veron, F., Thomas, M., and Kambhamettu, C. (2008). "The mean and turbulent flow structure of a weak hydraulic jump." *Physics of Fluids*, 20(3), 035106.

Moffat, R. J. (1988). "Describing the Uncertainties in Experimental Results." *Experimental Thermal and Fluid Science*, Vol. 1, pp. 3-17.

Parshah, M., Sotiropoulos, F., and Porté-Agel, F. (2010). "Estimation of Power Spectra of Acoustic-Doppler Velocimetry Data Contaminated with Intermittent Spikes." *ASCE Journal of Hydraulic Engineering*, 136(6), 368-378.

Pearson, B., Krogstad, P., and van de Water, W. (2002). "Measurements of the turbulent energy dissipation rate." *Physics of Fluids*. 14(3), pp. 1288-1290.

Peterka, A. J. (1984). "Hydraulic design of stilling basins and energy dissipators." *Engineering Monograph No. 25*, 8th Ed. US Bureau of Reclamation, Denver, USA.

Politis, D. N., and White, H. (2004). "Automatic Block-Length Selection for the Dependent Bootstrap." *Econometric Reviews*, Vol. 23, No., 1, pp. 53-70.

Pope, S. (2000), *Turbulent Flows*, Cambridge University Press, New York, USA

Chapter 5: Turbulence Characteristics of Submerged Hydraulic Jumps with Baffle Blocks

Precht E., Janssen, F., and Huettel, M. (2006). "Near-bottom performance of the Acoustic Doppler Velocimeter (ADV) – a comparative study." *Aquatic Ecology* 40, pp. 481–492.

Romagnoli, M., Garcia, C. M., and Lopardo, R. A. (2012). "Signal processing technique and uncertainty analysis of ADV turbulence measurements on free hydraulic jumps." *ASCE Journal of Hydraulic Engineering*, 138(4), 353-357.

Rouse, H., Siago, T. T., and Nagaratnam, S. (1958). "Turbulence characteristics of the hydraulic jump." *J. Hyd. Div.*, 84(HY1), 1-30.

Song, S., and Eaton, J.K. (2004). "Reynolds number effects on a turbulent boundary layer with separation, reattachment, and recovery." *Experiments in Fluids*, Vol. 36, pp. 246–258.

SonTek Technical Notes, (1997). "Pulse Coherent Doppler Processing and the ADV Correlation Coefficient." 6837 Nancy Ridge Drive, Suite A, San Diego, CA 92121. 5 pp.

Svendsen, IB A., Veeramony, J., Bakunin, J., and Kirby, J. T. (2000). "The flow in weak turbulent hydraulic jumps." *J. Fluid Mech.*, Vol. 418, pp. 25-57.

Taylor, G. I. (1938). "The Spectrum of Turbulence." *Proceedings of the Royal Society of London. Series A, Mathematical and Physical Sciences*, Vol. 164, No. 919, pp. 476-490.

Velmex Inc. (2002). *VXM Stepping Motor Controller User's Manual*, Bloomfield, NY, USA.

Voulgaris, G. and Trowbridge, J. H. (1998). "Evaluation of the Acoustic Doppler Velocimeter (ADV) for Turbulence Measurements." *J. Atmos. Ocean. Technol.*, Vol. 15(1), pp. 272-289.

Wahl, T. L. (2000). "Analyzing ADV data using WinADV." *Proc. Conf. on Water Resources Engineering and Water Resources Planning and Management*, Reston, VA.

Wahl, T. L. (2003). "Discussion of 'Despiking Acoustic Doppler Velocimeter Data,' by D. Goring and V. Nikora." *ASCE J. Hydraul. Eng.* 129(6), pp. 484-487.

Chapter 5: Turbulence Characteristics of Submerged Hydraulic Jumps with Baffle Blocks

Wernersson, E., and Trägårdh, C. (2000). "Measurements and analysis of high-intensity turbulent characteristics in a turbine-agitated tank.", *Experiments in Fluids*. 28(6), pp. 532-545.

Wu, H., and Patterson, G. K. (1989). "Laser-Doppler measurements of turbulent-flow parameters in a stirred mixer." *Chemical Engineering Science*, Vol. 44, No. 10, pp. 2207-2221.

Wu, S., and Rajaratnam, N. (1996). "Transition from hydraulic jump to open channel flow." *J. Hydr. Engrg.*, 122(9), 526-528.

Wu, S., and Rajaratnam, N. (1995). "Effect of Baffles on Submerged Flows." *J. Hydr. Engrg.*, 121(9), 644-652.

Zobeyer, A.T.M.H., Jahan, N., Islam, Z., Singh, G., and Rajaratnam, N. (2010). "Turbulence characteristics of the transition region from hydraulic jump to open channel flow." *J. Hydraul. Res.*, 48(3), 395-399.

Zoubir, A. M., and Iskander, D. R. (2004). *Bootstrap Techniques for Signal Processing*, Cambridge University Press, New York.

Chapter 6: Conclusions and Recommendations for Future Research

Conclusions

The transition from a supercritical flow to a subcritical one through a hydraulic jump helps in dissipating the excess kinetic energy of the flow which could otherwise scour the downstream channel. Supercritical flows occur downstream of most hydraulic structures such as spillways, chutes, sluice gates, and drops. Hydraulic jump stilling basins are utilized in such locations to stabilize the jump, decrease streamwise extent and increase energy dissipation. The functioning of stilling basins is enhanced by introducing baffle blocks. The guidelines for designing stilling basins such as the USBR standards are based on free jump conditions disregarding the effects of submergence. However, in practice, the tailwater depth may increase; e.g. as a result of backwater from a downstream structure and submerge the jump. The objective of the current study was to investigate the effects of submergence on the performance of a submerged jump with baffle blocks downstream of a sluice gate. To achieve the goals, an experimental study was arranged in which a wide range of Froude numbers, submergence factors, and block size (height and width), location and arrangement (one-row and two-row) were covered. An acoustic Doppler velocimeter (ADV) was used to measure the three-dimensional instantaneous velocity components of the flow field.

The simplified one-dimensional momentum equation was used to derive a theoretical equation for the drag force acting on the blocks. An empirical equation was also presented for the back-up depth; i.e. the depth just downstream of the gate. The energy dissipation efficiency of submerged jumps with blocks was found to be a function of F_1 and S . The efficiency first increases with submergence, reaching its maximum, then slightly decreasing. The maximum energy dissipation efficiency of submerged jumps with blocks was shown to be more than the efficiency of the free jump, and a free jump with the same blocks at

the same F_1 . However, the difference decreases with increasing Froude number. The energy dissipation efficiency of submerged jumps with blocks is larger than that of free jumps at first but the efficiency decreases as tailwater depth increases.

Preliminary experiments using dye injection and high-speed camera revealed the fact that the two flow regimes observed in submerged jumps with two-dimensional baffle walls existed when three-dimensional baffle blocks were present. At small tailwater depths (low submergence factors), the supercritical jet, in the centerplane, was deflected by the blocks towards the water surface. The deflected jet created a bulge on the water surface at the boundary between the forward and backward flows and this flow is referred to as the Deflected Surface Jet (DSJ) regime. For large submergences, the flow in the centerplane first separated from the bed just upstream of the block face then reattached to the bed just downstream of the blocks. This flow regime is referred to as the Reattaching Wall Jet (RWJ) regime. It was observed that the performance of the blocks was different in these two flow regimes. Empirical equations were derived to estimate S_1 and S_2 the critical values of the submergence factor that predict which flow regime will occur. These empirical equations were found to predict the flow regime accurately 85% of the time. The DSJ regime, which occurred at smaller submergence factors, was found to be the more efficient in terms of energy dissipation than the RWJ regime; since the energy dissipation efficiency decreases as S increases. In both flow regimes, the effect of the height, width, location and number of rows of the blocks on energy dissipation efficiency was found to be insignificant. However, these parameters had a significant influence on the flow regime. When the blocks are further away from the gate; e.g. for $x_b/y_1=40$, the formation of the RWJ regime was prevented at all F_1 and S values within the studied range. Employing a second row of blocks or narrower blocks also increased the magnitude of the submergence factor required for the formation of the RWJ regime. In practice if a submerged jump with blocks is to be used as an energy dissipator, the designer should ensure that the flow is in the DSJ regime.

The block characteristics should be specified so that for the design tailwater depth, the critical submergence factor for the DSJ regime (S_I), from Eq. (3-3), is greater than the design submergence factor.

The mean flow fields showed that, in the centerplane, the deflection of the incoming supercritical stream at the blocks occurs at a sharper angle in the DSJ flow regime compared to the RWJ regime. In the DSJ flow regime, the deflection of the jet in the centerplane approaches 85° ; while the deflection angle in the RWJ flow regime, with the same Froude number, did not exceed 50° . The deflection angle of the flow in the off-centerplane at the same station was approximately 12° in both flow regimes. The difference between the deflection angles of the flow in the centerplane and the off-centerplane results in a large shear interface between the two planes. The maximum longitudinal velocity in the centerplane in both flow regimes is rapidly reduced at the blocks. In the DSJ regime, it takes a distance of about five block heights for the maximum velocity to drop by approximately 80%. This reduction of the maximum velocity is gradual in the RWJ regime; e.g. at $x/y_I=20$ the dimensionless maximum velocity u_m/U_I in the DSJ regime is approximately 30% less than that in the RWJ regime. It was observed that the reduction of u_m in the off-centerplane flow in both flow regimes follows a similar pattern to the centerplane but the reduction is delayed; i.e. the reduction of u_m in the off-centerplane is both shifted and at a slower rate compared to the centerplane. However, further downstream for $x/y_I \geq 20$, the reduction of u_m in both shows has a similar pattern. The width of the submerged jet was studied in terms of the jet half-width and it was observed that, in both flow regimes, the jet width is comparable to that of the wall jet upstream of the blocks. At the blocks, however, the width in the off-center plane increases sharply and reaches magnitudes which are larger than those in the corresponding free hydraulic jumps. In the centerplane of both flow regimes the flow is deflected upwards by the blocks and does not behave like a wall jet. The blocks cause the

jet-like flow in the off-centerplane to expand 5.8 and 4.3 times faster than a wall jet or submerged jump, in the DSJ and RWJ flow regimes respectively.

This experimental study of submerged hydraulic jumps with baffle blocks showed that the flow in the DSJ regime is more effective in reducing the longitudinal component of the velocity than the RWJ regime. This DSJ flow regime was also found to have a shorter streamwise length; i.e. a shorter recirculating region. The length of the RWJ flow regime was comparable to that of the corresponding submerged jump without blocks. That is, a shorter stilling basin is required for the DSJ flow regime compared to the RWJ regime, and, as a result, the DSJ regime imposes less construction costs. This supports the conclusion that a submerged hydraulic jump with baffle blocks is an efficient method of dissipating the excess kinetic energy of the incoming supercritical jet as long as the DSJ flow regime is maintained. Hydraulic jump stilling basins can operate effectively under submerged conditions, if they are designed such that the DSJ regime occurs over the entire range of tailwater depths that are likely to occur.

The study of the turbulent flow field showed that both planes in the two flow regimes are influenced by the presence of the blocks. The turbulence intensities and turbulent kinetic energy drop at the blocks and the rate of this reduction is larger in the DSJ flow regime. It is shown that, in the DSJ regime, the sharp deflection of the centerplane flow associated with a mild deflection of the flow in the off-centerplane creates a large velocity gradient which, in turn, results in a considerable mixing shear interface. As a result, the mean and turbulent kinetic energies are rapidly dissipated just downstream of the blocks. The largest energy dissipation rates were observed in the off-centerplane of the DSJ regime, which decreased the turbulence levels in a short distance. In the RWJ regime and the submerged jump without blocks, however, the turbulence levels persist for a long distance.

Chapter 6: Conclusions and Recommendations

The results of this study showed that the presence of the blocks in a submerged hydraulic jump can enhance the energy dissipation provided that the DSJ flow regime occurs. In the DSJ regime, large velocity gradients created by the deflection of the incoming flow, result in a shear mixing which rapidly decays the velocity and turbulent kinetic energy in as short distance. It is found that the DSJ flow regime of submerged hydraulic jumps with blocks can be used as an efficient energy dissipator. Equations were provided to be used in practice such that the design of the blocks ensures the occurrence of the DSJ regime under a practical range.

Recommendations for Future Research

The following is a list of recommendations for future studies:

- Numerical modeling of a submerged hydraulic jump with baffle blocks
- Experimental study of the effects of submergence on hydraulic jumps downstream of other hydraulic structures such as spillways
- Study of the effects of chute blocks and end sill on the flow pattern under submerged flow conditions
- Experimental study of the fluctuating pressure field acting on the bed and blocks.

Appendix 1: Some Observations on Submerged Hydraulic Jumps with Blocks¹

Introduction

Hydraulic jumps occur in water distribution and irrigation networks downstream of hydraulic structures such as spillways, sluice gates, and drops. These structures are usually designed for a specific tailwater depth corresponding to the design discharge, so that the jump is restricted to a length not more than the length of the stilling basin. However, the flow rate and hence the tailwater depth are subject to change; as a result, the location of the jump can vary. Usually a tailwater depth in excess of the one required for the free jump is maintained to ensure that the jump will not be swept away. If the flow rate is larger than the design discharge, the tailwater depth will be greater than the one required for a free jump. These situations are common in low head hydraulic structures including low diversion dam spillways and gates. Under such conditions the hydraulic jump will be submerged. The purpose of stilling basins downstream of these types of hydraulic structures is to dissipate the excess kinetic energy of the supercritical flow in a hydraulic jump. When the jump is submerged, the energy dissipation rate, being a function of submergence, will be less than that of the free jump (Rajaratnam 1967). In submerged jumps the flow behavior, including jet expansion and streamwise velocity decay, differ significantly from a free jump (Rajaratnam 1967).

Baffle walls and blocks are often used to stabilize the jump, decrease its length and to increase energy dissipation. Performance of baffle walls and blocks in free hydraulic jumps has been studied by numerous researchers (e.g. Rajaratnam 1964, Basco and Adams 1971, Rajaratnam and Murahari 1971, Ohtsu

¹ A version of this chapter has been published. Habibzadeh, A., Loewen, M. R., and Rajaratnam, N. (2011), *34th Biennial Congress of the International Association for Hydro-Environment Engineering and Research (IAHR)*, Proceedings CD pp. 2460-2467, 26 June to 6 July, Brisbane, Australia.

Appendix 1: Some Observations on Submerged Hydraulic Jumps with Blocks

et al. 1991, and Hager 1992). Submerged hydraulic jumps have also been the subject of many papers (e.g. Long et al. 1990 and Dey and Sarkar 2008). However, submerged jumps with baffles (walls or blocks) have received much less attention. Wu and Rajaratnam (1995) studied submerged flows with baffle walls and observed that the flow could be classified into two regimes. For low submergences the incoming stream, after impacting the baffle wall, is deflected towards the water surface and a region of circulating flow was established. This type of flow was called the “Deflected Surface Jet” (DSJ) regime. When the tailwater depth was larger than a certain amount, the incoming jet was first deflected away from the bed and then impinged on the bed again. This flow regime was called the “Reattaching Wall Jet” (RWJ). The growth of the jet and the distribution of the velocity in the jet were studied. Habibzadeh et al. (2010) conducted a preliminary study on the flow properties of submerged jumps with baffle blocks. A general theoretical equation for the drag force on blocks was derived. The energy dissipation in submerged jumps with blocks was also compared with free jumps. The energy dissipation efficiency, defined as the ratio of the dissipated energy to the initial energy of the supercritical flow in the submerged jump to that in the free jump, was found to be a function of submergence with the maximum efficiency being slightly larger than in the corresponding free jump. The energy dissipation efficiency was found to gradually decrease as submergence increased.

In the present paper, mean flow properties of a submerged jump are studied for one Froude number with two submergences. Some observations of the mean velocity field within the jump are also reported.

Experimental Setup

The experiments were conducted in a horizontal flume with a width of 46.7 cm, height of 60 cm and length of 7.5 m. The flume had glass side walls and an aluminum bed. The flow rate was measured using a magnetic flowmeter in the

Appendix 1: Some Observations on Submerged Hydraulic Jumps with Blocks

supply pipe. The flow first entered a head tank equipped with a sluice gate with a streamlined lip and an opening of $y_l=1.9$ cm. A tailgate at the downstream end of the flume was used to adjust the tailwater depth. A PVC sheet was placed on the aluminum bed to facilitate mounting of blocks. A schematic plan and longitudinal view of the experimental set-up is shown in Figure A1.1.

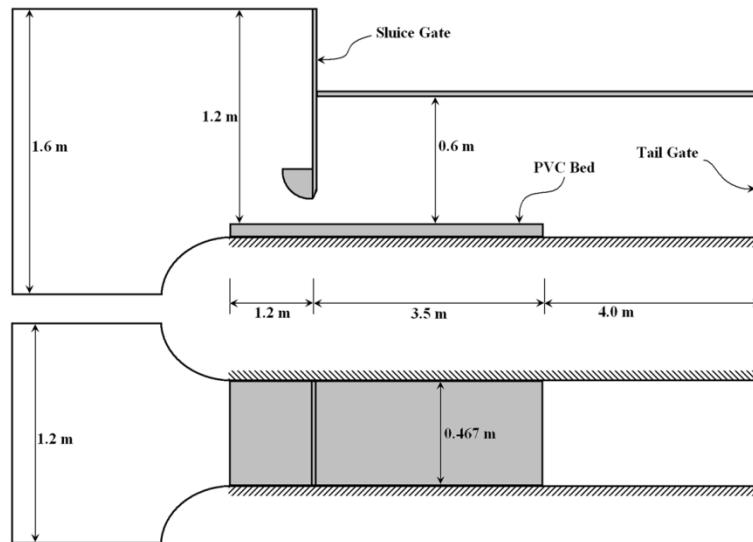


Figure A1.1 Schematic view of the experimental set-up.

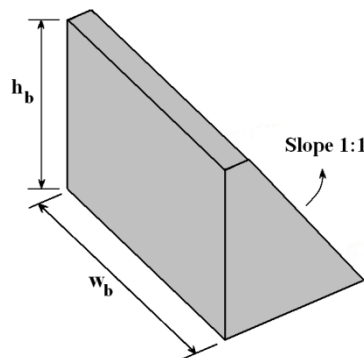


Figure A1.2 Shape and parameters of the blocks.

Three dimensional baffle blocks were made of PVC sheets following the standard designs of USBR stilling basins (Peterka 1984). The block height was set equal to $h_b=3.81$ cm which corresponds to a ratio of $h_b/y_l=2$. The width of the blocks and the space between them was set to $w_b=w_s=4.5$ cm; i.e. five blocks were required corresponding to a blockage ratio of 0.5. The blocks were mounted on

Appendix 1: Some Observations on Submerged Hydraulic Jumps with Blocks

the PVC bed at a distance of $x_b=19.1$ cm from the gate corresponding to $h_b/y_1=10$. The shape of the blocks as well as their dimensions is shown in Figure A1.2.

A point gauge with an accuracy of 0.1 mm was used to measure the water surface profiles. A NorTek Vectrino+ Acoustic Doppler Velocimeter (ADV) was used to measure 3D velocities at a sampling frequency of 100 Hz. The raw data was filtered using the method of Goring and Nikora (2002) to remove spikes prior to calculation of the three velocity components.

Two experiments were conducted for a gate Froude number of $F_1 \approx 4.6$ and submergence factors of $S=0.52$ and 1.73. Here, submergence factor is defined as $S=(y_t - y_2)/y_2$, where y_t is the tailwater depth and y_2 is the jump sequent depth based on the Belanger equation.

Results and Analysis

At the Froude number studied, it was observed that for low submergences, the incoming jet was deflected towards the water surface, similar to the flow over a baffle wall (Wu and Rajaratnam 1995). Although in the case of 3D baffle blocks there is a gap between adjacent blocks but the main flow field behaved like the 2D baffle wall case where the flow impacts a 2D continuous obstacle. This flow regime is referred to as the Deflected Surface Jet (DSJ) regime. In DSJ regime, the flow consisted of a small region of re-circulating flow which extended from the gate up to the blocks. Figure A1.3 shows several flow visualization images created using dye-injection. Dye was injected at three different locations; i.e. upstream of the blocks in the $z=0$ plane, on the block centerline (Figure A1.3a and d), upstream of the blocks at the center of the gap between the blocks ($z=4.5$ cm plane) (Figure A1.3b and e), and behind the middle block (c and f). It can be observed in Figure 3a, b, and c that in all three locations there is rapid mixing of the dye downstream of the blocks.

For larger submergences, it was observed that the flow separates from the bed after impacting the blocks. The flow then re-attaches to the bed downstream

Appendix 1: Some Observations on Submerged Hydraulic Jumps with Blocks

of the block and continues to grow as a re-attached wall jet. This was similar to the behavior observed in flow over a baffle wall (Wu and Rajaratnam 1995) where it was referred to as the “Reattaching Wall jet” (RWJ) regime. The separation and reattachment of the flow is visualized in Figure A1.3d where the dye is mixed over only a small region around the block compared with Figure 3a where the dye rapidly mixes over the entire depth. Figure A1.3e shows the gradual expansion of the jet in the gap between the blocks. Comparing with Figure A1.3b, it is obvious that the growth of the jet is much more gradual in the RWJ regime. Finally, in Figure A1.3f it can be seen that dye injected behind the block is trapped in a small region representing the standing eddy.

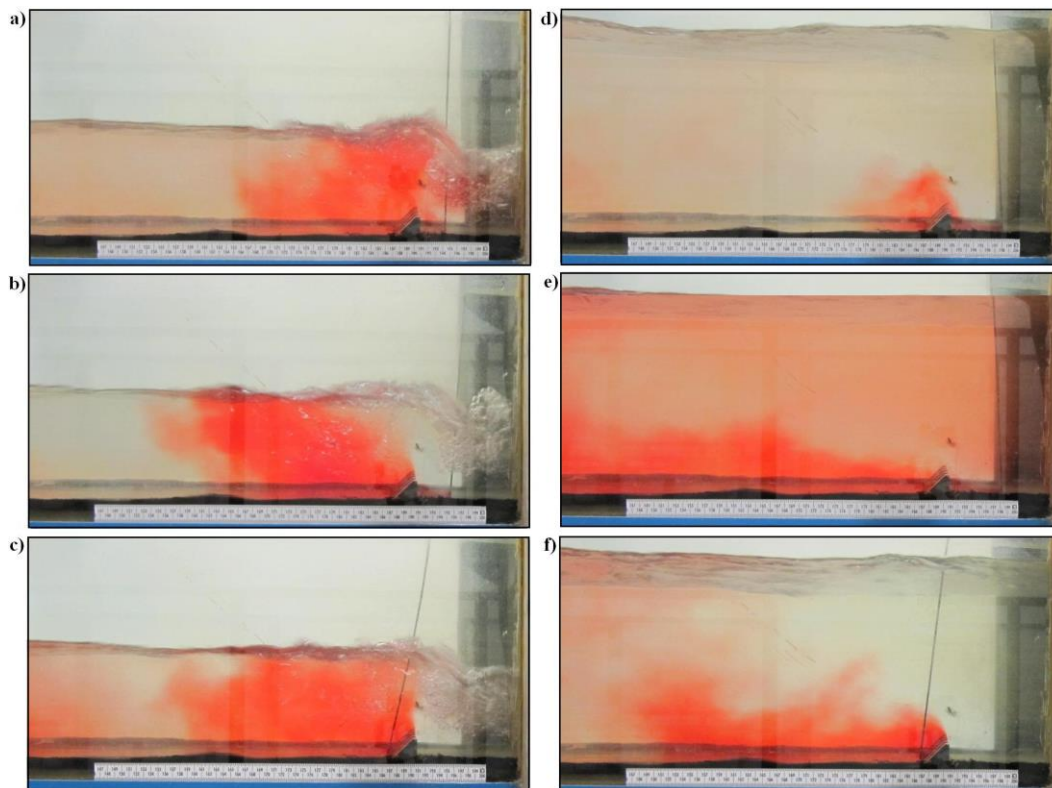


Figure A1.3 Flow visualization for DSJ (a, b, and c) and RWJ regimes (d, e, and f) (dye injected in the $z=0$ plane (a and d), $z=4.5$ cm plane (b and e), and behind the block (c and f)).

Longitudinal velocity (u) profiles for the DSJ flow regime are shown in Figure A1.4 for $F_1=4.59$ and $S=0.52$. In this figure, the u velocity profiles are plotted at six sections downstream from the gate along the centerline of the flume

Appendix 1: Some Observations on Submerged Hydraulic Jumps with Blocks

($z=0$, this plane coincides with the center of the middle block) and along the plane passing through the center of the space between blocks ($z=4.5$ cm).

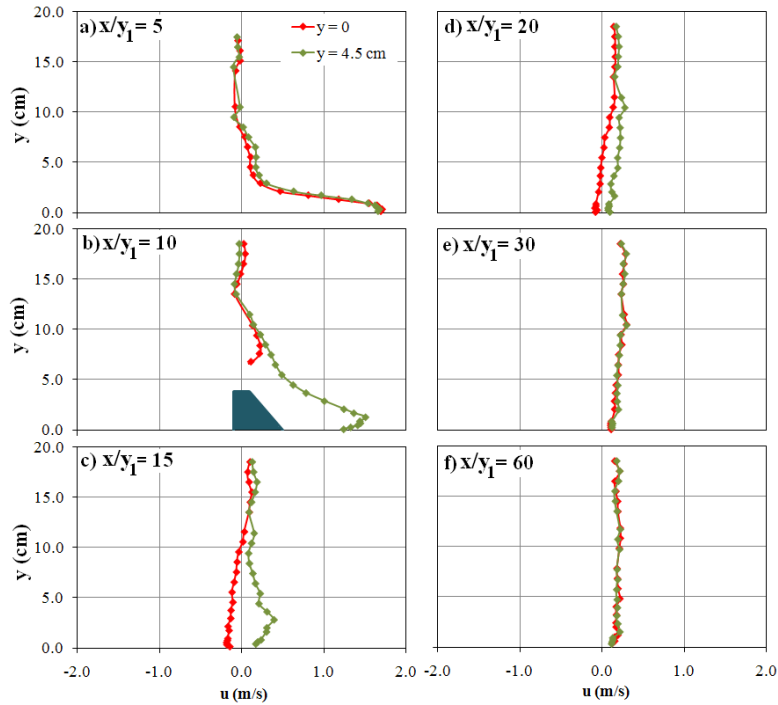


Figure A1.4 u -velocity profiles of the DSJ regime for $F_1=4.59$ and $S=0.52$ at $z=0$ and $z=4.5$ cm

The flow in the gap diffuses similar to a wall jet (see Figure A1.4); however, along the block centerline the jet decelerates and rapidly decays (see Figure A1.4). It is evident that the flow around the block is three-dimensional but upstream of the block and downstream of it at a distance of $x/y_1 \geq 30$, there is no transverse variation in the longitudinal velocity i.e. the flow is two-dimensional. Along the centerline, the supercritical jet impacts the block front face and deflects towards the water surface. This results in an almost 90° change in flow direction which is associated with a high shear layer above the block. This deflected jet entrains fluid at the block crest, creating a backward flow right above the block (see Figure A1.4b). This phenomenon shapes the longitudinal velocity profile above the block (see Figure A1.4b). There is a recirculating region downstream of the block which extends up to $x/y_1=20$.

Appendix 1: Some Observations on Submerged Hydraulic Jumps with Blocks

The streamlines for the DSJ regime in the planes at $z=0$ and $z=4.5$ cm are shown in Figure A1.5. In the $z=4.5$ cm plane, a recirculating region can be observed which extends up to the blocks. Downstream of the blocks, the flow starts recovering to the gravity driven flow. However, the flow features on the centerline are quite different. The deflected (almost) vertical jet entrains fluid from both upstream and downstream sides of the blocks. This creates an eddy couple joined together above the blocks. Obviously, the size of eddy upstream of the block is restricted by the gate; hence, an asymmetric flow pattern is formed. The upstream eddy is identical in both planes while the flow downstream is different in the two planes. In the $z=4.5$ cm plane the jet continues to expand similar to a wall jet but at a much faster rate. In the $z=0$ cm -plane, the deflected jet, after hitting the water surface, plunges towards the bed forming a larger eddy which includes the recirculating zone behind the block.

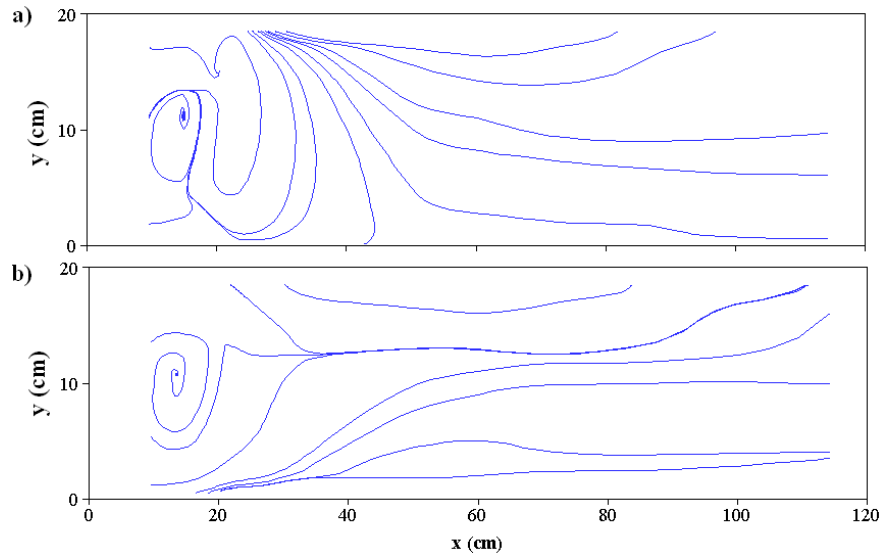


Figure A1.5 Sketch of the streamlines of the DSJ regime at (a) $z=0$ and (b) $z=4.5$ cm

Considering the flow further downstream; i.e. $x \approx 50$ cm in Figure A1.5, it can be seen that the flow in the $z=4.5$ cm plane is inclined towards the water surface following the trajectory of a two dimensional wall jet. However, the flow in the centerline plane is inclined in the opposite direction; i.e. towards the bed. This pattern reveals the fact that the flow just downstream of the block is three

Appendix 1: Some Observations on Submerged Hydraulic Jumps with Blocks

dimensional and is associated with regions of very high shear. These shear layers increase the mixing which results in high energy dissipation. This transition occurs in a short length due to high mixing and further downstream at $x/y_1 \geq 30$, the flow lacks any transverse variation and becomes a two dimensional flow. In this flow regime, waves of small amplitudes were travelling downstream of the jump which resulted in a fluctuating tailwater. This may be a direct result of the transport of turbulence downstream.

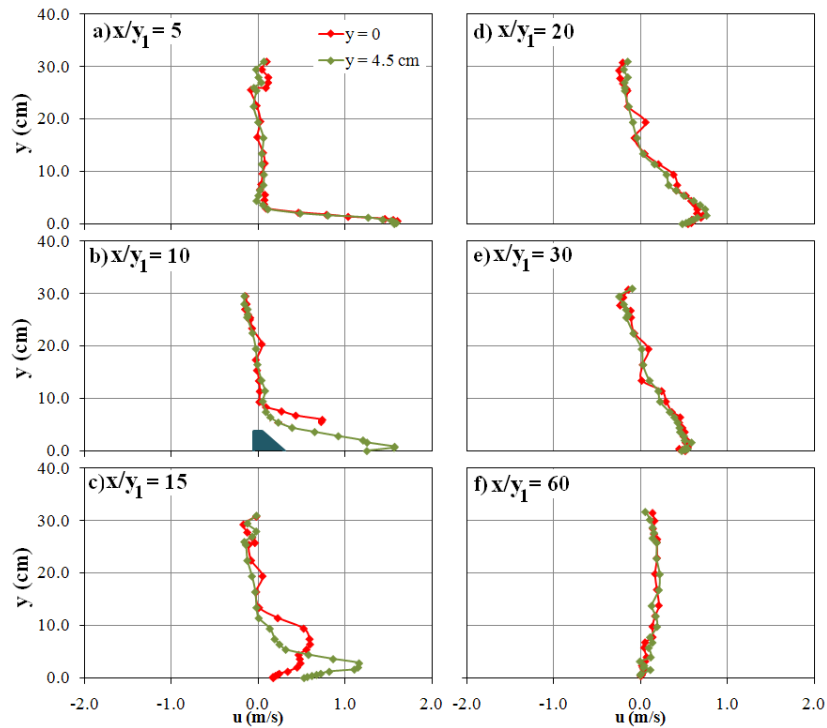


Figure A1.6 u -velocity profiles of the RWJ regime ($F_1=4.63$, $S=1.73$) for $z=0$ and $z=4.5$ cm

The RWJ flow regime was observed for a Froude number of $F_1=4.63$ and a submergence of $S=1.73$ for which the longitudinal velocity profiles are shown in Figure A1.6. The flow reattachment was associated with a large recirculating region on top. This surface roller had a length of approximately one meter. A small confined eddy was also formed downstream of the block extending up to a length of approximately 10 cm corresponding to approximately two block heights.

Appendix 1: Some Observations on Submerged Hydraulic Jumps with Blocks

The supercritical jet behaved similar to a wall jet upstream of the block (Figure A1.6a) and continued to expand like a wall jet along the $z=4.5$ cm plane. While in the center-plane, the flow first detached from the bed (Figure A1.6b) then reattached to the bed (Figure A1.6c) and after a short length a reattached wall jet is developed with negligible transverse variation (Figure A1.6d, e, and f).

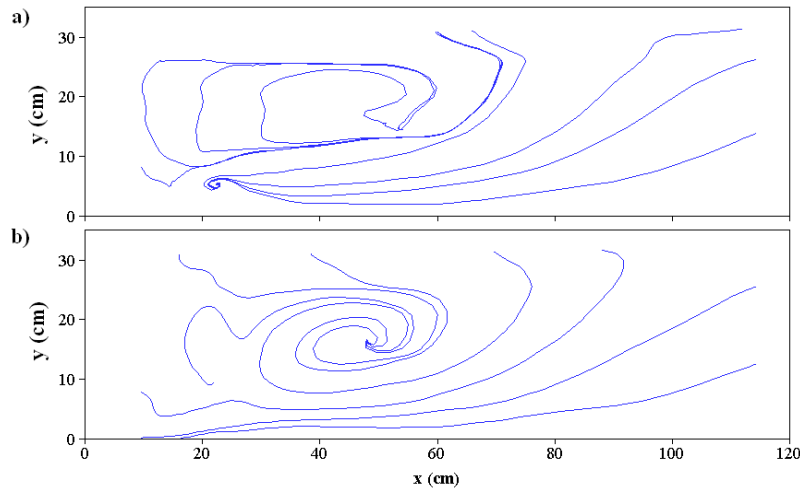


Figure A1.7 Sketch of the streamlines of the RWJ regime for (a) $z=0$ and (b) $z=4.5$ cm

Figure A1.7 shows the streamlines for the RWJ regime in two planes at $z=0$ (centerline) and $z=4.5$ cm. The flow patterns in the two planes are very similar except for the flow in the vicinity of the block. The flow in the $z=4.5$ cm plane behaves like a wall jet similar to the DSJ regime. On the centerline, however, the flow is significantly influenced by the block. The jet impacts the block and is separated from the bed but just downstream of the block, it reattaches to the bed. Downstream of the reattachment point, the flow expands similar to a wall jet. This flow regime is associated with an almost horizontal water surface (negligible gradient). The waves travelling downstream of the jump are also smaller in amplitude than the DSJ regime. Comparing the flow in the two planes in Figure A1.7, it was concluded that the flow pattern is almost identical and the surface roller is slightly altered by the presence of the block. This means that the flow recovers to a two dimensional flow in a much shorter length. This indicates that the block has only a minor effect on the flow. This is the case for large

submergences (RWJ regime) where the energy dissipation efficiency of the flow is reduced (Habibzadeh et al., 2010).

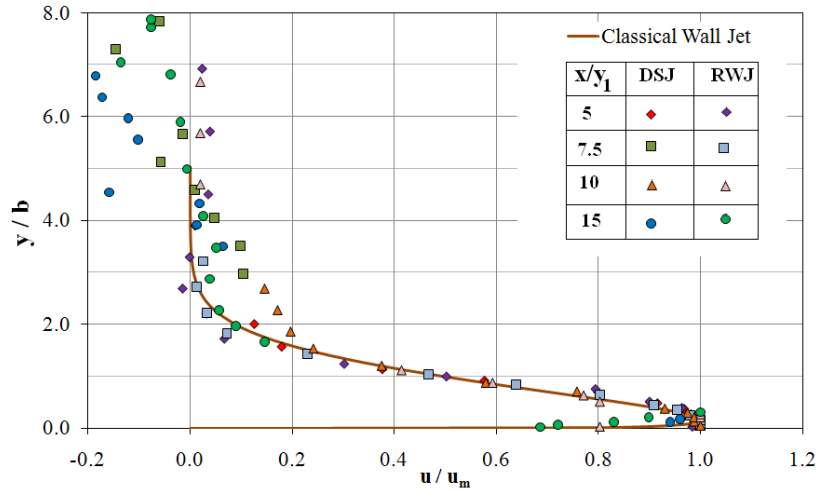


Figure A1.8 Nondimensional velocity profiles along the $z=4.5$ cm plane

The longitudinal velocity profile in turbulent jets can be presented in a nondimensional form if the maximum velocity u_m is used as the velocity scale and the jet half-width b (height at which $u=u_m/2$ and velocity gradient is negative) is used as the vertical length scale (Rajaratnam 1976). Such a plot is presented in Figure A1.8. This Figure shows the dimensionless velocity profiles for the two flow regimes in the $z=4.5$ cm plane. The curve for the wall jet is also shown in this figure. It can be observed that the flow in this plane closely follows the wall jet trend; i.e. velocity profiles are self-similar. The velocity distribution deviates from the wall jet curve near the water surface due to the presence of the surface roller.

To study the three dimensional features of the flow, the transverse velocity (v component) was investigated for both DSJ and RWJ regimes in the $z=4.5$ cm plane. The transverse velocity was significant only in the vicinity of the block. Just downstream of the block, there is a region of large transverse flow in both regimes. In this region, the flow is deflected towards the recirculating region behind the block by the pressure gradient (Coanda effect), resulting in a highly

Appendix 1: Some Observations on Submerged Hydraulic Jumps with Blocks

three dimensional flow. For the DSJ regime, this region extends further downstream compared to the RWJ regime. The vertical extent of the significant transverse velocity region is also larger in the case of DSJ flow. As mentioned before, for larger submergences; i.e. for RWJ regime, the influence of the block on flow characteristics is much less noticeable than in the DSJ regime. In the RWJ regime the only effect of the blocks is to temporarily detach the jet from the bed. And slightly downstream of the block, the transverse velocity decays and the flow becomes two dimensional.

The decay of the maximum velocity along the streamwise direction of flow occurs more gradually in the case a submerged jump compared to a wall jet. It was observed that the maximum longitudinal velocity is drastically reduced at the block section. The flow experiences high mixing which results in a faster expansion of the jet which in turn increases the rate of velocity decay. Further downstream of the block, the maximum velocity was much smaller than in a wall jet. For $x/y_j \geq 20$ the maximum velocity became negligible; i.e. open channel flow was established. Based on these results, it can be concluded that the use of baffle blocks significantly accelerates the decay of the maximum velocity which otherwise would be an unfavorable characteristic of submerged jumps.

The supercritical jet in a submerged jump expands at a slower rate compared to a wall jet, in addition to having a slower rate of velocity decay. This means that the maximum velocity in submerged jumps prevails for a longer distance while occurring at a closer distance from the bed. It was observed that the jet expands much faster than in a wall jet. The deviation of the half-width of the jet from the equation for a wall jet starts to be significant at the block section and continues to increase further downstream. After a certain distance downstream of the block, the jet becomes completely diffused and the flow recovers to a gravity driven flow. The rate of expansion is slightly faster for the DSJ regime. Considering this, it can be deduced that the baffle blocks cause the maximum

Appendix 1: Some Observations on Submerged Hydraulic Jumps with Blocks

velocity to decay more rapidly and they also cause faster expansion of the supercritical jet in submerged jumps.

Summary and Conclusion

Two experiments were conducted at a Froude number of approximately 4.6 and submergence factors of 0.52 and 1.73 to study the mean flow field in submerged hydraulic jumps with baffle blocks. It was observed that at the lower submergence, the flow forms a deflected surface jet defined as the DSJ regime. The DSJ consists of a small surface roller confined by the gate and block followed by a large recirculating region downstream of the block. At the higher submergence the flow at a formed a reattaching wall jet defined in the centerline plane. This flow behavior is defined as the RWJ regime. In both regimes the flow in a plane passing through the space between blocks, expands similar to a wall jet but with a faster rate of expansion. The flow behind the block experiences a high level of variation in three dimensions which was most significant in the DSJ regime. In the RWJ regime the three dimensional flow features were limited to a small standing eddy behind the block which had a height approximately equal to the block height and a length of two to three times the block height. By comparison, the DSJ regime had a large region of three-dimensional flow which resulted in larger mixing interface. Based on the observations, submergence influences the flow behavior to a large extent. For low submergence; i.e. DSJ regime, the flow field is highly three dimensional while for large submergence (RWJ regime) the three dimensional flow features are limited to a small region behind the blocks. Reduced three-dimensionality of the flow results in less mixing which in turn results in lower energy dissipation efficiency.

References

Basco, D. R., and Adams, J. R. (1971). Drag forces on baffle blocks in hydraulic jumps. *J. Hyd. Div.*, 97(HY12), 2023-2035.

Appendix I: Some Observations on Submerged Hydraulic Jumps with Blocks

- Dey, S., and Sarkar, A. (2008). Characteristics of Turbulent Flow in Submerged Jumps on Rough Beds. *J. Engrg. Mech.*, 134(1), 49-59.
- Goring, D. G., Nikora, V. I. (2002). Despiking acoustic doppler velocimeter data. *J. Hydr. Engrg.*, 128(1), 117-126.
- Habibzadeh, A., Wu S., Ade F., Rajaratnam, N., and Loewen, M. R. (2010). An Exploratory Study on Submerged Hydraulic Jumps with Blocks. Accepted for publication in the ASCE *J. Hydr. Engrg.*
- Hager, W. H. (1992). *Energy dissipators and hydraulic jump*. Kluwer, London.
- Long, D., Steffler, P. M., and Rajaratnam, N. (1990). LDA study of flow structure in submerged hydraulic jump. *J. Hydraul. Res.*, 28(4), 437-460.
- Ohtsu, I., Yasuda, Y., and Yamanaka, Y. (1991). Drag on vertical sill of forced jump. *J. Hydraul. Res.*, 29(1), 29-47.
- Peterka, A. J. (1984). *Hydraulic design of stilling basins and energy dissipators*. Engineering Monograph No. 25, 8th Ed. US Bureau of Reclamation, Denver, USA.
- Rajaratnam, N. (1976). *Turbulent Jets*. Elsevier Scientific Publishing Co., Amsterdam, The Netherlands.
- Rajaratnam, N. (1967). *Hydraulic Jumps*. *Advances in Hydroscience* Vol. 4, Academic Press Inc., 197-280.
- Rajaratnam, N. (1964). The forced hydraulic jump. *Water Power*, Part I - January and Part II - February.
- Rajaratnam, N., and Murahari, V. (1971). A contribution to forced hydraulic jumps. *J. Hydraul. Res.*, 9(2), 217-240.
- Wu, S., and Rajaratnam, N. (1995). Effect of Baffles on Submerged Flows. *J. Hydr. Engrg.*, 121(9), 644-652.

Appendix 2: Data Quality and Analysis

*Error Analysis*¹

A series of experiments were conducted in which measurements of the tailwater depth, back-up depth and discharge were repeated to estimate the uncertainty associated with these measurements. The standard deviation of the measured values was used to estimate the uncertainty of the data. It was found that the discharge could be measured with an uncertainty of ± 0.2 L/s. The uncertainties in the tailwater (y_t) and back-up depth (y_3) were found to be ± 0.05 cm and ± 0.10 cm, respectively. Measurements of the gate opening and the flume width were accurate to ± 0.01 cm and ± 0.14 cm, respectively. These uncertainties propagate to the dependent variables and the magnitude of these errors was used to assess the statistical significance of the results. The propagated error in S was calculated to be ± 0.02 . In terms of the repeatability of the experiments, it was observed that the gate Froude number could be reproduced with an accuracy of ± 0.05 , which corresponds to errors in the magnitude of F_l of less than 2%.

ADV Measurements

Data Quality

The ADV measures the Doppler shift between the transmitted and reflected acoustic waves and converts this into velocity. Along with velocity measurements, other parameters are computed by the ADV software (Vectrino) including the correlation coefficient (COR) and the signal-to-noise-ratio (SNR). The COR is a data quality parameter and the SNR is a measure of signal strength compared to the background noise (SonTek 1997). For mean velocity measurements, 30% and 5 dB are the recommended minimum recommended

¹ A version of this sub-section has been published in: Habibzadeh, A., Wu, S., Ade, F., Rajaratnam, N., and Loewen, M. R., *ASCE Journal of Hydraulic Engineering*, 137(6), 706-710, June 2011. DOI: [http://dx.doi.org/10.1061/\(ASCE\)HY.1943-7900.0000347](http://dx.doi.org/10.1061/(ASCE)HY.1943-7900.0000347)

Appendix 2: Data Quality and Analysis

values for COR and SNR, respectively (SonTek 1997). When the ADV is being used in clear water, seeding particles can be used to improve the SNR. The particles act as acoustic wave scattering targets and improve the acoustic reflections from water and increase SNR values. Spherichel[®] (Potters Industries LLC, Valley Forge, PA, USA) was used as the seeding particle in this project. This seeding material consists of hollow glass spheres with a median diameter of 10 μm and a density of 1100 kg/m^3 . It was observed that without the seeding particles, the SNR values were not satisfactory; i.e. typically less than 10 dB. As a result, approximately 5 kg of Spherichel[®] was added to the sump tank which had a volume of 300 m^3 , resulting in a seed concentration of 0.0167 kg/m^3 .

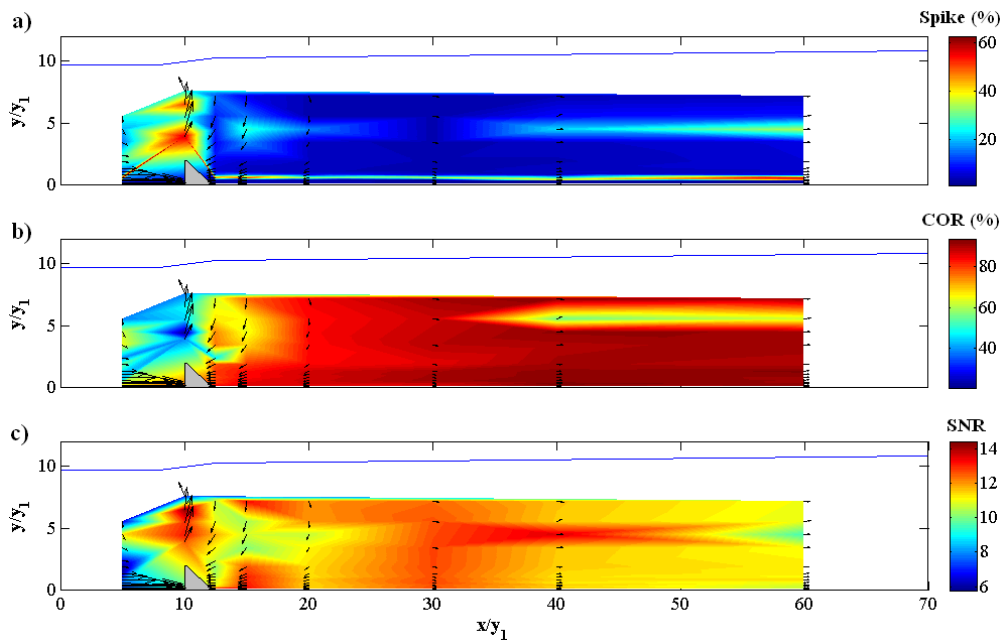


Figure A2.1 Distribution pattern for the spikes (a), correlation coefficients (b), and signal-to-noise ratios (c) of the u-velocity in the centerplane of the DSJ flow regime (run BB3).

The distribution of the spikes, correlation coefficients and signal-to-noise ratios for the u-velocity of the DSJ flow regime are shown in Figure A2.1 and Figure A2.2 for the centerplane and off-centerplane, respectively. It can be observed in these figures that the low-quality data; i.e. large percentage of spikes, low COR percentage and low SNR values, are concentrated at stations upstream

Appendix 2: Data Quality and Analysis

of the blocks and in the vicinity of the blocks. These regions are the locations where larger turbulence intensities were also observed. This is expected because it is known that the ADV performs poorly in such regions.

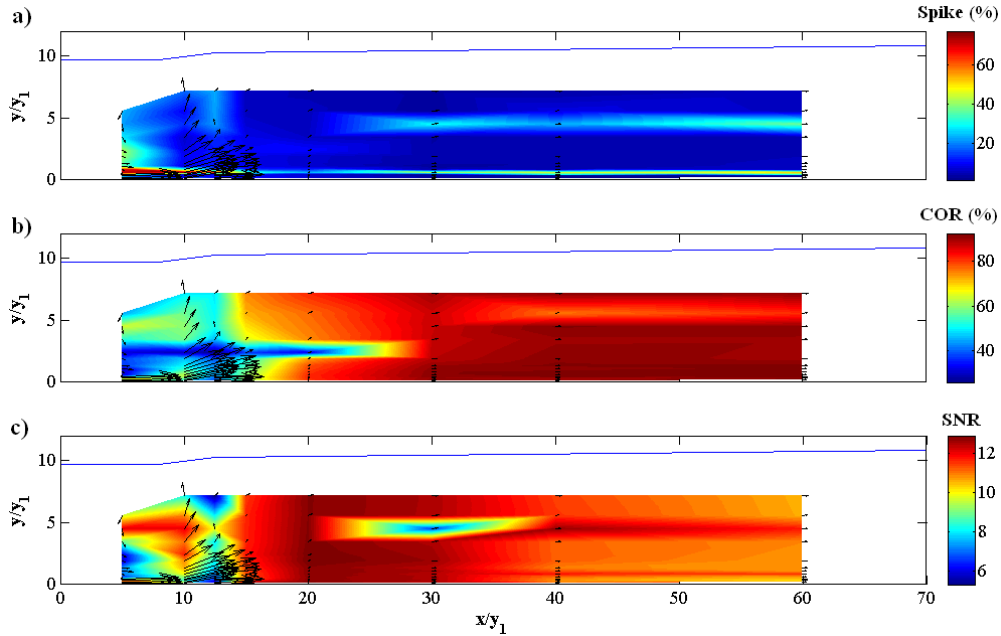


Figure A2.2 Distribution pattern for the spikes (a), correlation coefficients (b), and signal-to-noise ratios (c) of the u-velocity in the off-centerplane of the DSJ flow regime (run BB3).

A comparable diagram is shown for the distribution of the spikes, COR and SNR for the u-velocity of the RWJ flow regime in Figure A2.3 and Figure A2.4 for the centerplane and off-centerplane, respectively. Similar to the DSJ regime, low-quality data are mainly observed in the regions around the blocks. That is, the regions where the deflection and reattachment of the jet occurs have larger turbulence intensities and velocity gradients which reduce the performance of the ADV.

Appendix 2: Data Quality and Analysis

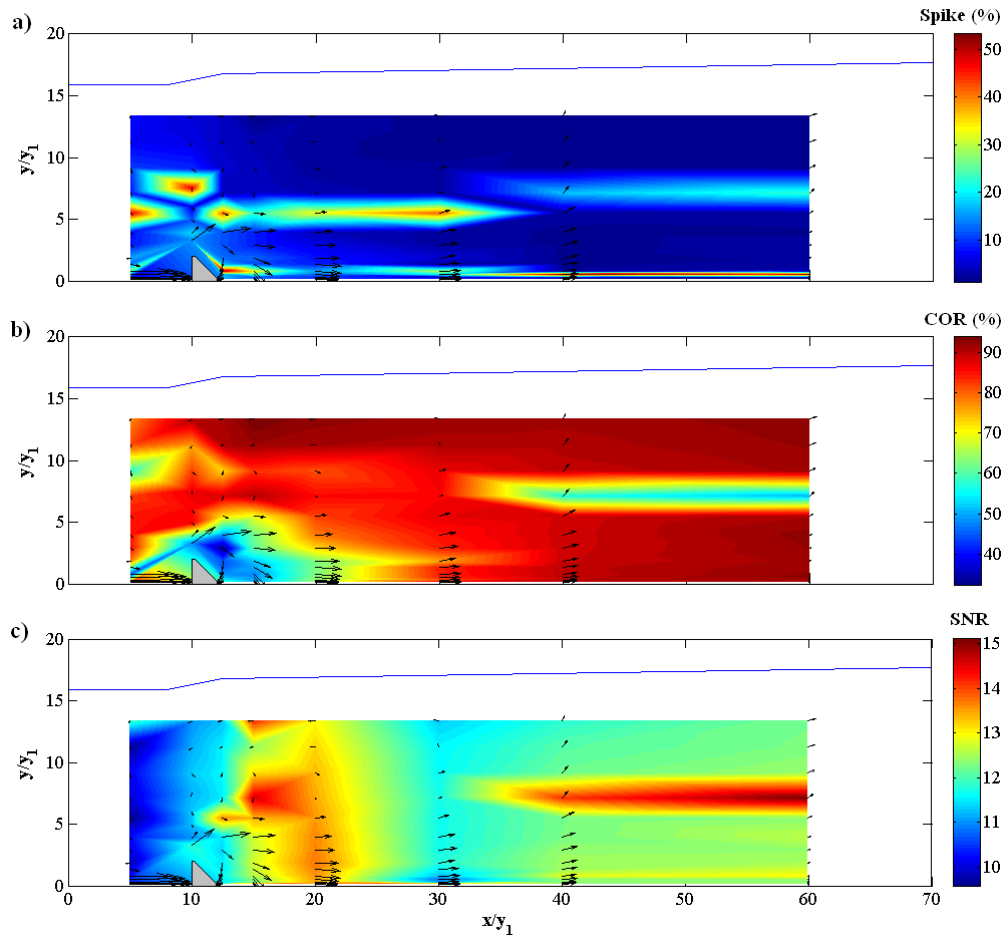


Figure A2.3 Distribution pattern for the spikes (a), correlation coefficients (b), and signal-to-noise ratios (c) of the u-velocity in the centerplane of the RWJ flow regime (run BB4).

Appendix 2: Data Quality and Analysis

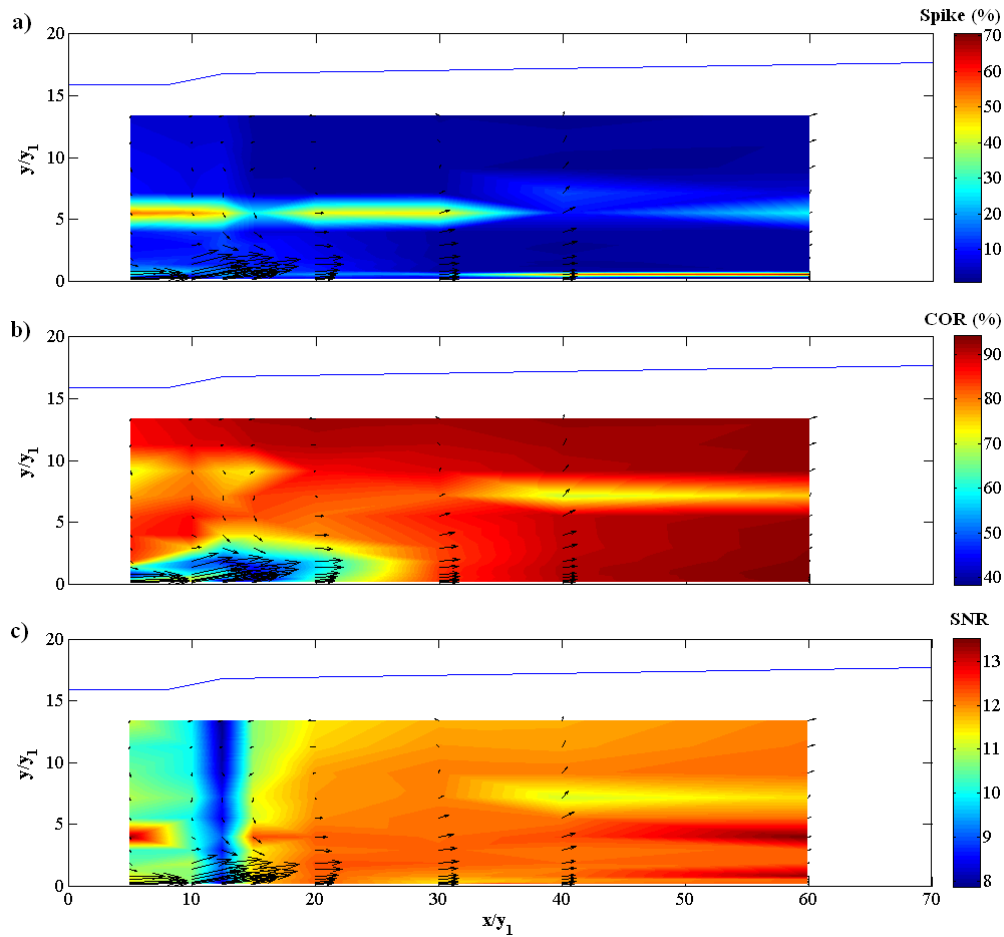


Figure A2.4 Distribution pattern for the spikes (a), correlation coefficients (b), and signal-to-noise ratios (c) of the u-velocity in the off-centerplane of the RWJ flow regime (run BB4).

Sampling Duration

A sensitivity analysis was conducted to find the appropriate sampling duration. In this sensitivity analysis, 30-minute long time series of instantaneous velocities were gathered at a number of points located at various distances from the gate and heights from the bed. Time-averaged velocities were then computed using different lengths of the 30-minute time series. It was assumed that the 30-minute time-averaged value was free of any sensitivity to the sampling duration. The computed time-averaged velocities computed for shorter durations were compared with the values calculated using the entire 30-minute time series and the difference in percent was calculated. A diagram of such comparison is shown

Appendix 2: Data Quality and Analysis

in Figure A2.5 for the u velocity (a) as well as the longitudinal RMS velocity (b). It was found that the time-averaged velocities computed using time series with durations of one minute or greater had magnitudes that were within 4% of the values computed using the 30-minute time series. As a result, a sampling duration of one minute was used for time-averaged measurements and each resulting time series was comprised of 6,000 instantaneous velocity samples (i.e. one minute duration sampled at 100 Hz). Also, it was observed that a minimum sampling duration of 5 minutes is required for measuring the turbulence properties to reduce the error to less than 4%. Hence, a sampling duration of five minutes was used for turbulence measurements.

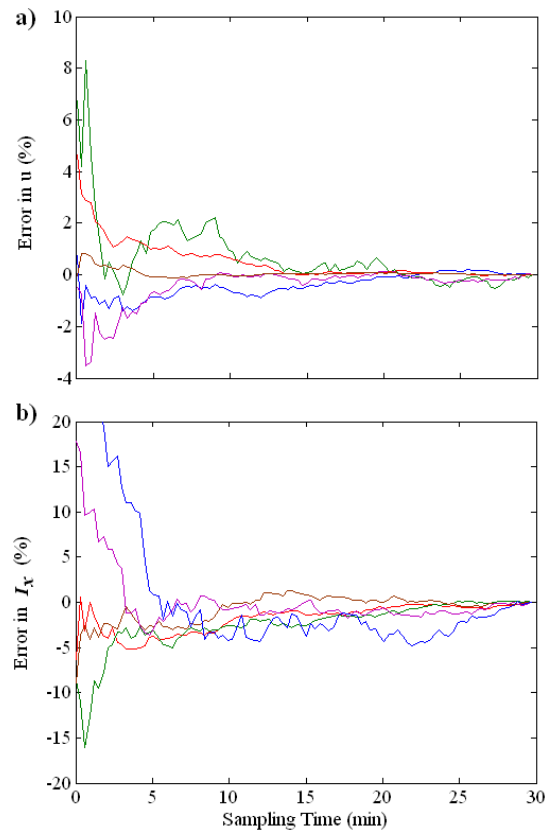


Figure A2.5 Sensitivity of the measured u (a) and I_x (b) to sampling duration (colors represent different measurement points).

Accuracy Compared to LDA

Measurement of turbulence parameters using the ADV involves some uncertainties due to several sources. The errors present in turbulence measurements can be classified into two groups. First, errors due to the physical limitations of the measuring device; i.e. the relatively large sampling volume of the ADV compared to the turbulence length scales. Secondly, statistical errors in sampling a random signal which result in scatter in measurements conducted in repeated experiments (Garcia et al. 2006).

Table A2.1. The range of parameters in the replicate experiments.

Run	F_I	S	x/y_I
R1	3.19	0.85	8, 30, 48
R2	5.49	0.63	16, 40, 64
R3	8.19	0.24	12, 36, 68

To evaluate the effect of the ADV sampling volume size, replicate experiments of submerged hydraulic jumps without blocks were conducted with identical F_I and S values to Long et al. (1990). Three experiments (R1, R2, and R3) were conducted for which the F_I , S and x/y_I values are tabulated in Table A2.1. These experiments were selected such that they cover the range of F_I and x/y_I values in the current study. The only difference between these experiments and the ones by Long et al. (1990) was the opening of the gate (other than using the ADV instead of the LDA); i.e. in Long et al.'s (1990) selected three experiments the gate opening was 2.5, 2.5, and 1.5 cm, respectively, compared to 1.9 cm in the present study.

It was observed that the overall trends of the measurements made using the two devices are similar; however, the turbulence parameters estimated from the ADV data are considerably smaller than the corresponding values estimated from the LDA data by Long et al. (1990). To quantify the differences in the measurements by ADV and LDA, the depth-averaged values of the parameters at each station were compared and the results are presented in Table A2.2. That is, the values in this table are results of comparison between nine stations. In this

Appendix 2: Data Quality and Analysis

table, RE represents the standard error computed as the percentage ratio of the difference between the ADV and LDA measurements to the LDA measurement. Also, SAD stands for the sum-of-absolute deviations and SSD stands for sum-of-squared-deviations.

Table A2.2. The range of the ADV measurement errors compared to LDA.

Parameter	RE (%)			SAD	SSD
	min	max	average		
I_x	-14.4	4.2	-4.2	0.056	0.00049
I_y	-42.0	-22.6	-30.3	0.268	0.00873
$\hat{\tau}_R$	-76.2	193.4	14.7	0.014	0.00006

It can be observed in Table A2.2 that the nondimensional I_x values are scattered within a band with an approximately -14% to +4% relative error with the average RE being only 4%. The nondimensional I_y values are, however, always underestimated by 23% to 42% with an average of 30%. The largest magnitudes of the relative error are observed for the Reynolds stress with a range from +193% to -76% and an average of 15%, despite having small SAD and SSD values (due to the small absolute magnitudes of the Reynolds stress). In summary, the average relative error of I_x , I_y and $\hat{\tau}_R$ estimated from ADV data compared to Long et al.'s (1990) LDA estimates was -4%, -30% and 15%, respectively. From this comparison it can be concluded that the ADV measurements are sufficiently accurate for the current project.

Uncertainty

The other source of error in ADV measurements is the statistical error in sampling a random signal. The estimation of this sampling error provides a good approximation of the total error when the other error components are relatively small (Garcia et al. 2006). To evaluate the significance of this error, uncertainty analysis is used. The uncertainty analysis provides a data range for the measured parameter within which the true value, for the selected confidence limit, is located. If the parameter being analyzed has a normal probability distribution, standard methods are available to approximate the confidence intervals (Moffat

Appendix 2: Data Quality and Analysis

1988). These methods require the standard error of the parameter to be known which can be estimated for uncorrelated data with any arbitrary probability distribution using the equations available in the literature (Benedict and Gould 1996). For correlated data such as velocity time series, however, equations for the standard error of the mean and variance are only available (Bendat and Piersol 2010). No equations are available to compute the standard error of parameters such as turbulence time and length scales or energy dissipation rate which are dependent on the correlation structure of the turbulent velocity field (Garcia et al. 2006).

An alternative method for such complicated parameters is the bootstrap technique introduced by Efron (1979). The standard bootstrap method can be used to evaluate the confidence intervals for uncorrelated data with any complex structure (Efron and Tibshirani 1993). However, Kusch (1989) introduced the moving block bootstrap method which preserves the correlation structure and, hence, can be used for correlated data. This method is based on randomly re-sampling the signal using blocks with a certain length (Zoubir and Iskander 2004). This procedure is repeated and the error and confidence intervals are estimated using the repeated re-samples. It is recommended to have 200 and 1000 replications for the estimation of error variance and confidence interval, respectively (Efron and Tibshirani 1993). Regarding the optimum length of the blocks, there are general methods available in the literature; e.g. Politis and White (2004). Garcia et al. (2006) applied the moving block bootstrap successfully to ADV turbulence measurements. They also presented an empirical equation for the optimum length of the blocks based on the ADV sampling time and the turbulence integral time scale. Herein, the moving block bootstrap with the optimum block length provided by Garcia et al. (2006) with 1000 repetitions was used to evaluate the confidence intervals of all turbulence parameters.

To study the uncertainty of the ADV measurements, the coefficient of variation (CV) and the relative error (RE) were calculated for the 1000

Appendix 2: Data Quality and Analysis

replications of the moving block bootstrap. Here, CV is equal to the ratio of the standard deviation to the mean of the 1000 replications calculated for each parameter. Also, RE for each parameter is defined as,

$$RE = \frac{X_r - X_o}{X_o} \times 100 \quad 2-1$$

where, X_o and X_r represent the values of parameter X obtained from the original measured time series and from the 1000 replications, respectively.

The distribution pattern of the CV and RE magnitudes for the I_x measurements are shown in Figure A2.6 and Figure A2.7 for the centerplane and off-centerplane of the DSJ flow regime, respectively. Similar plots for the RWJ flow regime are shown in Figure A2.8 and Figure A2.9 for the centerplane and off-centerplane, respectively. It can be observed that, in both cases, largest magnitudes of CV and RE are observed in the shear layer upstream of the blocks and also at the location where the deflection and reattachment of the jet occurs.

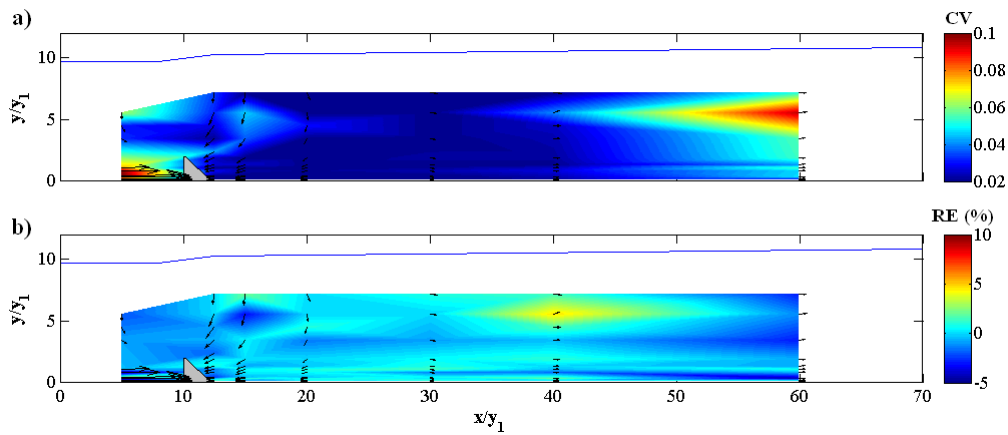


Figure A2.6 Distribution pattern of the coefficient of variation (a) and relative error (b) of I_x in the centerplane of the DSJ flow regime (run BB3).

Appendix 2: Data Quality and Analysis

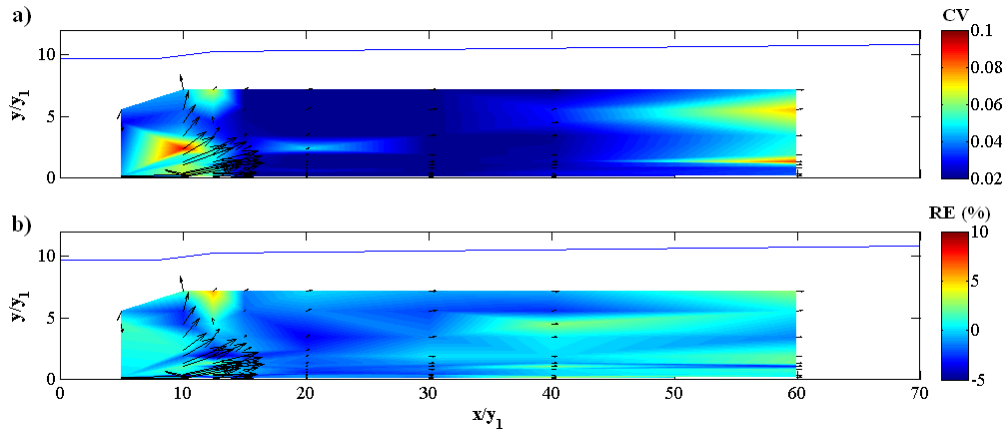


Figure A2.7 Distribution pattern of the coefficient of variation (a) and relative error (b) of I_x in the off-centerplane of the DSJ flow regime (run BB3).

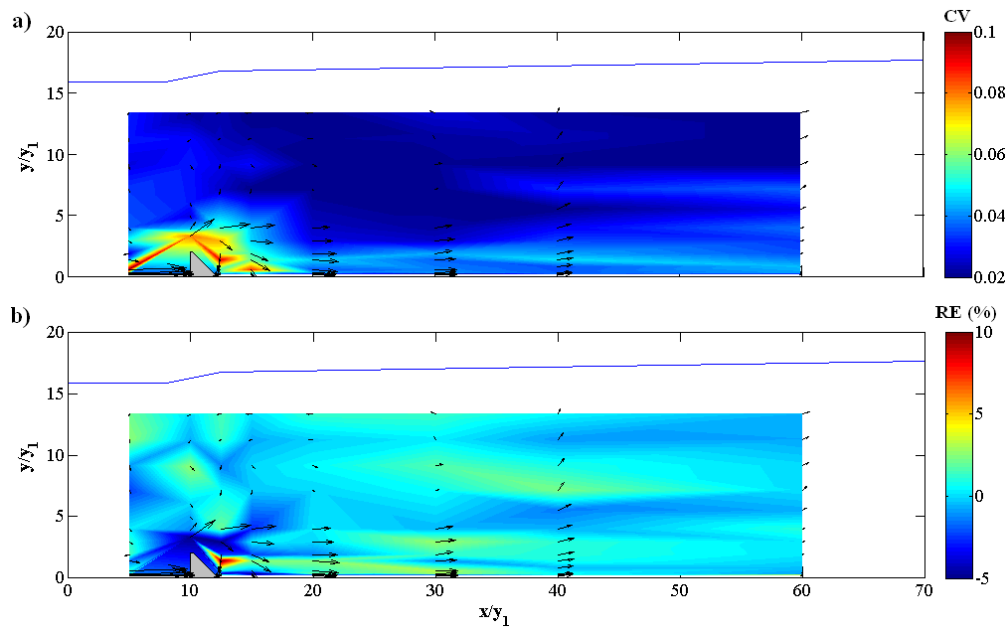


Figure A2.8 Distribution pattern of the coefficient of variation (a) and relative error (b) of I_x in the centerplane of the RWJ flow regime (run BB4).

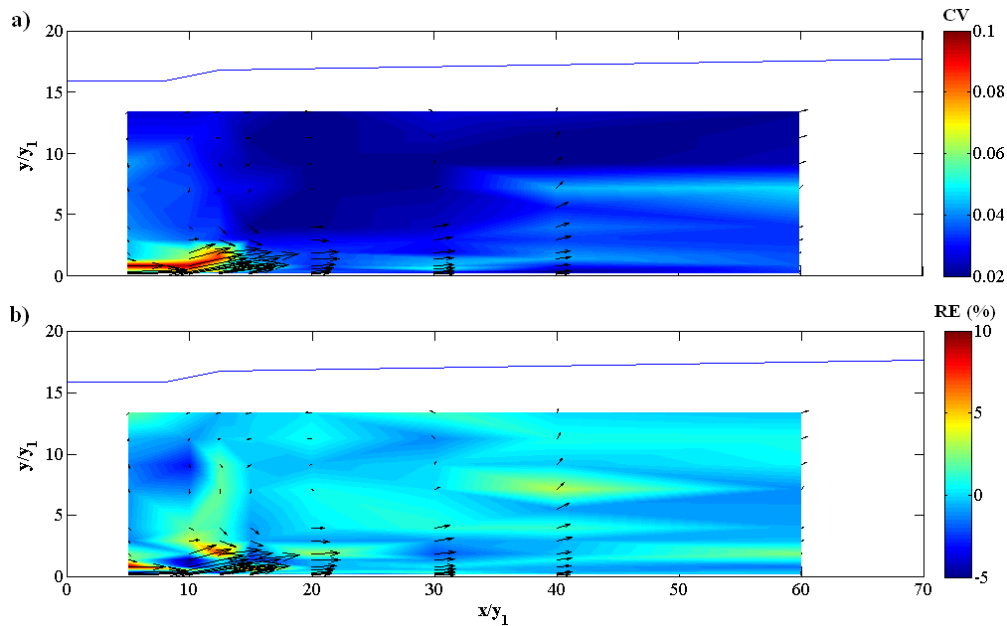


Figure A2.9 Distribution pattern of the coefficient of variation (a) and relative error (b) of I_x in the off-centerplane of the RWJ flow regime (run BB4).

References

- Bendat, J. S., and Piersol, A. G. (2010). *Random Data: Analysis and Measurement Procedures*, Fourth Edition, John Wiley & Sons.
- Benedict, L. H., and Gould, R. D. (1996). "Towards better uncertainty estimates for turbulence statistics." *Experiments in Fluids*, 22, pp. 129-136.
- Efron, B. (1979). "Bootstrap Methods: Another Look at the Jackknife." *The Annals of Statistics*, Vol. 7, No. 1, 1-26.
- Efron, B., and Tibshirani, R. J. (1993). "An Introduction to the Bootstrap." *Monographs on Statistics and Applied Probability 57*, Chapman and Hall Inc. New York.
- Garcia, C. M., Jackson, P. R., and Garcia, M. H. (2006). "Confidence intervals in the determination of turbulence parameters." *Experiments in Fluids*, 40, pp. 514-522.
- Kunsch, H. R. (1989). "The Jackknife and the Bootstrap for General Stationary Observations." *The Annals of Statistics*, Vol. 17, No. 3, pp. 1217-1241.

Appendix 2: Data Quality and Analysis

Long, D., Steffler, P. M., and Rajaratnam, N. (1990). "LDA study of flow structure in submerged hydraulic jump." *J. Hydraul. Res.*, 28(4), 437-460.

Moffat, R. J. (1988). "Describing the Uncertainties in Experimental Results." *Experimental Thermal and Fluid Science*, Vol. 1, pp. 3-17.

Politis, D. N., and White, H. (2004). "Automatic Block-Length Selection for the Dependent Bootstrap." *Econometric Reviews*, Vol. 23, No., 1, pp. 53-70.

SonTek Technical Notes, (1997). "Pulse Coherent Doppler Processing and the ADV Correlation Coefficient." 6837 Nancy Ridge Drive, Suite A, San Diego, CA 92121. 5 pp.

Zoubir, A. M., and Iskander, D. R. (2004). *Bootstrap Techniques for Signal Processing*, Cambridge University Press, New York.